Numerical analysis and long-term dynamics of Fourier-type pseudo-spectral schemes applied to the Klein-Gordon equation

Gafari Abiodun Lukumon
217081936

UKZN, Westville Campus, 2024.

Numerical analysis and long-term dynamics of Fourier-type pseudo-spectral schemes applied to the Klein-Gordon equation

by

Gafari Abiodun Lukumon

1st May, 2024.

Submitted in fulfilment of the academic
requirements for the degree of
Doctor of Philosophy in Mathematics,
University of KwaZulu-Natal (UKZN),
School of Mathematics, Statistics and Computer Science,
Westville Campus,
Durban, 4000.

As the candidate's supervisors, we have approved this thesis for submission.

Signature: _____ Name: Prof. S. Shindin Date:_____

Signature: _____ Name: Prof. N. Parumasur Date: _____

Preface

The work described in this thesis was carried out in the School of Mathematics, Statistics and Computer Science at University of KwaZulu-Natal, Durban,South Africa from January 2019 to April 2024, under the supervision of Professor Sergey Shindin and Professor Nabendra Parumasur.

This study represents original work by the author and has not otherwise been submitted in any form for any degree or diploma to any other tertiary institution. Where use has been made of the work of others, it is duly acknowledged in the text.

Gafari Abiodun Lukumon.

Declaration 1 - Plagiarism

I, Gafari Abiodun Lukumon, declare that

1. The research reported in this thesis, except where otherwise indicated, is my original research.

2. This thesis has not been submitted for any degree or examination at any other university.

3. This thesis does not contain other personal data, pictures, graphs or other information, unless specifically acknowledged as being sourced from other persons.

4. This thesis does not contain other persons' writing, unless specifically acknowledged as being sourced from other researchers. Where other written sources have been quoted, then:

    a. Their words have been re-written but the general information attributed to them has been referenced

    b. Where their exact words have been used, then their writing has been placed in italics and inside quotation marks, and referenced.

5. This thesis does not contain text, graphics or tables copied and pasted from the Internet, unless specifically acknowledged, and the source being detailed in the thesis and in the References section.

Signed _____

Acknowledgment

I humbly attribute all glory and adoration to the Almighty God, whose grace has blessed me with sound health, guidance, and strength, enabling me to navigate and conquer challenges along this journey.

I extend my deepest appreciation to my esteemed supervisors, Professor Sergey Shindin and Professor Nabendra Parumasur, whose patient guidance, encouragement, and unwavering support have been instrumental since our journey began in 2017 (first as an MSc student). Without their mentorship and steadfast commitment, overcoming the obstacles encountered would have been daunting. I am immensely grateful for their invaluable contributions to my academic and personal growth. Special recognition is also extended to Madam Desiree Govender and the youngest member of the Shindin household, affectionately known as "Professor Shindin's Junior" for accommodating my inquiries beyond regular office hours. I extend my sincere apologies for any inconvenience caused and express thanks for their patience and understanding.

I am profoundly thankful to the University of KwaZulu-Natal, South Africa, for providing tuition remission and fostering a conducive study environment equipped with modern facilities.

Special gratitude is extended to my beloved parents, Mr. and Mrs. Luku-

mon Olomini, my cherished wife, Mrs. Mariam Lukumon (nee Adegoke), my children - Asake, Ayinde, and Abeni Lukumon, as well as Fatima, Adam, Nimotallah and other siblings, in-laws, friends, family, and well-wishers for their love, prayers, support, encouragement, advice, and endurance throughout my academic journey.

I am grateful for the support and mentorship of Chief Ahmed Raji (SAN) and Professor Aneshkumar Maharaj, as well as the assistance and camaraderie of Dr. Ayegbusi Rasheed, Dr. Olabisi Aluko and my other colleagues at the school.

My heartfelt appreciation also goes to all my teachers and advisors. Though limitations of space prevent me from mentioning each name individually, I extend my gratitude to everyone who contributed, in various capacities, to the success of this endeavor. Your support has been invaluable, and I am sincerely thankful.

Abstract

This thesis investigates the Klein-Gordon equation (KGE) using a combined theoretical and numerical approach. We develop a robust numerical approximation scheme for the KGE that demonstrates good convergence properties for various data types and explore the long-time behavior of semi-discrete KGE solutions near finite- and infinite-dimensional invariant subsets of an appropriate space.

In the first part of the thesis, we establish convergence results for the semi-discrete, Fourier pseudo-spectral spatial approximation of the KGE with smooth potentials. We present an extensive stability and convergence analysis for finite Sobolev regularity data in $\mathbb{T}$ and $\mathbb{R}$, as well as for smooth data from Gevrey classes in $\mathbb{T}$. We demonstrate that the convergence rate is algebraic in the first case and (sub-)geometric in the second case.

The second part of the thesis deals with the numerical studies of the long-time dynamics of semi-discrete numerical solutions in periodic settings. Through an extensive set of simulations, we show that the pseudospectral semi-discretization is capable of preserving finite- and infinite-dimensional invariant structures over very long time intervals.

Contents

1 Introduction **1**

1.1 The Klein-Gordon equation 1

1.2 Contemporary studies on well-posedness for the nonlinear KGE 3

1.3 Contemporary studies of numerics for the nonlinear KGE . . . 6

1.4 Aims and objectives of the study 9

2 Preliminaries **12**

2.1 Banach spaces 12

2.2 Hilbert spaces 16

2.3 Hilbert-Sobolev Scale of Periodic Functions 18

2.4 Hilbert-Gevrey Scale of Periodic Functions 20

2.5 The continuous and discrete Fourier expansions 21

2.5.1 The continuous Fourier expansion 21

2.5.2 The discrete Fourier expansion 23

2.6 Two inequalities 24

3 Convergence of pseudospectral schemes in $\mathbb{T}$ and $\mathbb{R}$ for $H^s \times$

H^{s-1} **data** **26**

3.1 A priori estimates 27

3.2 Convergence 33

3.3 Extension to the real line 36

4 Geometric convergence **38**

4.1 Wellposedness in the Gevrey settings 38

4.2 Consistency estimates 40

4.3 Error estimates 41

4.4 Extension to the real line 44

5 Long time behaviour of the KGE solutions **45**

5.1 Dynamics associated to the Sine-Gordon equation 45

5.2 The spectrum of $\mathcal{L}_{(u,v)}$ in periodic settings 47

5.3 Finite-gap solutions 50

5.4 Small amplitude real finite-gap solutions 51

5.5 Finite-gap KAM tori 52

5.6 Finite-dimensional KAM theory near the origin 54

5.7 Infinite dimensional Nekhoroshev-type theories near the origin 58

6 Numerical simulations **60**

6.1 Accuracy in finite time intervals 60

6.1.1 Practical Implementation 61

6.1.2 Simulations 63

6.2 Long time behaviour near n-gap tori 66

6.3 Long time preservation of harmonic actions 70

7 Conclusion **101**

Chapter 1

Introduction

1.1 The Klein-Gordon equation

In the field of applied mathematics, finding analytical solutions to certain evolution equations can be extremely challenging, leading us to resort to numerical approaches. Various numerical methods are available for different types of problems, but when dealing with regular domains, spectral methods are highly regarded for their accuracy and computational efficiency [17, 22, 56, 63, 88]. Spectral methods comprise a collection of techniques that represent solutions of a d ifferential equation as finite linear combinations of globally defined basis functions, where the coefficients are chosen to ensure the closest possible satisfaction of the differential equation and boundary conditions [17, 22, 56, 63, 88].

This thesis focuses on the theoretical and numerical analyses of a Fourier-type pseudo-spectral method in the context of the Klein-Gordon equation (KGE). The nonlinear KGE is given by

$$u_{tt} = a^2\Delta u - \mathcal{V}'(u), \quad t > 0, \quad u(x,0) = u_0, \quad u_t(x,0) = v_0, \tag{1.1.1}$$

where $\mathcal{V}(\cdot)$ is a given non-negative potential, $\mathcal{V}(0) = \mathcal{V}'(0) = 0$, $\Delta u = u_{tt}$ and u is defined in Ω, where $\Omega \in \{\mathbb{T}, \mathbb{R}\}$. Such models arises in a variety of practical applications including theoretical physics, quantum field theory, nonlinear optics, solid state physics, applied sciences and engineering [31, 64, 12, 10, 1, 87]. The concrete form of the potential $\mathcal{V}(\cdot)$ depends on the physical phenomenon under consideration, e.g. (1.1.1), with $\mathcal{V}(u) = 1 - \cos(u)$, (the so called Sine-Gordon or SGE equation) is widely used in the modeling of shallow waves, $\mathcal{V}(u) = \frac{u^3}{3} - \frac{u^2}{2}$ has applications in solid state physics, see e.g. [31], and $\mathcal{V}(u) = \cosh(u) - 1$ is used in describing the behavior of quantum impurities in certain materials and the interaction of dislocations in crystals [75], etc.

The problem (1.1.1) is Hamiltonian, i.e. introducing

$$U = \begin{pmatrix} u \\ v \end{pmatrix} = \begin{pmatrix} u \\ u_t \end{pmatrix}, \quad \mathcal{J} = \begin{pmatrix} 0 & 1 \\ -1 & 0 \end{pmatrix},$$

and

$$\mathcal{H}(u,v) = \frac{a}{2}\|u_x\|_0^2 + \frac{1}{2}\|v\|_0^2 + \int_\Omega \mathcal{V}(u)dx, \quad \Omega \in \{\mathbb{T}, \mathbb{R}\}, \quad \|u\|_0^2 = \int_\Omega |u|^2 dx,$$

it is easy to verify that (1.1.1) is equivalent to

$$U_t = \mathcal{J}\nabla\mathcal{H}(U), \quad t > 0, \tag{1.1.2a}$$

$$U_0 = (u_0, v_0)^T. \tag{1.1.2b}$$

Formally,

$$\frac{d}{dt}\mathcal{H}(u,v) = \frac{1}{2}\int_\Omega (2vv_t + 2a^2u_{xt}u_x + 2u_t\mathcal{V}'(u))dx.$$

Using equation (1.1.1), integrating by parts and taking into account that v is 2ℓ-periodic, we infer that

$$\begin{aligned}\frac{d}{dt}\mathcal{H}(u,v) &= \int_\Omega (v[a^2u_{xx} - \mathcal{V}'(u)] + a^2v_xu_x + v\mathcal{V}'(u))dx \\ &= a^2\int_\Omega(-v_xu_x + v_xu_x)dx + (vu_x)|_{\partial\Omega} = 0.\end{aligned}$$

From the above, we conclude that the quantity $\mathcal{H}(u,v)$ is conserved along classical solutions of (1.1.1). In applications, the quantity $\mathcal{H}(u,v)$ represents total energy of a physical system under consideration. For example, in the SGE scenario, $\|u_t\|_0^2$ represents the kinetic energy of the wave, $\|u_x\|_0^2$ represents its potential energy, and $\int_\Omega \mathcal{V}(u)dx$ represents the self-energy of the wave so that $\mathcal{H}(u,v)$ is the total energy of a wave propagating in the spatial domain Ω.

Many authors have worked on KGE/SGE, including both its numerical and analytical aspect. We shall present a review of these in the coming sections.

1.2 Contemporary studies on well-posedness for the nonlinear KGE

Well-posedness and related studies. For a given evolution system like KGE to be well-posed, one must ensure that solutions exist, are uniquely determined by input data (that normally involves a number of initial and boundary conditions) and depend on the data continuously. Mathematical studies that are pertinent to well-posedness of the nonlinear KGE have attracted a substantial number of authors [89, 18, 47, 48, 44, 62, 72, 73, 79, 81, 96, 100, 99].

The pioneering works by K. Jörgens, J.L Lions and F.E. Browder, [60, 69,

20], laid the foundation for the modern well-posedness theory of KGE and related models. Building upon these foundational works, recent research has extended well-posedness results to various physically relevant scenarios. These extensions consider settings such as higher dimensions ($d > 1$), rapidly growing potentials $\mathcal{V}(u)$ and diverse classes of input data. The specific detail of these results depend heavily on three key factors:

(i) The type of nonlinearity $\mathcal{V}(u)$, implying that different nonlinearities lead to distinct well-posedness conditions.

(ii) The dimensionality of the spatial domain, meaning that well-posedness results often vary depending on the number of spatial dimensions.

(iii) The regularity and size of initial data, e.g., small or large input can influence well-posedness outcomes.

A vast amount of effort in the literature is directed towards local and global well-posedness for the KGE with general power-type nonlinearities, see e.g. [47, 48, 72, 84] and references therein. These classes of works are mainly focused on the existence of local and global weak solutions in the energy space $H^1(\mathbb{R}^d) \times L^2(\mathbb{R}^d)$, $d \geq 1$. Depending on the nonlinearity sign and on the size of input data one has two distinct scenarios: the weak solutions exists globally for any data; the weak solutions exists globally for small data and blow-up in finite time for data above a certain threshold.

The basic results of these types are found in [47, 48]. The authors demonstrate existence and uniqueness of global weak solutions in the energy space $H^1(\mathbb{R}^d) \times L^2(\mathbb{R}^d)$ for general power-type nonlinearities, satisfying

$$|\mathcal{V}(u)| \leq |u|^p, \quad p \leq \begin{cases} \infty, & n = 1, 2, \\ 1 + \frac{4}{n-2}, & n \geq 3. \end{cases}$$

In the settings of [47, 48], the total energy $\mathcal{H}(u, v)$ (see definition in Section 1.1) carried by the weak solutions is sign definite. As a consequence, global solvability is independent of the initial data (u_0, v_0).

The situation is significantly much more complicated, in the case when the total energy $\mathcal{H}(u, v)$ (the Hamiltonian) is sign indefinite. Multiple authors contributed to this problem, see in particular [72, 100, 84] and references therein. For the same power-type nonlinearity as above, the solutions are global if $\mathcal{H}(u_0, v_0) < c$, blow-up when $\mathcal{H}(u_0, v_0) > c$ and both scenarios are possible in the border case of $\mathcal{H}(u_0, v_0) = c$. The concrete value of c is not easy to determine explicitly, see however [84] for some sharp results in this direction.

It is well known that the wave operator does not have smoothing properties similar to those of operators of parabolic type. However, in the simplest linear settings it preserves the original regularity of the input data. In the general KGE case equipped with power-type nonlinearities, this phenomenon was investigated in great detail by a number of authors, see in particular [18].

As compared to power-type nonlinearities, much less is known about general smooth potentials $\mathcal{V}(u)$. In this direction, we can cite the relatively recent works of [57] in $H^1(\mathbb{R}^2) \times L^2(\mathbb{R}^2)$ and of [79] in $H^s(\mathbb{R}^d) \times H^s(\mathbb{R}^d)$, both dealing with exponential-type potentials; and the work of [82] on analytic KGE solutions, equipped with general analytic potentials in $d = 1$.

It is worth mentioning that apart from stand-alone KGE equation, there exists vast literature dealing with the well-posedness of coupled hyperbolic systems of KGE type, see [66] for the results in this direction.

Long-time dynamics in near integrable settings. In the special cases of $\mathcal{V}(u) = 1 - \cos(u)$, $\mathcal{V}(u) = \cosh(u) - 1$ and $d = 1$, the resulting PDEs are known to be completely integrable. That is, in the classical settings both problems have a complete countable family of first integrals that are in involution. Hence, in complete analogy with finite-dimensional Hamiltonian ODEs, the exact solution associated to sufficiently regular initial data can be constructed using geometric methods. A vast amount of literature (specifically in physics) is dedicated to construction of such solutions. The classical references are [81, 96], for the inverse scattering transform and multi-soliton solutions in $\mathbb{R}$; and [11], for the exact geometric integration of SGE and hyperbolic SGE (hSGE) in the periodic settings $\mathbb{T}$.

Presently, the long-time dynamics of SGE and hSGE in $\mathbb{T}$ is well understood. For input data from $H^2(\mathbb{T}) \times H^1(\mathbb{T})$ all solutions are quasi-periodic in time. Note however that in realistic settings, we always deal with small perturbations of the idealized mathematical models. Hence, a lot of effort was directed towards building a Hamiltonian perturbation theory similar to the famous KAM theory for ODEs, see [94] for the works in this direction. Note, however, that, the current state-of-art results are far from being complete and/or satisfactory. We provide a more detailed discussion in Chapter 5.

1.3 Contemporary studies of numerics for the nonlinear KGE

In the numerical analysis realm, a number of semi- and fully- discrete schemes were proposed in the literature. In particular, study of three finite-difference approximations of the nonlinear KGE that respect the symplectic structure

of the equation in periodic settings is done in [35]. M. Dehghan and A. Shokri in [28] employ radial basis functions. Their scheme appears to be very similar to a finite-difference method and was successfully applied to solve one-dimensional nonlinear KGE with quadratic and cubic nonlinearities. The numerical techniques for the solution of nonlinear KGE based on the finite-difference and collocation methods are presented by [65]. The validity of these techniques is demonstrated with examples. Further details on classical finite-difference methods for solving nonlinear KGE can be found in [14, 38, 55].

In [93], a fully discrete approach targeting a damped nonlinear Klein-Gordon equation (KGE) in one dimension is implemented. The paper extensively discusses the numerical treatment of damped nonlinear Klein-Gordon equation, employing a variational method in conjunction with a finite element approach. It introduces a semi-discrete algorithm featuring quadratic interpolation functions and Gauss-Legendre quadrature for numerical integrations. The study further implements a Runge-Kutta method for advancing numerical solutions in time. The study is illustrated by numerous simulations.

Numerical schemes based on Chebyshev-type wavelet spectral approximations for solving the KGE and SGE are presented in [58]. The authors approach yields sparse differentiation matrices which significantly reduces the computational cost of the algorithm. The approach transforms the given problem into a system of algebraic equations that can be easily integrated in time using standard methods for ODEs. On the other hand, the development of schemes associated with Legendre-type wavelets is discussed in [101]. As in [58], this approach saves memory and computation time by leveraging the hierarchical scale structure of Legendre wavelets. The paper includes 1D and 2D examples to demonstrate the validity and applicability of the new technique. The numerical results presented in the paper demonstrate the

exponential convergence of the algorithm.

Fast and accurate fourth-order time-stepping schemes, coupled with the discrete Fourier transform, are proposed in [77]. Although the semidiscretized in space differential operator is not diagonal, it is implemented as in the approach of the diagonal case. On one hand, this reduces computational time on another hand the scheme preserves key qualitative features of the KGE model, in particular the total energy of numerical solutions is conserved.

A Legendre-type pseudo-spectral scheme for solving initial-boundary value problems of nonlinear KGE is developed in [68]. The authors investigate the stability and convergence of numerical solutions. Their numerical method exhibits high accuracy and extends to multi-dimensional settings.

A variant of the pseudo-spectral method for solving the nonlinear KGE is proposed in [53]. The approach introduces modifications to the conventional pseudo-spectral method aiming to improve its performance in solving the KGE. The numerical simulations demonstrate high accuracy and stability of the numerical scheme over long time intervals. Notably, even for moderate number of modes retained in spatial approximation and for large integration time steps, the proposed method remains robust and reliable.

A pseudo-spectral Fourier-type method for finding localized spherical soliton solutions of $(3+1)$-dimension KGE is presented in [37], where the classical fourth-order Runge-Kutta method is employed to perform time integration.

The continuous flow generated by KGE is symplectic, hence design of suitable high order time-stepping (marching) schemes preserving this structure is an important issue. In this direction, in [70], a class of symmetric and arbitrary high-order marching schemes suitable for time integration of KGE is proposed. The construction makes use of two-point Hermite interpola-

tion polynomials, which are applied directly to approximate integrals in the variation-of-constants formula. The high accuracy of the resulting scheme is demonstrated in a number of practical simulations.

The numerical comparison of implicit and exponential time-differencing methods in context of ϕ^4 KGE is performed in [36], where it was established that the former techniques are more accurate than the latter. Similarly, B. Weizhu and D. Xuanchun in [97], compared finite-difference and Fourier-type pseudo-spectral schemes combined with a Gaustschi-type exponential integrators for solving KGE in the non-relativistic limit region.

Further discussion of spectral and finite-element methods in context of KGE can be found in [24, 29, 32, 9, 4].

1.4 Aims and objectives of the study

The KGE is a fundamental model that spans various fields, from quantum mechanics to relativistic quantum field theory. Despite its widespread applications, significant gaps exist in our understanding of the KGE model.

(i) It is worth mentioning that most of numerical schemes developed in the literature and reviewed in the previous section deal with the KGE posed on bounded spatial domains. When the domain is unbounded, it is standard to truncate it and then apply conventional schemes designed for bounded domains. It is clear that doing so, we loose some information about solutions of the KGE model. To the best of our knowledge there exists no rigorous treatment of the numerical error induced by domain truncation.

It is one of the purposes of the present thesis to demonstrate that this er-

ror is properly controlled, provided the truncated domain is sufficiently large to capture the essential features of the input data.

(ii) The spectral methods in general are known to converge extremely fast. In context of various types of spectral schemes applied to KGE the (sub-)geometric convergence rate was reported by large number of researchers. However, to the best of our knowledge, rigorous mathematical proofs have not appeared in the numerical literature.

In Chapter 4, we employ the ideas of [82] to demonstrate (sub-)geometric convergence for analytic data.

(iii) In a number of realistic scenarios, the pseudo-spectral Fourier-type schemes can be viewed as a small Hamiltonian perturbation of the SGE and/or the linear wave equation (LWE). In these cases, it is natural to expect that the qualitative behaviour of the semidiscrete flow resembles closely the flow generated by the SGE/LWE. Despite multiple attempts to construct an infinite dimensional analogue of KAM theory, the available results are far from being satisfactory. The available results rely on assumptions which are extremely pessimistic.

In Chapter 6, we provide comprehensive numerical simulations, indicating that the long-time dynamics of semidiscrete solutions is close to the dynamics of the unperturbed SGE/LWE models for a much wider set of parameters than predicted by available theories.

Chapter 1 reviews some existing results from the literature on well-posedness and numerics of KGE. In Chapter 2, we provide the necessary background in functional analysis that is used throughout our work.

In Chapter 3, an analogue of well-posedness for the Fourier-type pseudospec-

tral discretizations is discussed, with a specific focus on convergence in both $\mathbb{T}$ and $\mathbb{R}$. Geometric convergence of the Fourier-type schemes is covered in Chapter 4.

Chapter 5 provides a detailed review of available results, concerning KGE with general smooth/analytic potentials in both $\mathbb{T}$ and $\mathbb{R}$. The special focus is given to the long time behaviour of solutions in near completely integrable regime.

Chapter 6 concludes the thesis with simulations, addressing convergence theories of Chapters 3 and 4 in finite time intervals, illustrating long-time behavior of numerical solutions near n-gap tori and numerical near preservation of harmonic actions over large time intervals.

Finally, the main theoretical results of the thesis, in particular those of Chapters 3, 4 and partially 6 are published in

[89] S. Shindin, N. Parumasur, G. Lukumon (2022). Numerical analysis of Fourier pseudospectral methods for the Klein-Gordon equation with smooth potentials, *Afrika Matematika*, 33(3):85
https://doi.org/10.1007/s13370-022-01021-9

The work done in this thesis is a continuation of my MSc disseration

[71] Lukumon, G. A. (2018). Numerical solution of the Klein-Gordon equation in an unbounded domain (M.Sc. dissertation).
https://researchspace.ukzn.ac.za/handle/10413/16319

Chapter 2

Preliminaries

The purpose of this Chapter is twofold. First, we assemble together basic facts from functional analysis that are relevant for our study. Second, we fix a notation that is used consistently throughout the thesis.

2.1 Banach spaces

All results listed below are classical, and we refer readers to e.g. [19, 39, 67, 86].

Banach spaces. A linear vector space X over $\mathbb{R}$ or $\mathbb{C}$, equipped with a function $\|\cdot\| : X \to \mathbb{R}$ such that:

(i) $\|u\| \geq 0$ and $\|u\| = 0$ if and only if $u = 0$;

(ii) $\|\alpha u\| = |\alpha|\|u\|$;

(iii) $\|u + v\| \leq \|u\| + \|v\|$;

hold for every $u, v \in X$ and $\alpha \in \mathbb{R}$, is called a *normed linear vector space*. The function $\|\cdot\|$ itself is called a *norm* in X. A norm $\|\cdot\|$ in X induces a topology (*strong topology*). In particular, a sequence $\{u_n\}_{n\geq 0} \subset X$ converges strongly to an element $u \in X$, iff $\lim_{n\to\infty} \|u_n - u\| = 0$.

As usual, we say that a sequence $\{u_n\}_{n\geq 0} \subset X$ is *Cauchy* iff for every $\varepsilon > 0$ and all $n, m \geq N_\varepsilon$, we have $\|u_n - u_m\| < \epsilon$, provided N_ε is sufficiently large. A normed linear vector space is called *complete/Banach* iff all Cauchy sequences in X converge in norm to an element of X.

A subset $Y \subset X$ is said to be *everywhere dense* in a Banach space X if its strong closure equals X, i.e. if $\overline{Y} = X$. A Banach space X is called *separable* if it contains at least a countable everywhere dense subset.

The following two examples are standard:

(i) The spaces ℓ^p, $1 \leq p \leq \infty$ of real-valued sequences $u = (u_n)_{n\geq 0}$, equipped with the norms

$$\|u\|_p = \Big(\sum_{n\geq 0} |u_n|^p\Big)^{1/p}, \quad 1 \leq p < \infty,$$
$$\|u\|_\infty = \sup_{n\geq 0} |u_n|,$$

are Banach spaces. In the case of $1 \leq p < \infty$, these spaces are separable.

(ii) Let Ω be an open measurable subset of $\mathbb{R}^n$. The Lebesgue spaces $L^p(\Omega)$, $1 \leq p \leq \infty$ of measurable p-integrable (equivalence classes of) functions, equipped with the norms

$$\|u\|_p = \Big(\int_\Omega |u(x)|^p dx\Big)^{1/p}, \quad 1 \leq p < \infty,$$
$$\|u\|_\infty = \operatorname{ess\,sup}_{x\in\Omega} |u(x)|,$$

are Banach spaces. As in the previous example for $1 \leq p < \infty$, these spaces are separable.

Linear maps. A linear map $F : X \to Y$ between two Banach spaces X and Y is *bounded* iff

$$\|F\|_{X\to Y} = \sup_{\|x\|_X=1} \|Fx\|_Y < \infty.$$

Since Banach spaces are bornological, all bounded linear maps as above are continuous. The collection of all bounded (equivalently continuous) linear maps from X to Y is denoted by $L(X, Y)$ — it is again a Banach space with respect to the induced norm $\|F\|_{X\to Y}$.

A linear continuous map $F \in L(X, Y)$ is *compact* iff images of bounded subsets of X are precompact in Y. A bounded injective linear map $J : X \to Y$ is called an *embedding* of X into Y. The embedding J is compact if it is compact as a linear map from X into Y. When X is a subspace of Y and J acts as the identity on X, we speak about *canonical embeddings* and write $X \hookrightarrow Y$.

Dual spaces. Given a Banach space X, the space $L(X, \mathbb{C})$ of all bounded linear functionals on X is denoted by X' and is called the *topological dual* of X. The operator norm

$$\|f\|_{X\to\mathbb{R}} = \|f\|_{X'} = \sup_{\|u\|_X=1} |fu|,$$

turns X' into a Banach space.

We may repeat the procedure described above and define the second dual $X'' = (X')'$ and the map $J : X \to X''$ that to each $u \in X$ assigns the linear functional $u'' \in X''$ acting on $f \in X'$ according to the formula

$$u''f = fu.$$

It turns out that J is a continuous linear embedding (*natural embedding*) of X into X''. In general, J is not onto, i.e. JX is a proper linear subspace of X''. In the important case when J is an isomorphism, i.e. when $JX = X''$, we say that the space X is *reflexive*.

We remark that due to the symmetry, the connection between $u'' \in X''$, $u \in X$ and $f \in X'$ is often expressed as

$$u''f = fu = \langle u, f \rangle.$$

The bilinear form $\langle \cdot, \cdot \rangle$ is called the *duality pairing*.

Weak and weak-$*$ convergences. Given a sequence $\{u_n\}_{n\geq 0} \subset X$ (respectively, $\{f_n\}_{n\geq 0} \subset X'$), we say that $u \in X$ (respectively $f \in X'$) is its *weak limit* (respectively, *week-$*$ limit*) if

$$\lim_{n\to\infty} \langle u_n, f \rangle = \langle u, f \rangle, \quad \text{(respectively, } \lim_{n\to\infty} \langle u, f_n \rangle = \langle u, f \rangle),$$

holds for all $f \in X'$ (all $u \in X$).

It is a elementary exercise to verify that strong convergence yields weak in X and that weak convergence in X yields weak-$*$ convergence in X''. Further, in reflexive Banach spaces the notions of weak and weak-$*$ convergences are equivalent. The following two results are standard, see e.g. in [19, 39, 40, 67, 86, 90]:

Lemma 2.1.1. *Bounded subset of reflexive Banach spaces are weakly compact*

Lemma 2.1.2. *Bounded subsets of X', dual of a Banach space X, are weak-$*$ compact.*

In the case of Lebesgue spaces $L^p(\Omega)$, $1 \leq p \leq \infty$, in addition to the weak/weak-$*$ convergence, we say that a sequence $\{u_n\}_{n\geq 0}$ *converges almost everywhere (a.e.)* to u in Ω iff

$$\lim_{n\to\infty} \sup_{\varepsilon>0} \lambda(\{x \in \Omega | |u_n(x) - u(x)| > \varepsilon\}) = 0,$$

where λ denotes the standard Lebesgue measure in $\mathbb{R}^n$.

The following results can be found e.g. in [40, 90].

Lemma 2.1.3. *Assume $\{u_n\}_{n\geq 0}$ converges strongly to $u \in L^p(\Omega)$, $1 \leq p < \infty$. Then there exists a subsequence that converges a.e. to u in Ω. If $p = \infty$, the sequence itself converges a.e. to u in Ω.*

Lemma 2.1.4. *Let $\{u_n\}_{n\geq 0}$ be a bounded sequence in $L^p(\Omega)$, $1 \leq p < \infty$. If $u_n \to u$ a.e. in Ω, then $u \in L^p(\Omega)$ and u_n converges weakly to u in $L^p(\Omega)$.*

2.2 Hilbert spaces

The subsequent theoretical and numerical analyses of the KGE rely on the theory of Hilbert spaces. Below, we list briefly several results from this theory. All of them are standard and we refer readers to [13, 19, 39, 67, 86] for further details.

Hilbert spaces. A linear vector space H over $\mathbb{C}$, equipped with a sesquilinear positive definite form $\langle \cdot, \cdot \rangle : H \times H \to \mathbb{C}$, is called an *Euclidean /inner product* space. The form $\langle \cdot, \cdot \rangle$ itself is called an *inner product* in H. The positive definite form $\langle \cdot, \cdot \rangle$ induces a norm on H via the formula

$$\|u\| = \sqrt{\langle u, u \rangle}.$$

It is readily verified that $\|\cdot\|$ is indeed a norm, so that H is a normed linear vector space under the induced norm $\|\cdot\|$. Euclidean spaces that are complete with respect to the induced norm are called *Hilbert spaces*. The standard examples of Hilbert spaces are ℓ^2 and $L^2(\Omega)$, equipped with the natural inner products

$$\langle u, v\rangle = \sum_{k\geq 0}^{n} u_k\overline{v_k} \quad \text{and} \quad \langle u, v\rangle = \int_\Omega u\bar{v}dx.$$

By the Riesz representation theorem, for every element $f \in H'$ there exist a unique member $u_f \in H$, so that $f = \langle u_f, \cdot\rangle$ in H'. Hence, the dual space H' identifies naturally with the space H itself and, subsequently, every Hilbert space is reflexive.

Orthogonal bases. Given a Hilbert space H, we say that $u, v \in H$ are mutually *orthogonal* if $\langle u, v\rangle = 0$ and *orthonormal* if, in addition, $\|u\| = \|v\| = 1$. A collection $\{u_\alpha\}_{\alpha\in A} \subset H$ of mutually orthogonal vectors is an *orthogonal basis* of H if its linear span is everywhere dense in H.

Using the Axiom of Choice it is readily verified that every Hilbert space has an orthonormal basis. Furthermore, if H is separable then the basis is at most countable. The latter fact is of fundamental importance for Numerical Analysis and Approximation Theory. Indeed, since every separable Hilbert space H has a countable orthonormal basis $\{u_n\}_{n\geq 0} \subset H$, every member $u \in H$ is given by its Fourier series

$$u = \sum_{n\geq 0} \hat{u}_n u_n, \quad \hat{u}_n = \langle u_n, u\rangle, \quad n \geq 0,$$

that converges strongly in H and, for any $u, v \in H$, the *Parseval identities*

hold

$$\langle u, v\rangle = \sum_{n\geq 0} \hat{u}_n \overline{\hat{v}_n}, \quad \|u\|^2 = \sum_{n\geq 0} |\hat{u}_n|^2.$$

Furthermore, if $u \in H$, $H_k = \text{span}\{u_n\}_{n=0}^k$ and $S_k(u) = \sum_{n=0}^k \hat{u}_n u_n$, $k \geq 0$, we have

$$\inf_{v\in H_k} \|u - v\| = \|u - S_k(u)\|.$$

That is, the partial Fourier sum $S_k(u)$ provides the best approximation to $u \in H$ in the finite dimensional space H_k, $k \geq 0$. The extremal property lays a foundation for the large class of practical computational algorithms known as spectral methods.

In the next section, we turn our attention to the specific Hilbert-Sobolev scale of 2ℓ-periodic functions. Members of this scale serve as natural phase spaces for the flow generated by the KGE.

2.3 Hilbert-Sobolev Scale of Periodic Functions

In this thesis, we utilize the following scale of Hilbert spaces:

$$H^s(-\ell, \ell) = \{u \mid \|u\|_s := \|\mathcal{A}^{s/2}u\|_0\}, \quad s \in \mathbb{R}, \tag{2.3.1}$$

where $\mathcal{A}$ is the $L^2(-\ell, \ell)$ realization of the operator

$$\mathcal{A} = I - \partial_{xx}, \tag{2.3.2}$$

equipped with the periodic boundary condition and $\|\cdot\|_0$ stands for the norm of $L^2(-\ell, \ell)$. Each of the spaces $H^s(-\ell, \ell)$ is a Hilbert space under the inner

product

$$\langle u, v\rangle_s = \langle \mathcal{A}^{s/2}u, \mathcal{A}^{s/2}v\rangle_0, \quad s \in \mathbb{R}. \tag{2.3.3}$$

Furthermore, we have

$$H^s(-\ell, \ell) \hookrightarrow H^t(-\ell, \ell), \quad s > t,$$

with the embedding being dense and compact. Additionally, we have

$$H^s(-\ell, \ell) \hookrightarrow C_b[-\ell, \ell], \quad s > \tfrac{1}{2},$$

where $C_b[-\ell, \ell]$ is the space of bounded and continuous functions in $[-\ell, \ell]$. The family $\{H^s(-\ell, \ell)\}_{s\in\mathbb{R}}$ is a complex interpolation scale, i.e.,

$$[H^{s_0}(-\ell, \ell), H^{s_1}(-\ell, \ell)]_\theta = H^{s_0(1-\theta)+s_1\theta}(-\ell, \ell), \tag{2.3.4}$$

for $s_0, s_1 \in \mathbb{R}$ and $\theta \in (0, 1)$.

Viewing $\langle\cdot, \cdot\rangle_0$ as the duality pairing in $H^s(-\ell, \ell)$, we have

$$(H^s(-\ell, \ell))' = H^{-s}(-\ell, \ell), \quad s \in \mathbb{R}. \tag{2.3.5}$$

Each of the spaces $H^s(-\ell, \ell)$ is separable with the class $C^\infty(-\ell, \ell)$ being dense in each of $H^s(-\ell, \ell)$. The collection of complex exponentials

$$\{\phi_n\}_{n\in\mathbb{Z}} = \left\{\frac{1}{2\sqrt{\ell}} e^{-\frac{i\pi n}{\ell}x}\right\}_{n\in\mathbb{Z}},$$

provides a complete orthonormal basis in each of $H^s(-\ell, \ell)$, for $s \in \mathbb{R}$. In terms of Fourier coefficients, we have

$$\langle u, v\rangle_{H^s} = \sum_{n\in\mathbb{Z}} \Big(1 + \tfrac{\pi^2 n^2}{\ell^2}\Big)^s \hat{u}_n \bar{\hat{v}}_n, \tag{2.3.6}$$

where $\hat{u}_n = \langle u, \phi_n \rangle_{L^2}$ and $\hat{v}_n = \langle v, \phi_n \rangle_{L^2}$ are the classical Fourier coefficients of u and v, respectively. In particular, the Hilbert matrices associated with closed operators ∂_x^n, for $n \in \mathbb{N}_0$, are diagonal.

In the following section, we discuss briefly operators and forms defined on the scale of $H^s(-\ell, \ell)$.

2.4 Hilbert-Gevrey Scale of Periodic Functions

In Chapter 4, we deal with the geometric convergence of semidiscrete approximations to the SGE/KGE. To control the covergence rate, we make use of the following class of functions:

$$G^s_{\rho,\theta}(-\ell,\ell) = \left\{ u \;\middle|\; \|u\|_{G^s_{\rho,\theta}} := \|\mathcal{A}^{s/2} e^{\rho \mathcal{A}^{\theta/2}} u\|_{L^2} \right\}, \tag{2.4.1}$$

where the operator $\mathcal{A}$ is defined in (2.3.2), and $s \in \mathbb{R}$, $\rho > 0$, and $\theta \in (0, 1]$ [82, 43, 42].

The space $G^s_{\rho,\theta}(-\ell, \ell)$ is a Hilbert space under the inner product:

$$\langle u, v \rangle_{G^s_{\rho,\theta}} = \sum_{n \in \mathbb{Z}} \left[1 + \left(\frac{\pi n}{\ell} \right)^2 \right]^s e^{2\rho \left(1 + \left(\frac{\pi n}{\ell}\right)^2\right)^{\theta/2}} \hat{u}_n \bar{\hat{v}}_n,$$

where $\hat{u}_n$ and $\hat{v}_n$ are the classical Fourier coefficients of functions u and v, respectively. It is noteworthy that the functions in $G^s_{\rho,1}(-\ell, \ell)$ are analytic in the strip:

$$\mathcal{S} = \{ |\Im z| < \rho \},$$

due to the rapid decay of their Fourier coefficients. The spaces $G^s_{\rho,\theta}(-\ell, \ell)$

are intermediate between $H^s(-\ell,\ell)$ and $G^s_{\rho,1}(-\ell,\ell)$, as it is easy to see that

$$G^s_{\rho,1}(-\ell,\ell) \hookrightarrow G^s_{\rho,\theta}(-\ell,\ell) \hookrightarrow H^s(-\ell,\ell), \quad s \in \mathbb{R}, \quad \rho > 0, \quad \theta \in (0,1].$$

Moreover, it is easy to verify that

$$[H^{s_0}(-\ell,\ell), G^{s_1}_{\rho,\theta}(-\ell,\ell)]_\delta = G^{s_0(1-\delta)+s_1,\delta}_{\delta\rho,\theta}(-\ell,\ell),$$

for all $s_0, s_1 \in \mathbb{R}$, $\rho > 0$, $\theta \in (0,1]$, and $\delta \in [0,1]$.

The class $G^s_{\rho,\theta}(-\ell,\ell)$ proves particularly useful in studying geometric or subgeometric convergence of spectral methods.

2.5 The continuous and discrete Fourier expansions

In this thesis, we make use of the periodic boundary conditions and the classical trigonometric Fourier basis. With this approach, all differential operators are diagonal in the frequency space and, as a result, associated spectral schemes allow very efficient practical implementation. In this section, we list briefly the key properties of the classical trigonometric Fourier basis.

2.5.1 The continuous Fourier expansion

Let $L^p(-\ell,\ell)$, $1 < p < \infty$, be the usual Lebesgue space of p-integrable 2ℓ-periodic functions, $\mathbb{P}_n = \text{span}\left\{e^{-i\frac{\pi k}{\ell}x},\ |k| \le n\right\}$ and $\mathcal{P}_n : L^2(-\ell,\ell) \to \mathbb{P}_n$ be the orthogonal projector from $L^2(-\ell,\ell)$ to $\mathbb{P}_n$, i.e.

$$\mathcal{P}_n[u] = \tfrac{1}{2\ell} \sum_{|k|\le n} \hat{u}_k e^{i\frac{\pi k x}{\ell}}, \quad \hat{u}_k = \left\langle u, e^{i\frac{\pi k x}{\ell}} \right\rangle_{L^2_p} = \int_{-\ell}^{\ell} u(x) e^{-i\frac{\pi k x}{\ell}} dx. \qquad (2.5.1)$$

Study of the operator $\mathcal{P}_n$ is one of the key components of the classical Fourier analysis and the constructive approximation theory (see e.g. [21, 92, 91, 74, 51]). At present properties of $\mathcal{P}_n$ are well understood. In particular, the collection of complex exponents $\left\{e^{-i\frac{\pi k}{\ell}x},\ k\in\mathbb{Z}\right\}$ is dense in $L^p(-\ell,\ell)$, $1\le p<\infty$ and $\lim_{n\to\infty}\mathcal{P}_n[u]=u$ in the sense of $L^p(-\ell,\ell)$, $1<p<\infty$, (see e.g. [21, 74, 51]). Since the convergence in norm implies convergence in measure, it is fairly easy to show that a subsequence of $\{\mathcal{P}_n[u]\}_{n\ge0}$ converges a.e. to $u\in L^p(-\ell,\ell)$, $1<p<\infty$. In fact, according to the famous Carleson-Hunt theorem (see [50]), the sequence $\{\mathcal{P}_n[u]\}_{n\ge0}$ itself converges a.e. in $(-\ell,\ell)$.

In the case of regular periodic integrable functions, the convergence rate is algebraic (see [21, 74]), i.e.

$$\|(\mathcal{I}-\mathcal{P}_n)[u]\|_{W^{s,p}}\le c_p\big(\tfrac{\pi n}{\ell}\big)^{s-r}\|u\|_{W^{r,p}},\quad 0\le s\le r,\quad 1<p<\infty,\quad (2.5.2)$$

where $W^{s,p}$ is the standard Sobolev space of order s and integrability exponent p, $c_p>0$ depends on p only and, in particular, $c_2=1$. In connection with the inequality (2.5.2), we remark that $\mathcal{P}_n$ and differentiation commute, hence $\mathcal{P}_n[u]$ delivers the best approximation in the Hilbert-Sobolev settings of $H^s(-\ell,\ell)$.

The convergence rate is geometric/subgeometric, provided u has stronger regularity. In particular, for functions from the Gevrey classes (see Section 2.4) we have

$$\|(\mathcal{I}-\mathcal{P}_n)[u]\|_{H^s}\le\big(\tfrac{\pi n}{\ell}\big)^{s-r}\exp\left\{-\rho\big(\tfrac{\pi n}{\ell}\big)^{\theta}\right\}\|u\|_{G^r_{\rho,\theta}},\quad s\le r.\qquad (2.5.3)$$

2.5.2 The discrete Fourier expansion

The continuous Fourier approximation $\mathcal{P}_n[u]$ requires exact evaluation of inner product integrals, which, apart from trivial cases, is impossible. In practice, one has to resort to numerical quadratures. In the sequel, we employ the composite mid-point rule:

$$\int_{-\ell}^{\ell} f(x)dx \approx I_n[f] := \tfrac{2\ell}{2n+1} \sum_{j=0}^{2n} f(x_j), \quad x_j = \tfrac{2\ell(j-n)}{2n+1}, \quad 0 \le j \le 2n. \quad (2.5.4)$$

Using formula (2.5.4), the continuous Fourier coefficients are approximated by their discrete counterparts

$$\breve{u}_k = I_n[u\overline{\phi_k}] =: \langle u, \phi_k \rangle_n, \quad |k| \le n, \tag{2.5.5a}$$

and give rise to the discrete Fourier expansion

$$\mathcal{I}_n[u](x) = \tfrac{1}{2\ell} \sum_{|k|\le n} \breve{u}_k e^{\frac{i\pi k}{\ell}x}. \tag{2.5.5b}$$

Formulas (2.5.5) provide a one-to-one linear correspondence between values $u(x_j)$, $0 \le j \le 2n$ of u at the quadrature nodes and the discrete Fourier coefficients $\breve{u}_k$, $-n \le k \le n$. The direct and inverse transformation matrices are Fourier [17, 22, 56, 88] and, as a consequence, either of the transforms require $\mathcal{O}(n \log_2 n)$ floating point operations using the classical divide-and-conquer strategy.

Unlike $\mathcal{P}_n$, the discrete operator $\mathcal{I}_n$ is undefined for general $L^p(-\ell, \ell)$ functions. Nevertheless, in the case of regular data the approximation properties of $\mathcal{I}_n$ are identical to those of $\mathcal{P}_n$. In particular, we have[1] [74]

$$\|(\mathcal{I} - \mathcal{I}_n)[u]\|_{W^{s,p}} \le c\big(\tfrac{\pi n}{\ell}\big)^{s-r} \|u\|_{W^{r,p}}, \quad 0 \le s \le r, \quad 1 \le r, \quad 1 < p < \infty. \tag{2.5.6}$$

[1]The proof of inequality (2.5.7), as given in [74], deals with the integer values of $r \ge 1$ and $0 \le s \le r$, the general case follows from the standard interpolation argument.

As shown in [83],

$$\|(\mathcal{I}-\mathcal{I}_n)[u]\|_{H^s} \le c_s \|(\mathcal{I}-\mathcal{P}_n)[u]\|_{H^s}, \quad s > \tfrac{1}{2}, \tag{2.5.7}$$

with $c_s > 0$ depending on $s > \frac{1}{2}$ only. Hence,

$$\|(\mathcal{I}-\mathcal{I}_n)[u]\|_{H^s} \le c_s \big(\tfrac{\pi n}{\ell}\big)^{s-r} \exp\Big\{-\rho\big(\tfrac{\pi n}{\ell}\big)^{\theta}\Big\} \|u\|_{G^r_{\rho,\theta}}, \quad \tfrac{1}{2} < s \le r. \tag{2.5.8}$$

2.6 Two inequalities

In the analysis of our scheme in Chapter 3, we make an explicit use of the following two inequalities (see e.g. [82])

$$\|u^n\|_{G^r_{\rho,\theta}} \le c_{r,n} \|u\|^n_{G^r_{\rho,\theta}}, \quad r > \tfrac{1}{2}, \tag{2.6.1a}$$

$$\|u\|_{G^r_{\rho,\theta}} \le e^{\frac{1}{2}} \|u\|_{H^r} + (2\rho)^{\frac{q}{\theta}} \|u\|_{G^{r+q}_{\rho,\theta}}, \quad q \ge 0, \quad 0 < \theta \le 1. \tag{2.6.1b}$$

To obtain inequality (2.6.1a), we combine the Minkowski and Hölder inequalities, to obtain

$$\begin{aligned}
\|u^n\|^2_{G^r_{\rho,\theta}} &= \tfrac{1}{2\ell} \sum_{k\in\mathbb{Z}} \Big[1 + \big|\tfrac{\pi k}{\ell}\big|^2\Big]^r \exp\Big(2\rho\big[1 + \big|\tfrac{\pi k}{\ell}\big|^2\big]^{\frac{\theta}{2}}\Big) \left[\sum_{\substack{(k_1,\dots,k_n)\in\mathbb{Z}^n \\ k_1+\cdots+k_n=k}} \prod_{j=1}^n |\hat{u}_{k_j}|\right]^2 \\
&\le \tfrac{n^r}{2\ell} \sum_{k\in\mathbb{Z}} \left[\sum_{\substack{(k_1,\dots,k_n)\in\mathbb{Z}^n \\ k_1+\cdots+k_n=k}} \prod_{j=1}^n \exp\Big(\rho\big[1 + \big|\tfrac{\pi k_j}{\ell}\big|^2\big]^{\frac{\theta}{2}}\Big) |\hat{u}_{k_j}| \sum_{j=1}^n \Big[1 + \big|\tfrac{\pi k_j}{\ell}\big|^2\Big]^{\frac{r}{2}}\right]^2 \\
&\le n^{r+2} \left[\tfrac{1}{2\ell} \sum_{k\in\mathbb{Z}} \exp\Big(\rho\big[1 + \big|\tfrac{\pi k}{\ell}\big|^2\big]^{\frac{\theta}{2}}\Big) |\hat{u}_k|\right]^{2(n-1)} \|u\|^2_{G^r_{\rho,\theta}} \le c_{r,n} \|u\|^{2n}_{G^r_{\rho,\theta}},
\end{aligned}$$

with

$$0 < c_{r,n} \le n^{r+2} (2\ell)^{n-1} \left[\sum_{k\in\mathbb{Z}} \Big[1 + \big|\tfrac{\pi k}{\ell}\big|^2\Big]^{-r}\right]^{n-1} < \infty, \quad r > \tfrac{1}{2}.$$

For the inequality (2.6.1b), we combine the interpolation

$$\|u\|_{H^{r\theta+s(1-\theta)}} \leq \|u\|_{H^r}^{\theta}\|u\|_{H^s}^{1-\theta}, \quad r,s \in \mathbb{R}, \quad \theta \in (0,1)$$

and Young's inequalities. This gives

$$\begin{aligned}
\|u\|_{G^r_{\rho,\theta}}^2 &= \sum_{n\geq 0} \tfrac{(2\rho)^n}{n!}\|u\|^2_{H^{r+\frac{n\theta}{2}}} \leq \sum_{n\geq 0} \tfrac{(2\rho)^n}{n!}\|u\|_{H^r}^{\frac{4q}{2q+n\theta}}\|u\|^{\frac{2n\theta}{2q+n\theta}}_{H^{r+q+\frac{n\theta}{2}}} \\
&\leq \sum_{n\geq 0} \tfrac{1}{n!}\left[\tfrac{2q}{2q+n\theta}\|u\|^2_{H^r} + (2\rho)^{n+\frac{2q}{\theta}}\tfrac{n\theta}{2q+n\theta}\|u\|^2_{H^{r+q+\frac{n\theta}{2}}}\right] \\
&\leq e\|u\|^2_{H^r} + (2\rho)^{\frac{2q}{\theta}}\|u\|^2_{G^{r+q}_{\rho,\theta}}
\end{aligned}$$

and the inequality (2.6.1b) follows.

Chapter 3

Convergence of pseudospectral schemes in $\mathbb{T}$ and $\mathbb{R}$ for $H^s \times H^{s-1}$ data

In this Chapter, we present a Fourier-type pseudo-spectral scheme and discuss its convergence in periodic settings. The finite propagation speed of the group, associated with the linear wave operator, allows us to extend these results to the case on the real line (see Section 4.4).

We fix some $\ell > 0$ and consider the weak formulation of the problem (1.1.1) in the periodic settings, i.e., the problem of finding a pair of 2ℓ-periodic functions $(u, v) \in C([0,T], H^1(-\ell,\ell)\times L^2(-\ell,\ell))$, with $(u_t, v_t) \in C([0,T], L^2(-\ell,\ell)\times H^{-1}(-\ell,\ell))$, so that the identities

$$\langle (u,v)_t, (\phi_1,\phi_2)\rangle = \langle v, \phi_1\rangle - a^2\langle \partial_x u, \partial_x\phi_2\rangle - \langle \mathcal{V}'(u), \phi_2\rangle, \tag{3.0.1a}$$

$$(u(0), v(0)) = (u_0, v_0) \in H^1(-\ell,\ell)\times H^\gamma(-\ell,\ell), \quad \gamma \geq 0, \tag{3.0.1b}$$

hold for all $(\phi_1, \phi_2) \in L^2(-\ell,\ell)\times H^1(\ell,\ell)$.

In the finite dimensional space $\mathbb{P}_n$, we approximate equations (3.0.1) by the means of the formula

$$\langle (u_n, v_n)_t, (\phi_1, \phi_2) \rangle = \langle v_n, \phi_1 \rangle - a^2 \langle \partial_x u_n, \partial_x \phi_2 \rangle - \langle \mathcal{I}_n[\mathcal{V}'(u_n)], \phi_2 \rangle, \quad (3.0.2a)$$

$$(u_n(0), v_n(0)) = (\mathcal{I}_n[u_0], \mathcal{I}_n[v_0]), \quad (3.0.2b)$$

where (ϕ_1, ϕ_2) is an arbitrary element of $\mathbb{P}_n^2$. We show that $\{(u_n, v_n)\}_{n \geq 1}$ converges strongly to a unique weak solution (u, v) of equations (3.0.1), provided the initial data and the potential $\mathcal{V}$ are sufficiently regular.

3.1 A priori estimates

To begin, we observe that the finite dimensional ODE (3.0.2) is Hamiltonian, i.e., ODE (3.0.2) is equivalent to

$$\tfrac{d}{dt} U_n = \mathcal{J} \nabla \mathcal{H}_n(U_n), \quad t > 0, \quad (3.1.1a)$$

$$U_n(0) = \mathcal{I}_n[U_0], \quad (3.1.1b)$$

where

$$U_n = \begin{pmatrix} u_n \\ v_n \end{pmatrix} = \begin{pmatrix} u_n \\ u_{n,t} \end{pmatrix}, \quad \mathcal{J} = \begin{pmatrix} 0 & 1 \\ -1 & 0 \end{pmatrix}$$

and

$$\mathcal{H}_n(U_n) = \tfrac{1}{2} \|v_n\|_{L^2}^2 + \tfrac{a^2}{2} \|\partial_x u_n\|_{L^2}^2 + I_n[\mathcal{V}(u_n)]. \quad (3.1.1c)$$

The Hamiltonian formulation (3.1.1) indicates that the total energy $\mathcal{H}_n(U_n)$ is preserved along the numerical trajectories $U_n(t)$. Using this fact, we obtain

Lemma 3.1.1. *Assume $U_0 = (u_0, v_0) \in H^1(-\ell, \ell) \times H^\gamma(-\ell, \ell)$, $\gamma > \frac{1}{2}$, $\mathcal{V} \in C^2(\mathbb{R})$, $\mathcal{V} \geq 0$ and $\mathcal{V}(0) = \mathcal{V}'(0) = 0$. Then, for any $T < \infty$, the*

numerical solution (u_n, v_n) *of* (3.0.2) *satisfies*

$$(u_n, v_n) \in C([0,T], H^1(-\ell,\ell) \times L^2(-\ell,\ell)),$$
$$(u_{n,t}, v_{n,t}) \in C((0,T), L^2(-\ell,\ell) \times H^{-1}(-\ell,\ell)).$$

The respective norms are uniformly bounded in n *and* ℓ.

Proof. (a) Equations (3.0.2) define a system of ordinary differential equations (ODEs). If $\mathcal{V}(u) \in C^2(\mathbb{R})$, the vector field of the system is of class C^1 and the standard theory of ODE's implies existence of a unique solution

$$(u_n, v_n) \in C^1((0,T), \mathbb{P}_n^2) \cap C([0,T], \mathbb{P}_n^2),$$

for some $T > 0$. Along the numerical trajectories U_n, the Hamiltonian is preserved. Hence,

$$\|v_n\|_{L^2}^2 + a^2\|\partial_x u_n\|_{L^2}^2 + 2I_n[\mathcal{V}(u_n)] = 2\mathcal{H}_n(U_n(0))$$

and it follows that $\|v_n\|_{L^2}^2$, $\|\partial_x u_n\|_{L^2}^2$ and $I_n[\mathcal{V}(u_n)]$ are uniformly bounded for any $t > 0$. In particular,

$$\max\{|a|\|\partial_x u_n\|_{C([0,t],L^2)}, \|v_n\|_{C([0,t],L^2)}\} \le \sqrt{2}\mathcal{H}_n^{\frac{1}{2}}(U_n(0)), \quad t > 0. \tag{3.1.2}$$

Since

$$u_n(x-at,t) = u_n(x,0) + \int_0^t \big(v_n(x-a\tau,\tau) - a\partial_x u_n(x-a\tau,\tau)\big)d\tau,$$

we conclude that

$$\|u_n\|_{L^2} \le \|u_n(0)\|_{L^2} + 2^{\frac{3}{2}} t\mathcal{H}_n^{\frac{1}{2}}(U_n(0)), \quad t > 0, \tag{3.1.3a}$$
$$\|u_n\|_{C([0,t],H^1)} \le \|u_n(0)\|_{L^2} + \Big[\tfrac{1}{|a|} + 2^{\frac{3}{2}} t\Big]\mathcal{H}_n^{\frac{1}{2}}(U_n(0)). \tag{3.1.3b}$$

Estimates (3.1.2) and (3.1.3) indicate that the solution U_n does not blow up in a finite time and hence is globally defined.

(b) Since $u_{n,t} = v_n$, we have $\|u_{n,t}\|_{C((0,T),L^2)} \leq \sqrt{2}\mathcal{H}_n^{\frac{1}{2}}(U_n(0))$. It remains to bound $\|v_{n,t}\|_{C((0,T),H^{-1})}$. By virtue of the standard Sobolev embedding [3] and the estimate (3.1.3b), we have

$$\|u_n\|_{C([0,T],L^\infty)} \leq c\|u\|_{C([0,T],H^1)} \leq c\|u_n(0)\|_{L^2} + c\Big[\tfrac{1}{|a|} + 2^{\frac{3}{2}}T\Big]\mathcal{H}_n^{\frac{1}{2}}(U_n(0)), \tag{3.1.4}$$

where the embedding constant $c > 0$ is independent of ℓ. Further,

$$\begin{aligned} |\mathcal{V}'(u_n)| = \Big|\int_0^{u_n} \mathcal{V}''(s)ds\Big| &\leq \max\big\{|\mathcal{V}''(s)| \;\big|\; |s| \leq \|u_n\|_{C([0,T],L^\infty)}\big\}|u_n| \\ &\leq C(U_n(0),T)|u_n|, \end{aligned} \tag{3.1.5}$$

where in view of the estimate (3.1.4), the positive constant $C(U_n(0),T)$ depends on the initial data $U_n(0)$, terminal time T and the non-linearity $\mathcal{V}(u)$ only. Using equations (3.1.5) and (3.0.2a) with $\phi_1 = 0$, we infer that

$$\|v_{n,t}\|_{H^{-1}} \leq a^2\|\partial_t u_n\|_{L^2} + \sup\big\{|\langle \mathcal{I}_n[\mathcal{V}'(u_n)], \phi\rangle| \;\big|\; \|\phi_2\|_{H^1} = 1, \phi_2 \in \mathbb{P}_n\big\}.$$

Since the quadrature (2.5.4) is exact in $\mathbb{P}_{2n}$, for $\phi \in \mathbb{P}_n$ we have

$$\begin{aligned} |\langle \mathcal{I}_n[\mathcal{V}'(u_n)], \phi\rangle_{L^2}| &= |\langle \mathcal{I}_n[\mathcal{V}'(u_n)], \phi\rangle_n| \\ &\leq \|\mathcal{I}_n[\mathcal{V}'(u_n)]\|_{L^2}\|\phi\|_{L^2} \leq C(U_n(0),T)\|u_n\|_{L^2}\|\phi\|_{L^2}. \end{aligned}$$

The last two estimates yield the bound

$$\|v_{n,t}\|_{C((0,T),H^{-1})} \leq M(U_n(0),T), \tag{3.1.6}$$

with constant $M(U_n(0),T)$ that depends on the initial data $U_n(0)$, terminal time T and the non-linearity $\mathcal{V}(\cdot)$ only.

(c) To conclude the proof, we note that the estimates (3.1.2), (3.1.3) and (3.1.6) are uniform in n, provided the quantities $\mathcal{H}(U_n(0))$ and $\|u_n(0)\|_{L^2}$ are bounded independently of n.

In view of (2.5.7) and the commutativity of $\mathcal{P}_n$ and ∂_x, we have

$$\begin{aligned}
\|u_n(0)\|_{H^1} &\le \|u_0\|_{H^1} + \|(\mathcal{I}-\mathcal{I}_n)[u_0]\|_{H^1} \\
&\le \|u_0\|_{H^1} + c\|(\mathcal{I}-\mathcal{P}_n)[u_0]\|_{H^1} \le (1+c)\|u_0\|_{H^1}, \qquad (3.1.7a)\\
\|v_n(0)\|_{L^2} &\le \|v_0\|_{H^\gamma} + \|(\mathcal{I}-\mathcal{I}_n)[v_0]\|_{H^\gamma} \\
&\le \|v_0\|_{H^\gamma} + \|(\mathcal{I}-\mathcal{P}_n)[v_0]\|_{H^\gamma} \le (1+c)\|v_0\|_{H^\gamma}, \qquad (3.1.7b)
\end{aligned}$$

provided $\gamma > \frac{1}{2}$. In view of the estimate (3.1.7), we have also $\|u_n(0)\|_{L^\infty} \le c\|u_n(0)\|_{H^1}$. Using the last three bounds, we infer as in equation (3.1.5)

$$\begin{aligned}
I_n[\mathcal{V}(u_n(0))] &= \tfrac{2\ell}{2n+1}\sum_{j=0}^{n}\int_0^{u_n(x_j,0)}\int_0^s \mathcal{V}''(\tau)d\tau ds \\
&\le \tfrac{2\ell}{2n+1}\sum_{j=0}^{n}\left|\int_0^{u_n(x_j,0)} |\mathcal{V}''(\tau)|\cdot\big|u_n(x_j,0)-\tau\big|d\tau\right| \\
&\le \max\big\{|\mathcal{V}''(\tau)| \;\big|\; |\tau| \le \|u_n(0)\|_{L^\infty}\big\}\cdot\|u_n(0)\|_{L^\infty}^2 \\
&= B(\|u_0\|_{H^1})\cdot\|u_0\|_{H^1}^2,
\end{aligned}$$

where $B(\|u_0\|_{H^1})$ depends on the initial data u_0 and the nonlinearity $\mathcal{V}(\cdot)$ only. The calculations above show that

$$\mathcal{H}_n(U_n(0)) \le \frac{c}{2}\Big[\|v_0\|_{H^\gamma} + a^2\|u_0\|_{H^1}^2 + 2B(\|u_0\|_{H^1})\cdot\|u_0\|_{H^1}^2\Big], \qquad (3.1.8)$$

with a generic constant $c > 0$ independent of n and ℓ. The assertion of the Lemma follows directly from the estimates (3.1.2), (3.1.3b), (3.1.6), (3.1.7) and (3.1.8). □

In the case of regular initial data and smooth potentials $\mathcal{V}$, we have the following extension of Lemma 3.1.1.

Lemma 3.1.2. *If* $(u_0, v_0) \in H^{s+1}(-\ell,\ell)\times H^{s+\gamma}(-\ell,\ell)$ *and* $\mathcal{V} \in C^{s+2}(\mathbb{R})$,

with $s \geq 0$ *and* $\gamma > \frac{1}{2}$*, then*

$$(u_n, v_n) \in C([0,T], H^{s+1}(-\ell,\ell) \times H^s(-\ell,\ell)),$$
$$(u_{n,t}, v_{n,t}) \in C((0,T), H^s(-\ell,\ell) \times H^{s-1}(-\ell,\ell)),$$

uniformly in n *and* ℓ*.*

Proof. (a) Since $(u_n, v_n) \in \mathbb{P}_n^2$, it follows that:

$$(u_n, v_n) \in C([0,T], H^{s+1}(-\ell,\ell) \times H^s(-\ell,\ell)), \tag{3.1.9a}$$
$$(u_{n,t}, v_{n,t}) \in C((0,T), H^s(-\ell,\ell) \times H^{s-1}(-\ell,\ell)), \tag{3.1.9b}$$

for all $s > 0$ as in the finite dimensional space $\mathbb{P}_n^2$, all norms are equivalent. We show that the respective norms are uniformly bounded in n and ℓ.

(b) In equation (3.0.2a), we let $\phi_1 = \partial_x^{2(s+1)} u_n$ and $\phi_2 = \partial_x^{2s} v_n$, where $s \geq 0$ is an integer. Integrating by parts, using the periodicity of ϕ_1, ϕ_2, u_n and v_n, the Cauchy-Schwartz inequality and (2.5.7), we infer

$$\begin{aligned} \tfrac{d}{dt}\Big[a^2 \|\partial_x^{1+s} u_n\|_{L^2}^2 + \|\partial_x^s v_n\|_{L^2}^2\Big] &= 2\langle \partial_x^s \mathcal{I}_n[\mathcal{V}'(u_n)], \partial_x^s v_n\rangle \\ &\leq c\|\mathcal{V}'(u_n)\|_{H^s}^2 + \|\partial_x^s v_n\|_{L^2}^2, \end{aligned} \tag{3.1.10}$$

with $c > 0$ independent of n, ℓ, $\mathcal{V}$ and u_n. We estimate $\|\mathcal{V}'(u_n)\|_{H^s}$ using the Faa di Bruno formula [85]

$$\partial_x^s \mathcal{V}'(u_n) = \sum_{k=1}^{s} \mathcal{V}^{(k+1)}(u_n) \sum_{|\pi|=k} \prod_{\pi_i \in \pi} \partial_x^{|\pi_i|} u_n,$$

where the second sum runs over all partitions $\pi = \{\pi_1, \ldots, \pi_k\}$ of the set $\{1, \ldots, s\}$ that contain exactly k nonempty and disjoint subsets $\pi_i \subset \{1, \ldots, s\}$.

To begin, we observe that the same arguments as in Lemma 3.1.1 yield the

bound

$$|\mathcal{V}^{(1+k)}(u_n)| \leq |\mathcal{V}^{(1+k)}(0)| + \left| \int_0^{u_n} |\mathcal{V}^{(2+k)}(s)| ds \right|$$
$$\leq |\mathcal{V}^{(1+k)}(0)| + \max\big\{ |\mathcal{V}^{(2+k)}(s)| \;\big|\; |s| \leq \|u_n\|_{C([0,T],L^\infty)} \big\} \cdot \|u_n\|_{L^\infty}$$
$$\leq C_k(U_0, T), \quad k = 1, \ldots, s. \tag{3.1.11}$$

By virtue of Lemma 3.1.1, each quantity $C_k(U_0, T)$ is controlled by the regularity of $\mathcal{V}(\cdot)$, the terminal time T and $\|u_0\|_{H^1}$ and $\|v_0\|_{H^\gamma}$ only. Hence, using the Faa di Bruno formula, Young's inequality and the fact that $H^s(-\ell, \ell)$, $s > \frac{1}{2}$, are Banach algebras [3], we infer that

$$\|\mathcal{V}'(u_n)\|_{H^s} \leq \sum_{k=1}^{s} C_k(u_0, v_0, T) \sum_{|\pi|=k} \prod_{\pi_i \in \pi} \|u_n\|_{H^{|\pi_i|}} \leq F_s(\|u_n\|_{H^s}), \tag{3.1.12}$$

where $F_s(\cdot)$ is a polynomial of degree s, whose coefficients are controlled by the regularity of $\mathcal{V}(\cdot)$, the terminal time T and the quantities $\|u_0\|_{H^1}$ and $\|v_0\|_{H^\gamma}$ only.

(c) Combining the estimates (3.1.10) and (3.1.12), we infer that

$$\tfrac{d}{dt} \Big[a^2 \|\partial_x^{1+s} u_n\|_{L^2}^2 + \|\partial_x^s v_n\|_{L^2}^2 \Big] \leq c F_s^2(\|u_n\|_{H^s}) + \|\partial_x^s v_n\|_{L^2}^2, \tag{3.1.13}$$

for any integer $s \geq 0$.

The case $s = 0$ is settled in Lemma 3.1.1. Assuming $s = 1$, from Lemma 3.1.1, we have that $F_1(\|u_n\|_{C([0,T],H^1)})$ is uniformly bounded in n and ℓ. Hence, Gronwall's inequality applies and

$$a^2 \|\partial_x^2 u_n\|_{L^2}^2 + \|\partial_x v_n\|_{L^2}^2$$
$$\leq c \exp\{T\} \Big[a^2 \|\partial_x^2 u_n(0)\|_{L^2}^2 + \|\partial_x v_n(0)\|_{L^2} + T F_1(\|u_n\|_{C([0,T],H^1)}) \Big].$$

In view of equation (2.5.7) and as in part (c) of Lemma 3.1.1, we have

$$a^2 \|\partial_x^2 u_n(0)\|_{L^2} + \|\partial_x v_n(0)\|_{L^2} \leq c \big[a^2 \|u_0\|_{H^2}^2 + \|v_0\|_{H^1} \big].$$

Consequently,

$$(u_n, v_n) \in C([0,T], H^2(-\ell,\ell) \times H^1(-\ell,\ell)),$$

with the respective norms bounded independently of n and ℓ.

The uniform bound on $\|v_{n,t}\|_{C([0,T],L^2)}$ follows directly from equation (3.0.2), if we let $\phi_1 = 0$ and $\phi_2 = v_{n,t}$ and use the already proven fact that the norm $\|u_n\|_{C([0,T],H^2)}$ is uniformly bounded in terms of n and ℓ. This settles our claim for $s = 1$.

(d) With the aid of inequality (3.1.13), the process described in part (c) of the proof can be continued inductively for $s = 2, 3, \ldots$. We conclude that Lemma 3.1.2 holds for any integer $s \geq 0$, provided $(u_0, v_0) \in H^{s+1}(-\ell,\ell) \times H^{s+\gamma}(-\ell,\ell)$, $\gamma > \frac{1}{2}$ and $\mathcal{V} \in C^{s+2}(\mathbb{R})$. □

3.2 Convergence

We employ a priori estimates of Lemmas 3.1.1, 3.1.2 to show that the sequence $\{U_n\}_{n\geq 0}$ of pseudo-spectral numerical solutions converges strongly to a unique weak solution (u, v) of equation (3.0.1).

Theorem 3.2.1. *In the settings of Lemma 3.1.2, the sequence* $\{U_n\}_{n\geq 1}$*, defined by equation* (3.0.2)*, converges strongly to a unique weak solution*[1]

$$(u, v) \in C([0,T], H^{s+1}(-\ell,\ell) \times H^s(-\ell,\ell)),$$
$$(u_t, v_t) \in C([0,T], H^s(-\ell,\ell) \times H^{s-1}(-\ell,\ell)),$$

of (3.0.1)*. Moreover,*

$$\|u - u_n\|_{C([0,T],H^{r+1})} + \|u_t - u_{n,t}\|_{C([0,T],H^r)} \leq c_r \big(\tfrac{\ell}{\pi n}\big)^{s-r}, \quad 0 \leq r \leq s-1, \tag{3.2.1}$$

[1]For $s \geq 1$ the solution is in fact classical.

where the generic constants $c_r > 0$, $0 \le r \le s-1$, do not depend on n and ℓ.

Proof. (a) To begin, we show that the sequence $\{U_n\}_{n\ge 0}$ is Cauchy. For $n, m > 0$, we let $E = (e_n, e_{n,t})^T = U_{n+m} - U_n \in \mathbb{P}_{n+m}$. Directly from equation (3.0.2) it follows that

$$\begin{aligned}\langle (e_n, e_{n,t})_t, (\phi_1, \phi_2)\rangle &= \langle e_{n,t}, \phi_1\rangle - a^2\langle \nabla e_n, \nabla \phi_2\rangle \\ &\quad - \langle \mathcal{I}_{n+m}[\mathcal{V}'(u_{n+m})] - \mathcal{I}_n[\mathcal{V}'(u_n)], \phi_2\rangle, \qquad (3.2.2a)\\ (e_n(0), e_{n,t}(0)) &= ((\mathcal{I}_{n+m} - \mathcal{I}_n)[u_0], (\mathcal{I}_{n+m} - \mathcal{I}_n)[v_0]), \qquad (3.2.2b)\end{aligned}$$

for all $(\phi_1, \phi_2) \in \mathbb{P}_{n+m}$. Letting $(\phi_1, \phi_2) = (\partial_x^{2(k+1)} e_n, \partial_x^{2k} e_{n,t})$ in (3.2.2a), we infer, after integration by parts and some simplifications,

$$\begin{aligned}\tfrac{1}{2}\tfrac{d}{dt}\big[a^2\|\partial_x^{k+1} e_n\|_{L^2}^2 + \|\partial_x^k e_{n,t}\|_{L^2}^2\big] &= -\langle \partial_x^k(\mathcal{I} - \mathcal{I}_{n+m})[\mathcal{V}'(u_{n+m})], \partial_x^k e_{n,t}\rangle \\ &\quad + \langle \partial_x^k \mathcal{V}'(u_{n+m}) - \mathcal{V}'(u_n), \partial_x^k e_{n,t}\rangle + \langle \partial_x^k(\mathcal{I} - \mathcal{I}_n)[\mathcal{V}'(u_n)], \partial_x^k e_{n,t}\rangle. \qquad (3.2.3)\end{aligned}$$

On account of equations (2.5.7), (2.5.2) and (3.1.12)

$$\begin{aligned}\|(\mathcal{I} - \mathcal{I}_n)\mathcal{V}'(u_n)\|_{H^k} &\le c\|(\mathcal{I} - \mathcal{P}_n)\mathcal{V}'(u_n)\|_{H^k}, \quad 1 \le k \le s+1, \qquad (3.2.4a)\\ \|(\mathcal{I} - \mathcal{I}_n)\mathcal{V}'(u_n)\|_{H^k} &\le c\big(\tfrac{\ell}{\pi n}\big)^{s+1-k} F_{s+1}(\|u_n\|_{H^{s+1}}), \quad 0 \le k \le s, \qquad (3.2.4b)\end{aligned}$$

while the Leibniz rule, combined with the Faa di Bruno formula, yields initially

$$\begin{aligned}\partial_x^k[\mathcal{V}'(u_{n+m}) - \mathcal{V}'(u_n)] &= \partial_x^k\left[e_n \int_0^1 \mathcal{V}''(u_n + \tau e_n) d\tau\right] \\ &= \sum_{r=0}^{k} \tbinom{k}{r} \partial_x^r e_n \cdot \partial_x^{k-r}\left[\int_0^1 \mathcal{V}''(u_n + \tau e_n) d\tau\right]\end{aligned}$$

and then

$$\|\mathcal{V}'(u_{n+m}) - \mathcal{V}'(u_n)\|_{H^k} \le G_k(\|u_{n+m}\|_{H^k}, \|u_n\|_{H^k}) \cdot \|e_n\|_{H^k}, \qquad (3.2.5)$$

where $0 \leq k \leq s+1$, $G_{s+1}(\cdot,\cdot)$ is a bi-variate polynomial of degree at most $s+1$, whose coefficients are controlled by the regularity of $\mathcal{V}(\cdot)$, the terminal time T and the quantities $\|u_0\|_{H^1}$ and $\|v_0\|_{H^\gamma}$ only.

Combining equations (3.2.3), (3.2.4), (3.2.5) and making use of the Cauchy-Schwartz inequality, we infer

$$\begin{aligned}\tfrac{d}{dt}\big[a^2\|\partial_x^{k+1}e_n\|_{L^2}^2+\|\partial_x^k e_{n,t}\|_{L^2}^2\big] &\leq 3\|\partial_x^k e_{n,t}\|_{L^2}^2\\ &\quad+G_k^2(\|u_{n+m}\|_{H^k},\|u_n\|_{H^k})\cdot\|e_n\|_{H^k}^2\\ &\quad+2c\big(\tfrac{\ell}{\pi n}\big)^{2(s+1-k)}F_{s+1}^2(\|u_n\|_{H^{s+1}}),\end{aligned}\tag{3.2.6}$$

$0 \leq k \leq s$. On the other hand, letting $(\phi_1,\phi_2)=(\partial_x^{2k}e_n,0)$ in equation (3.2.2), integrating by parts and using the Cauchy-Schwartz inequality one more time, we have

$$\tfrac{d}{dt}\|\partial_x^k e_n\|_{L^2}^2 \leq \|\partial_x^k e_n\|_{L^2}^2+\|\partial_x^k e_{n,t}\|_{L^2}^2,\tag{3.2.7}$$

$0 \leq k \leq s$. Summing up all the inequalities (3.2.6) and (3.2.7) for $0 \leq k \leq r \leq s$, and making use of the classical Gronwall's lemma, we infer

$$\begin{aligned}&\|e_n\|_{C([0,T],H^{r+1})}+\|e_{n,t}\|_{C([0,T],H^r)}\\ &\qquad\leq C_r(U(0),T)\big[\|e_n(0)\|_{H^{r+1}}+\|e_{n,t}(0)\|_{H^r}+\big(\tfrac{\ell}{\pi n}\big)^{s+1-r}\big],\end{aligned}$$

where $0 \leq r \leq s$ and constants $C_r(U(0),T)$ are uniform in n and ℓ. In view of Lemma 3.1.2 and estimates (2.5.7), (2.5.2), we conclude

$$\|e_n\|_{C([0,T],H^{r+1})}+\|e_{n,t}\|_{C([0,T],H^r)} \leq c_r\big(\tfrac{\ell}{\pi n}\big)^{s-r},\quad 0\leq r\leq s-1,\tag{3.2.8a}$$

$$\|e_n\|_{C([0,T],H^{s+1})}+\|e_{n,t}\|_{C([0,T],H^s)} \leq c_s\left[\big(\tfrac{\ell}{\pi n}\big)^{\gamma}+\|(\mathcal{I}-\mathcal{P}_n)[u_n]\|_{H^{s+1}}\right],\tag{3.2.8b}$$

where the positive generic constants $c_r>0$, $0\leq r\leq s$, are independent of parameters n and ℓ.

(b) Bounds (3.2.8) indicates that the sequences $\{u_n\}_{n\geq 0}$, and $\{v_n\}_{n\geq 0}$ are Cauchy in the strong topology of $C([0,T],H^{s+1}(-\ell,\ell))$ and $C([0,T],H^{s}(-\ell,\ell))$, respectively. Furthermore directly from (3.2.2) it follows that $\{v_{n,t}\}_{n\geq 0}$ is Cauchy in $C((0,T),H^{s-1}(-\ell,\ell))$ (see parts (b) and (c) of Lemmas 3.1.1 and 3.1.2, respectively). We conclude that

$$(u_n,v_n)\to(u,v)\quad \text{strongly in } C([0,T],H^{s+1}(-\ell,\ell)\times H^{s}(-\ell,\ell)),$$
$$(u_{n,t},v_{n,t})\to(u_t,v_t)\quad \text{strongly in } C((0,T),H^{s}(-\ell,\ell)\times H^{s-1}(-\ell,\ell)).$$

From (3.2.5) we have also

$$\mathcal{V}'(u_n)\to\mathcal{V}'(u),\quad \text{strongly in } C([0,T],H^{s}(-\ell,\ell)),$$

while by construction of the discrete initial data, we have $U(0)=U_0$. Fixing $n>0$, $(\phi_1,\phi_2)\in\mathbb{P}_n^2$ and passing to the limit in (3.0.2), we see that for $U=(u,v)$ and $(\phi_1,\phi_2)\in\mathbb{P}_n^2$ (3.0.1) holds. Since $\cup_{n>1}\mathbb{P}_n^2$ is everywhere dense in $H^s(-\ell,\ell)\times H^{s+1}(-\ell,\ell)$, we conclude that (3.0.1a) holds in $[0,T]$ for all $(\phi_1,\phi_2)\in H^s(-\ell,\ell)\times H^{s+1}(-\ell,\ell)$. The uniqueness of regular U, satisfying (3.0.1a) and a prescribed initial condition, follows from the continuity of weak (classical when $s\geq 1$) solutions with respect to the initial data. The proof of this fact is trivial and is omitted. Hence, the first assertion of Theorem 3.2.1 is settled. The bound (3.2.1) is obtained by letting $m\to\infty$ in (3.2.8a). $\square$

3.3 Extension to the real line

The convergence results, obtained in previous paragraphs in periodic settings, extends readily to the case of the real line. Indeed, operator $\mathcal{L}=\mathcal{J}\,\mathrm{diag}(-1,a^2\Delta)$ (in a natural domain) generates a strongly continuous unitary group $\{e^{t\mathcal{L}}\}_{t\in\mathbb{R}}$ of bounded linear operators in the scale $H^{s+1}(-\ell,\ell)\times$

$H^s(-\ell,\ell)$. Further, by virtue of the finite speed propagation property of $\{e^{t\mathcal{L}}\}_{t\in\mathbb{R}}$ and by the standard variation of constant formula, classical solutions to the periodic initial value problem (3.0.1) satisfy

$$\operatorname{supp}(u,v)(t) \subset [x_0-\varepsilon-at, x_0+\varepsilon+at], \tag{3.3.1a}$$

provided

$$\operatorname{supp}(u_0,v_0) \subset [x_0-\varepsilon, x_0+\varepsilon], \tag{3.3.1b}$$

$$t < \tfrac{1}{a}\min\{\ell-x_0-\varepsilon, \ell+x_0-\varepsilon\}. \tag{3.3.1c}$$

Hence, any such solution, extended by zero outside of the spatial domain $(-\ell,\ell)$, satisfies (1.1.1) in the classical sense as long as (3.3.1b) and (3.3.1c) hold. This observation, together with the facts that the Schwartz class $\mathcal{D}(\mathbb{R})$ is dense in $H^s(\mathbb{R})$, $s\geq 0$, and that the generic constant $c_r>0$, appearing in (3.2.1) is uniform in ℓ, indicates that for

$$(u_0,v_0)\in H^{s+1}(\mathbb{R})\times H^{s+\gamma}(\mathbb{R}), \quad \mathcal{V}\in C^{s+2}(\mathbb{R}),$$

with $s\geq 0$, $\gamma>\frac{1}{2}$, $T<\infty$ and $\ell>0$ sufficiently large, the analogue of (3.2.1) holds, i.e.

$$\|u-u_n\|_{(C[0,T],H^{r+1}(\mathbb{R}))}+\|v-v_n\|_{(C[0,T],H^r(\mathbb{R}))}\leq c_r\big(\tfrac{\ell}{\pi n}\big)^{s-r}, \quad 0\leq r\leq s-1. \tag{3.3.2}$$

Chapter 4

Geometric convergence

4.1 Wellposedness in the Gevrey settings

The proof of Theorem 3.1.2 indicates that numerical errors are dominated by the errors in the input data. The convergence rate can be slightly increased to $\left(\frac{\ell}{\pi n}\right)^{s+1-r}$, $0 \le r \le s$, provided $(u_0, v_0) \in H^{m+1}(-\ell, \ell) \times H^m(-\ell, \ell)$, with $m \ge s+1$. For potentials $\mathcal{V}$ of finite regularity $s+2$, this bound is optimal. However, in many practical applications the potentials are known to be entire functions of u. As particular instances we mention: the quadratic and cubic potentials appearing in the field theory; potential $\mathcal{V}(u) = 1 - \cos u$ used in the modeling of shallow waves; double sine potentials $\mathcal{V}(u) = \sin u + \lambda \sin 2u$ describing spin waves; and hyperbolic potentials $\mathcal{V}(u) = 1 - \cosh u$ arising in quantum physics. Below, we show that for such potentials the convergence is in fact geometric. Our analysis is based on the recent result of S. Panizzi [82]. We reproduce its proof for the sake of completeness.

Lemma 4.1.1 ([82]). *Assume $\mathcal{V}(z) = \sum_{n\ge 2} \frac{V_n}{n!} z^n$ is an entire function and $(u_0, v_0) \in G^r_{\rho_0,\theta}(-\ell, \ell) \times G^{r+1}_{\rho_0,\theta}(-\ell, \ell)$, for some $\rho_0 > 0$, $r > \frac{1}{2}$ and $0 < \theta \le 1$.*

Then

$$(E^r_{\rho,\theta})^{\frac12}(t) \le (E^r_{\rho,\theta})^{\frac12}(0) + \int_0^t \Psi_0(\|u\|_{H^r})(\tau)d\tau < \infty, \quad t \ge 0, \tag{4.1.1a}$$

with

$$\rho(t) \ge \rho_0 \left[1 + \rho_0^{\frac{2-\theta}{\theta}} \tfrac{2-\theta}{2\theta} t \int_0^t \Psi_1(\|u\|_{G^r_{\rho,\theta}})(\tau)d\tau\right]^{-\frac{2\theta}{2-\theta}}, \tag{4.1.1b}$$

where $E^r_{\rho,\theta} = \|v\|^2_{G^r_{\rho,\theta}} + a^2\|u\|^2_{G^{r+1}_{\rho,\theta}}$, $c_{r,n}$ *is the positive constant appearing in* (2.6.1a) *and*

$$\Psi_0(z) = \sum_{n\ge1} \tfrac{|V_{n+1}-\delta_{1,n}|}{n!} c_{r,n} e^{\frac{n}{2}} z^n, \quad \Psi_1(z) = \sum_{n\ge1} \tfrac{|V_{n+1}-\delta_{1,n}|}{(n-1)!} c_{r,n} e^{\frac{n}{2}} z^n,$$

are entire functions.

Proof. (a) Assuming that $\rho = \rho(t)$ is a function of t, letting $(\phi_1, \phi_2) = (0, \mathcal{A}^{2r} e^{2\rho\mathcal{A}^\theta} v)$ in (3.0.1), after some simplifications we arrive at

$$\begin{aligned} \tfrac12 \tfrac{d}{dt} E^r_{\rho,\theta} &= \dot\rho E^{r+\frac\theta2}_{\rho,\theta} + \left\langle \mathcal{A}^r e^{2\rho\mathcal{A}^\theta}(u - \mathcal{V}'(u)), \mathcal{A}^r e^{2\rho\mathcal{A}^\theta} v \right\rangle \\ &\le \dot\rho E^{r+\frac\theta2}_{\rho,\theta} + \|u - \mathcal{V}'(u)\|_{G^s_{\rho,\theta}} \|v\|_{G^r_{\rho,\theta}}. \end{aligned} \tag{4.1.2}$$

Let $f(z) = z - \mathcal{V}'(z) = \sum_{n\ge1} \frac{f_n}{n!} z^n$. To bound $\|f(u)\|_{G^s_{\rho,\theta}}$, we employ (2.6.1a):

$$\|f(u)\|_{G^r_{\rho,\theta}} \le \sum_{n\ge1} \tfrac{|f_n|}{n!} c_{r,n} \|u\|^n_{G^r_{\rho,\theta}}. \tag{4.1.3}$$

Then the repeated application of (2.6.1b), with $q = 1 + \frac\theta2$, gives

$$\begin{aligned} \|f(u)\|_{G^r_{\rho,\theta}} &\le \sum_{n\ge1} \tfrac{|f_n|}{n!} c_{r,n} \|u\|^{n-1}_{G^r_{\rho,\theta}} \Big(e^{\frac12} \|u\|_{H^r} + (2\rho)^{\frac12+\frac1\theta} \|u\|_{G^{r+1+\frac\theta2}_{\rho,\theta}} \Big) \\ &\le \sum_{n\ge1} \tfrac{|f_n|}{n!} c_{r,n} e \|u\|_{H^r} \|u\|^{n-2}_{G^r_{\rho,\theta}} \Big(e^{\frac12} \|u\|_{H^r} + (2\rho)^{\frac12+\frac1\theta} \|u\|_{G^{r+1+\frac\theta2}_{\rho,\theta}} \Big) + \\ &+ (2\rho)^{\frac12+\frac1\theta} \sum_{n\ge1} \tfrac{|f_n|}{n!} c_{r,n} \|u\|^{n-1}_{G^r_{\rho,\theta}} \|u\|_{G^{r+1+\frac\theta2}_{\rho,\theta}} \\ &\le \sum_{n\ge1} \tfrac{|f_n|}{n!} c_{r,n} e^{\frac{n}{2}} \|u\|^n_{H^r} + (2\rho)^{\frac12+\frac1\theta} \sum_{n\ge1} \tfrac{|f_n|}{(n-1)!} e^{\frac{n}{2}} c_{r,n} \|u\|^{n-1}_{G^r_{\rho,\theta}} \|u\|_{G^{r+1+\frac\theta2}_{\rho,\theta}} \\ &= \Psi_0(\|u\|_{H^r}) + (2\rho)^{\frac12+\frac1\theta} \Psi_1(\|u\|_{G^r_{\rho,\theta}}) \|u\|_{G^{r+1+\frac\theta2}_{\rho,\theta}}, \end{aligned}$$

where, in view of the explicit formula for $c_{n,r}$ in (2.6.1a), both $\Psi_0(z)$ and $\Psi_1(z)$ are entire functions.

(b) Combining the last estimate with (4.1.2) and using the standard Young's inequality, we infer

$$\tfrac{1}{2}\tfrac{d}{dt}E^r_{\rho,\theta} \le \Psi_0(\|u\|_{H^r})\big[E^r_{\rho,\theta}\big]^{\frac{1}{2}} + \Big[\dot\rho + (2\rho)^{\frac{1}{2}+\frac{1}{\theta}}\Psi_1(\|u\|_{G^r_{\rho,\theta}})\Big]E^{r+\frac{\theta}{2}}_{\rho,\theta}.$$

Now Gronwall's inequality yields equation (4.1.1a), provided (4.1.1b) holds.

□

4.2 Consistency estimates

Let u be the exact weak solution of problem (3.0.1). For $n > 0$, we denote $(\hat u, \hat v) = (\mathcal{P}_n[u], \mathcal{P}_n[v])$ and $(\hat u(0), \hat v(0)) = (\mathcal{P}_n[u_0], \mathcal{P}_n[v_0])$. It is not difficult to verify that the spectral projection $(\hat u, \hat v)$ satisfies:

$$\begin{aligned}\langle(\hat u, \hat v)_t, (\phi_1, \phi_2)\rangle &= \langle \hat v, \phi_1\rangle - a^2\langle \partial_x \hat u, \partial_x\phi_2\rangle - \langle \mathcal{I}_n[\mathcal{V}'(\hat u)], \phi_2\rangle \\ &\quad + \langle \mathcal{D}_n[u], \phi_2\rangle, \qquad (4.2.1a)\\ (\hat u(0), \hat v(0)) &= (\mathcal{P}_n[u_0], \mathcal{P}_n[v_0]), \quad \text{for all} \quad (\phi_1, \phi_2) \in \mathbb{P}^2_n, \qquad (4.2.1b)\end{aligned}$$

where $\mathcal{D}_n[u] = \mathcal{I}_n[\mathcal{V}'(\hat u)] - \mathcal{P}_n[\mathcal{V}'(u)]$. We show that the defect $\mathcal{D}_n(u)$ is exponentially small, provided the exact solution is sufficiently regular.

Lemma 4.2.1. *If $\mathcal{V}(z)$ and (u_0, v_0) satisfy the assumptions of Lemma 4.1.1, then for any $\frac{1}{2} < s \le r$ and $t > 0$,*

$$\|\mathcal{D}_n[u]\|_{L^2} \le c\big(\tfrac{\pi n}{\ell}\big)^{s-r}\exp\Big\{-\rho\big(\tfrac{\pi n}{\ell}\big)^{\theta}\Big\}\Big[\Psi_2(\|u\|_{G^r_{\rho,\theta}}) + \Psi_3(\|u\|_{H^s})\|u\|_{G^r_{\rho,\theta}}\Big], \qquad (4.2.2)$$

where $c > 0$, depends on s only and

$$\Psi_2(z) = \sum_{n\ge1}\tfrac{|V_{n+1}|}{n!}c_{r,n}z^n, \quad \Psi_3(z) = \sum_{n\ge0}\tfrac{|V_{n+2}|}{n!}c_{s,n}z^n.$$

Proof. To bound $\mathcal{D}_n[u]$, we note that

$$\begin{aligned}\|\mathcal{D}_n(u)\|_{L^2} &= \|\mathcal{I}_n[\mathcal{V}'(\hat{u})] - \mathcal{V}'(\hat{u}) + \mathcal{V}'(\hat{u}) - \mathcal{P}_n[\mathcal{V}'(u)]\|_{L^2} \\ &\leq \|(\mathcal{I} - \mathcal{I}_n)[\mathcal{V}'(\hat{u})]\|_{L^2} + \|\mathcal{V}'(\hat{u}) - \mathcal{P}_n[\mathcal{V}'(u)]\|_{L^2} \\ &=: \|D_1\|_{L^2} + \|D_2\|_{L^2}.\end{aligned}$$

Using inequalities (2.5.8) and (2.6.1a), in the same way as in estimate (4.1.3) we obtain

$$\begin{aligned}\|D_1\|_{L^2} \leq \|D_1\|_{H^s} &\leq c_s\big(\tfrac{\pi n}{\ell}\big)^{s-r} \exp\Big\{-\rho\big(\tfrac{\pi n}{\ell}\big)^{\theta}\Big\} \|\mathcal{V}'(u)\|_{G^r_{\rho,\theta}}, \\ &\leq c_s\big(\tfrac{\pi n}{\ell}\big)^{s-r} \exp\Big\{-\rho\big(\tfrac{\pi n}{\ell}\big)^{\theta}\Big\} \Psi_2(\|u\|_{G^r_{\rho,\theta}}).\end{aligned}$$

Further, (2.5.3) combined with (2.6.1a) gives

$$\begin{aligned}\|D_2\|_{L^2} &\leq \|(\mathcal{I} - \mathcal{P}_n)[\mathcal{V}'(\hat{u})]\|_{L^2} + \|\mathcal{P}_n[\mathcal{V}'(\hat{u}) - \mathcal{V}'(u)]\|_{L^2} \\ &\leq \big(\tfrac{\pi n}{\ell}\big)^{-r} \exp\Big\{-\rho\big(\tfrac{\pi n}{\ell}\big)^{\theta}\Big\} \Psi_2(\|u\|_{G^r_{\rho,\theta}}) + \|\mathcal{V}'(\hat{u}) - \mathcal{V}'(u)\|_{L^2}.\end{aligned}$$

Finally, application of estimate (2.6.1a), with $\rho = 0$ followed by estimate (2.5.3), yields

$$\begin{aligned}\|\mathcal{V}'(\hat{u}) - \mathcal{V}'(u)\|_{L^2} &\leq \sum_{n\geq 1} \tfrac{|V_{n+1}|}{n!} \|\hat{u}^n - u^n\|_{L^2} \\ &\leq \sum_{n\geq 1} \tfrac{|V_{n+1}|}{n!} n c_{s,n-1} \|u\|_{H^s}^{n-1} \|(\mathcal{I} - \mathcal{P}_n)[u]\|_{H^s} \\ &\leq \big(\tfrac{\pi n}{\ell}\big)^{s-r} \exp\Big\{-\rho\big(\tfrac{\pi n}{\ell}\big)^{\theta}\Big\} \Psi_3(\|u\|_{H^s}) \|u\|_{G^r_{\rho,\theta}}.\end{aligned}$$

Combining all the inequalities together, we arrive at inequality (4.2.2). □

4.3 Error estimates

Equation (4.2.1) and Lemma 4.2.1 yield together

Theorem 4.3.1. *If $\mathcal{V}(z)$ and (u_0, v_0) satisfy the assumptions of Lemma 4.1.1, then for any $1 \leq r$, we have*

$$\|u-u_n\|_{(C([0,T]),H^1)}+\|v-v_n\|_{(C([0,T]),L^2)} \leq c\big(\tfrac{\pi n}{\ell}\big)^{1-r} \exp\Big\{-\rho\big(\tfrac{\pi n}{\ell}\big)^{\theta}\Big\}, \quad (4.3.1)$$

where $\rho = \rho(T)$ satisfies (4.1.1b) *and the generic constant $c > 0$ depends on $\|u_0\|_{G^r_{\rho_0,\theta}}$ and $\|v_0\|_{G^{r+1}_{\rho_0,\theta}}$ but is uniform in $n > 0$.*

Proof. (a) We subtract equation (3.0.2) from (4.2.1) and let $(e_1, e_2) = (\hat{u}, \hat{v}) - (u_n, v_n)$, $(\phi_1, \phi_2) = (e_1, e_2)$, to obtain

$$\frac{1}{2}\frac{d}{dt}\Big[\|e_2\|^2_{L^2} + a^2\|\nabla e_1\|^2_{L^2}\Big] = \langle \mathcal{D}_n[u], e_2\rangle - \langle \mathcal{I}_n[\mathcal{V}'(\hat{u}) - \mathcal{V}'(u_n)], e_2\rangle. \quad (4.3.2)$$

Since the quadrature is exact in $\mathbb{P}_n$, with the aid of the Cauchy-Schwarz and Young's inequalities, we infer

$$\begin{aligned}
\big|\langle \mathcal{I}_n[\mathcal{V}'(\hat{u}) - \mathcal{V}'(u_n)], e_2\rangle\big| &\leq \frac{2\ell}{2n+1}\sum_{j=0}^{2n} |e_2(x_j)| \left| \int_{\hat{u}(x_j)}^{u_n(x_j)} \mathcal{V}''(s)ds \right| \\
&\leq c\frac{2\ell}{2n+1}\sum_{j=0}^{2n} |e_2(x_j)||e_1(x_j)| \\
&\leq c\|e_1\|_{L^2}\|e_2\|_{L^2} \leq \frac{c}{2}\Big[\|e_1\|^2_{L^2} + \|e_2\|^2_{L^2}\Big],
\end{aligned}$$

where, by virtue of Theorem 3.2.1, the quantity

$$c = \max\Big\{\mathcal{V}''(s)\,\Big|\,|s| \leq \max\{\|u\|_{C([0,T],L^\infty)} + 1, \|u_n\|_{C([0,T],L^\infty)}\}\Big\} < \infty$$

is uniformly bounded for large values of $n > 0$. The last estimate, combined with (4.3.2), yields the bound

$$\frac{d}{dt}\Big[\|e_2\|^2_{L^2} + a^2\|\partial_x e_1\|^2_{L^2}\Big] \leq c\Big[\|e_1\|^2_{L^2} + \|e_2\|^2_{L^2}\Big] + \|\mathcal{D}_n[u]\|^2_{L^2}, \quad (4.3.3)$$

where as before, the generic constant $c > 0$ is independent of $n > 0$.

Similarly, letting $(\phi_1, \phi_2) = (e_1, 0)$ in (3.0.1) and (4.2.1) and using Young's inequality, we arrive at

$$\tfrac{d}{dt}\|e_1\|_{L^2}^2 \leq \|e_1\|_{L^2}^2 + \|e_2\|_{L^2}^2. \tag{4.3.4}$$

(b) We add (4.3.3) and (4.3.4) together and apply Gronwall's inequality to obtain

$$\|e_1\|_{(C([0,T]),H^1)} + \|e_2\|_{(C([0,T]),L^2)} \leq c\Big[\|e_{10}\|_{H^1} + \|e_{20}\|_{L^2} + \|\mathcal{D}_n[u]\|_{L^2([0,T]\times(-\ell,\ell))}\Big].$$

In view of Lemma 4.2.1 and (2.5.3), the last estimate yields the exponential bound

$$\|e_1\|_{(C([0,T]),H^1)} + \|e_2\|_{(C([0,T]),L^2)} \leq c\big(\tfrac{\pi n}{\ell}\big)^{1-r} \exp\Big\{-\rho\big(\tfrac{\pi n}{\ell}\big)^{\theta}\Big\},$$

where $c > 0$ is controlled (via (4.1.1)) by $\|u_0\|_{G^r_{\rho_0,\theta}}$ and $\|v_0\|_{G^{r+1}_{\rho_0,\theta}}$ but is independent on $n > 0$. Finally,

$$\begin{aligned}
\|u - u_n\|_{H^1} &\leq \|e_1\|_{H^1} + \|(\mathcal{I} - \mathcal{P}_n)[u]\|_{H^1},\\
\|v - v_n\|_{L^2} &\leq \|e_2\|_{L^2} + \|(\mathcal{I} - \mathcal{P}_n)[u]\|_{L^2}
\end{aligned}$$

and direct application of (2.5.3) completes the proof. □

It is noteworthy of mentioning that the spectral convergence rate is anticipated primarily for entire potentials. In such instances, for periodic KGE problems, the convergence rate manifests as spectral and is solely regulated by the Gevrey class of the initial data. However, the scenario becomes slightly more intricate when Fourier-type approximations are employed to solve initial value problems over the real line. In this context, spectral convergence is assured only if the space truncation parameter n increases at a pace exceeding a certain power of the domain truncation parameter ℓ.

4.4 Extension to the real line

As we did see in Chapter 3 — thanks to the finite propagation speed of the wave operator $e^{t\mathcal{L}}$, the convergence results can be extended from the periodic settings to the real line. Similarly, in the case of the Gevrey scale $G^r_{\rho_0,\theta}(-\ell,\ell)\times G^{r+1}_{\rho_0,\theta}(-\ell,\ell), r\in\mathbb{R}$, the family $\{e^{t\mathcal{L}}\}_{t\geq 0}$ is again a unitary group. However, extension of the bound (4.3.1) to the real line is a bit more complicated.

The major difficulty here is that the constant $c_{n,r}$, appearing in (2.6.1a), behaves as $\mathcal{O}(\ell^{2(n-1)})$. As a consequence, for entire potentials $\mathcal{V}$ of type $\sigma>0$ and order $p>0$ (i.e. if $\sup_{z\in\mathbb{C}} e^{-\sigma|z|^{-p}}|\mathcal{V}(z)|<\infty$), in a finite time intervals the following bound holds

$$E^r_{\rho,\theta}(T)\leq c\exp\bigl\{\sigma(\sqrt{e}\ell^2\|u\|_{H^r(\mathbb{R})})^{p+\varepsilon}\bigr\},$$

for any $\varepsilon>0$. In this situation, the analogue of (4.3.1) takes the form

$$\begin{aligned}\|u-u_n\|_{(C[0,T],H^1(\mathbb{R}))}+\|v-v_n\|_{(C[0,T],L^2(\mathbb{R}))}\\ \leq c\exp\Bigl\{\sigma(\sqrt{e}\ell^2\|u\|_{H^r(\mathbb{R})})^{p+\varepsilon}-\rho(T)\bigl(\tfrac{\pi n}{\ell}\bigr)^{\theta}\Bigr\}\end{aligned}\tag{4.4.1a}$$

and we see that the geometric convergence occurs, provided for any $\varepsilon>0$,

$$n\geq\mathcal{O}(\ell^{1+\frac{2p+2\varepsilon}{\theta}}).\tag{4.4.1b}$$

I.e., to preserve the spectral convergence rate in $\mathbb{R}$, the semidiscretization parameter n shall grow super-linearly as the domain truncation parameter ℓ increases.

Chapter 5

Long time behaviour of the KGE solutions

In this thesis, we are interested in the long time behaviour of semidiscrete approximations to the KGE near invariant subsets of the equation and to address this, we need a description of invariants sets of the SGE/LWE models.

5.1 Dynamics associated to the Sine-Gordon equation

It is well-known that the Sine-Gordon equation

$$u_{tt} = \Delta u - \sin(u), \quad x \in \mathbb{R}, \quad t > 0, \tag{5.1.1a}$$

$$u(0) = u_0, \quad u_t(0) = v_0, \tag{5.1.1b}$$

which is a particular type of KGE (1.1.1), with $\mathcal{V}(u) = 1 - \cos u$, is an example of a completely integrable Hamiltonian PDE [81]. This implies that in the periodic settings as well as in the real line, the problem has an infinite

family of first integrals that is sufficient to recover arbitrary solutions to the equation. Implicitly, these first integrals are described by the spectrum of Lax operator $\mathcal{L}_{(u,v)}$ that satisfies the equation

$$\partial_t \mathcal{L}_{(u(t),v(t))} = [\mathcal{A}_{(u(t),v(t))}, \mathcal{L}_{(u(t),v(t))}], \tag{5.1.2a}$$

where

$$\mathcal{L}_{(u,v)} = \begin{pmatrix} -J & 0 \\ 0 & 0 \end{pmatrix} \partial_x + \begin{pmatrix} A_{(u,v)} & B_{(u,v)} \\ B_{(u,v)} & 0 \end{pmatrix}, \tag{5.1.2b}$$

$$\mathcal{A}_{(u,v)} = \begin{pmatrix} -I & 0 \\ 0 & I \end{pmatrix} \partial_x - 2 \begin{pmatrix} 0 & JB_{(u,v)} \\ BJ_{(u,v)} & 0 \end{pmatrix}, \tag{5.1.2c}$$

$$J = \begin{pmatrix} 0 & 1 \\ -1 & 0 \end{pmatrix}, \quad A_{(u,v)} = \frac{i}{4}(v + u_x) \begin{pmatrix} 0 & 1 \\ 1 & 0 \end{pmatrix}, \quad B_{(u,v)} = \frac{1}{4} \begin{pmatrix} e^{\frac{iu}{2}} & 0 \\ 0 & e^{-\frac{iu}{2}} \end{pmatrix} \tag{5.1.2d}$$

and $[\mathcal{A}_{(u,v)}, \mathcal{L}_{(u,v)}] = \mathcal{A}_{(u,v)}\mathcal{L}_{(u,v)} - \mathcal{L}_{(u,v)}\mathcal{A}_{(u,v)}$ is the standard commutator. It is easy to verify that the point spectrum of operator $\mathcal{L}_{(u,v)}$, satisfying (5.1.2a) remains constant along classical solutions to the Sine-Gordon equations [75, 59, 64, 98].

In the real line, the discrete spectrum of operator $\mathcal{L}_{(u,v)}$, together with the asymptotic of eigenfunctions as $x \to \pm\infty$, can be used to recover the associated solutions to the Sine-Gordon equation via the inverse scattering transform, see [80, 2, 81, 23]. In the periodic settings, the situation is technically more complicated. Here, some solution (so called finite gap solutions) can be constructed from the eigenvalues of the operator $\mathcal{L}_{(u,v)}$ via algebro-geometric constructions and the general theory of Riemann surfaces, see [11, 76, 64, 33, 61].

In the latter case, the solutions are quasi-periodic in time and closely resemble quasi-periodic solutions of completely integrable Hamiltonian ODEs, i.e.

these solutions represent quasi-periodic motions on finite-dimensional tori. It is natural to expect (by analogy with the finite-dimensional KAM theory [95, 30, 94]) that the same is true for small Hamiltonian perturbations of the completely integrable Sine-Gordon equation.

It is worth mentioning that the the perturbations theory of completely integrable Hamiltonian ODEs is well established and goes back to the classical works of Lagrange, Jacobi, Linstedt, Poincare, Birkhoff and more recently to the works of Kolmogorov, Arnold, Moser, Nechoroshev, e.t.c , see e.g. [94] for the historical remarks. Relatively recently, a number of attempts were made to extend these results to the case of completely integrable semi- and quasi-linear Hamiltonian PDEs, see [11, 64, 5, 49, 41]. There are two major trends in the modern literature concerning perturbation theory of completely integrable Hamiltonian PDEs. The first one consists in the analysis of small Hamiltonian perturbations in a vicinity of a family of finite dimensional invariant tori embedded into an infinite dimensional phase space of the unperturbed completely integrable equation, see e.g. [15, 64] and references therein. The second approach deals directly with preservation of infinite-dimensional invariant structures. Unfortunately, very few results of these type (dealing with a very special problems) are available in the literature, see in particular [7, 46, 52, 8]. We provide a brief review below.

5.2 The spectrum of $\mathcal{L}_{(u,v)}$ in periodic settings

To describe the first type of results in context of small Hamiltonian perturbations of the Sine-Gordon equation, equipped with small periodic input data, we have to provide an explicit description of finite-dimensional invariant tori associated to the so called *finite-gap solutions* of the Sine-Gordon equation.

The spectrum of $\mathcal{L}_{(u,v)}$

Assuming that the potentials (u, v) are 2ℓ-periodic and sufficiently regular, i.e.

$$(u, v) \in C([0, T]; H^{s+1} \times H^s) \cap C^1((0, T); H^s \times H^{s-1}), \quad s \geq 1, \tag{5.2.1}$$

we view $(\mathcal{L}_{(u,v)}, \mathcal{D}(\mathcal{L}_{(u,v)}))$ as an unbounded linear operator acting on $H^s(-\ell, \ell)^4$, $s \in \mathbb{R}$, with the domain

$$\mathcal{D}(\mathcal{L}_{(u,v)}) = \{(f_+, f_-) \in H^{s+1}(-\ell, \ell)^2 \times H^s(-\ell, \ell)^2\}.$$

We note that $\mathcal{L}_{(u,v)}$ is closed and densely defined[1], however it is neither self-adjoint nor normal. To describe its spectrum, assume $\mu \in \mathbb{C} \setminus \{0, \infty\}$, $f = (f_+, f_-) \in H^s(-\ell, \ell)^2 \times H^{s-1}(-\ell, \ell)^2$ and $g = (g_+, g_-) \in H^{s-1}(-\ell, \ell)^4$. Then, the resolvent equation $(\mu I - \mathcal{L})f = g$ reads

$$\tfrac{d}{dx} f_+ = J\left(\mu I - A - \tfrac{1}{\mu} B^2\right) f_+ - J\left(g_+ + \tfrac{1}{\mu} B_n g_-\right), \tag{5.2.2a}$$

$$f_- = \tfrac{1}{\mu}(g_- + B f_+). \tag{5.2.2b}$$

Discarding the explicit formula (5.2.2b), we obtain a two-by-two system of linear inhomogeneous ODEs with periodic/anti-periodic coefficients for the unknown function f^+. The system can be integrated explicitly in terms of the fundamental solution matrix $\Phi_\mu(x, y)$ that satisfies

$$\frac{d}{dx}\Phi_\mu = J\left(\mu I - A - \tfrac{1}{\mu} B^2\right)\Phi_\mu = 0, \quad \Phi_\mu(y, y) = I. \tag{5.2.3}$$

Based on the standard theory of linear ODEs and our assumption (5.2.1), we can conclude that Φ_μ is a twice continuously differentiable function in either

[1]The claim follows from denseness of the standard Sobolev embeddings $H^s(-\ell, \ell) \hookrightarrow H^{s-1}(-\ell, \ell)$ and the fact that for smooth potentials, $\mathcal{L}_{(u,v)}$ is a bounded pertubation of the closed operator $\begin{pmatrix} -J & 0 \\ 0 & 0 \end{pmatrix} \partial_x$.

of the variable x and y. Expressed in terms of the monodromy operator

$$\mathcal{M}_\mu(x) := \Phi_\mu(x + 2\ell, x),$$

the formal solution to the periodic $(+)$ and anti-periodic $(-)$ resolvent equation (5.2.2) can be written as:

$$\begin{aligned} f_+ &= \Phi_\mu(x,0)\left(\mathcal{M}_\mu(0) \pm I\right)^{-1} \\ &\quad \times \left[\int_x^{2\ell} \Phi_\mu(2\ell,\tau) J \left[g_+(\tau) + \tfrac{1}{\mu} B(\tau) g_-(\tau)\right] d\tau \right. \\ &\qquad \left. + \int_0^x \Phi_\mu(0,\tau) J \left[g_+(\tau) + \tfrac{1}{\mu} B(\tau) g_-(\tau)\right] d\tau \right], \qquad (5.2.4a) \\ f_- &= \tfrac{1}{\mu}(g_- + B f_+), \qquad (5.2.4b) \end{aligned}$$

provided that $\mathcal{M}_\mu(0) \pm I$ is invertible.

From the last formula, it follows that $\mu \in \sigma(\mathcal{L}_{(u,v)})$ if and only if ± 1 are eigenvalues of the monodromy matrix $\mathcal{M}_\mu(0)$. Since the coefficient matrix in equation (5.2.3) is traceless and since $\det \Phi_\mu(y,y) = 1$, we have $\det \Phi_\mu(0) = 1$. Consequently $\mu \in \sigma(\mathcal{L}_{(u,v)})$ if and only if

$$\left[\tfrac{1}{2} Tr \mathcal{M}_\mu(0)\right]^2 = \Delta(\mu; u, v) = 1. \qquad (5.2.5)$$

The quantity $\Delta(\mu; u, v)$ is known as the discriminant of problem (5.2.3). The discriminant equation (5.2.5) completely determines the spectrum of operator $\mathcal{L}_{(u,v)}$. Using the discriminant equation (5.2.5), it is shown in [75] that

Lemma 5.2.1. *[75] For (u, v) as in (5.2.1), the spectrum of $\mathcal{L}_{(u,v)}$ is discrete and each eigenvalue has finite algebraic multiplicity. There exists $n_{(u,v)} > 0$ depending on the $H^{s+1} \times H^s$-norm ($s \geq 1$) of the potential (u, v) only and such that "positive" eigenvalues $\mu_n^{\pm}$ (respectively "negative" eigenvalues*

$-\mu_n^{\pm}$*), with* $|n| > n_{(u,v)}$ *are separated from the rest of the spectrum and satisfy*

$$|\mu_n^{\pm}| = \begin{cases} \frac{n}{2} + \mathcal{O}(n^{-1}), & n \to +\infty, \\ \frac{1}{8n} + \mathcal{O}(n^{-3}), & n \to -\infty. \end{cases} \tag{5.2.6}$$

Further, if the potential (u, v) *is real, every such isolated couple is either complex conjugate, i.e.* $\mu_n^{\pm} \notin \mathbb{R}$, $\mu_n^+ = \overline{\mu_n^-}$ *(both quantities are simple eigenvalues of* $\mathcal{L}_{(u,v)}$*); or* $\mu_n^+ = \mu_n^- \in \mathbb{R}$ *(both quantities correspond to a double eigenvalue of* $\mathcal{L}_{(u,v)}$*). Finally, along classical solutions to the Sine-Gordon equation, the spectrum of* $\mathcal{L}_{(u(t),v(t))}$ *is time independent and the algebraic multiplicities of eigenvalues remain constant.*

5.3 Finite-gap solutions

Among classical solutions to the Sine-Gordon Equation a significant subset known as *n-gap potentials* is of particular importance. These solutions are given by smooth 2ℓ periodic functions $(u(x,t), v(x,t))$, such that $\sigma(\mathcal{L}_{(u(t),v(t))})$ contains precisely $4n$ simple eigenvalues. In the theory of the SGE, it is a custom to use squared eigenvalues $\lambda = 16\mu^2$ and to rewrite the discriminant equation (5.2.5) in terms of the variable λ. An n-gap potential is defined by the property that the equation $\Delta^2(\lambda; u, v) = 1$ has precisely $2n$ simple roots, i.e.

$$\lambda_{\gamma_j}^{\pm}, \quad j = 1, 2, \cdots, n,$$

for some integers γ_j, $j = 1, 2, \cdots, n$. If (u, v) is real, the quantities

$$E_{2j-1} = \lambda_{\gamma_j}^+, \quad E_{2j} = \lambda_{\gamma_j}^-, \quad j = 1, \ldots, n,$$

represent complex conjugate pairs of simple λ-eigenvalues of the operator $\mathcal{L}_{(u,v)}$. Every such pair is called a gap.

Let $E = \big(E_1, \dots, E_{2n}\big) \in \mathbb{C}^{2n}$ be a fixed complex $2n$-vector as above. Since the periodic/anti-periodic discrete spectrum of the operator $\mathcal{L}_{(u,v)}$ is invariant under the SGE flow, the set of n-gap potentials with a fixed single spectrum E is also flow-invariant. The members of this set are given by the explicit formula [78, 75, 45, 11, 64]:

$$u(x,t;E,D) = 2i \ln \frac{\theta(i(Vx+Wt+D+\Delta))}{\theta(i(Vx+Wt+D))}, \tag{5.3.1}$$

where $\Delta = (\ell, \cdots, \ell) \in \mathbb{R}^{2n}$ is the vector of half periods, $D = \mathbb{T}^{2n}$, and $V, W \in \mathbb{C}^{2n}$,

$$\theta(z) = \sum_{m \in \mathbb{Z}^n} \exp\left(i\ell \langle Bm, m\rangle + \frac{i\pi}{\ell} \langle m, z\rangle \right), \quad z \in \mathbb{C}^n,$$

is the Riemann theta function associated to the algebraic curve

$$\Gamma = \left\{ (z,\lambda) \in \mathbb{C}^2 \,|\, z^2 = \lambda \prod_{i=1}^{n} (\lambda - E_i) \right\}$$

and B is the Riemann matrix containing b-periods of curve Γ, see [78, 75, 45, 11, 64] and references therein for further details.

5.4 Small amplitude real finite-gap solutions

In the sequel, we are interested in small amplitude real finite-gap solution. The reality condition imposes an additional restriction on the spectrum of $\mathcal{L}_{(u,v)}$, i.e. for such potentials we must have [75]

$$\lambda^{\pm}_{\pm n} = \overline{\lambda^{\mp}_{\pm n}}, \quad \lambda^{\pm}_{\pm n} \cdot \lambda^{\mp}_{\mp n} = 1, \quad n \in \mathbb{Z}. \tag{5.4.1}$$

Accordingly, we let $\gamma = \{\gamma_1, \cdots, \gamma_n\} \subset \mathbb{N}^n$ and define the set

$$\hat{\mathcal{R}}^n_{\gamma,\delta} = \big\{ r \in \mathbb{R}^n \,\big|\, |r| \le \delta,\, j = 1, \dots, n \big\},$$

that describes sizes of spectral gaps at positions γ, i.e. $\mathrm{Im}(\lambda^+_{\pm\gamma_j} - \lambda^-_{\pm\gamma_j}) = r_j$, for some solution (u, v) of the SGE. It is shown in [64] that for sufficiently small values of $\delta > 0$, $0 \in \hat{\mathcal{R}}^n_{\gamma,\delta}$ and there exists a one-to-one map $r \mapsto E = (\lambda^{\pm}_{\pm\gamma_j})_{j=1}^n$, so that within E, (5.4.1) holds. It is unknown if $\hat{\mathcal{R}}^n_{\gamma,\delta}$ is connected in $\mathbb{R}^n$, accordingly we let

$$\begin{aligned}
&\mathcal{R}^n_{\gamma,\delta} = \text{connected component of } \hat{\mathcal{R}}^n_{\gamma,\delta} \text{ that contains } 0,\\
&\mathcal{T}^n_{\gamma,\delta} = \bigcup_{r\in\mathcal{R}^n_{\gamma,\delta}} \mathcal{T}^n_{\gamma,\delta}(r),\\
&\mathcal{T}^n_{\gamma,\delta}(r) = \left\{(u,v)(x,t;E(r),\tilde{D})|\tilde{D}\in\mathbb{T}^n\right\}, \quad r\in\mathcal{R}^n_{\gamma,\delta}.
\end{aligned}$$

The following result is established in [64]

Theorem 5.4.1. *[64] On $\mathcal{R}^n_{\gamma,\delta}$, the map $r \mapsto (V, W)$, where V and W are velocities from* (5.3.1)*, is one-to-one and analytic. The image of $\mathcal{R}^n_{\gamma,\delta} \times \mathbb{T}^n$ under the map defined by* (5.3.1) *is an analytic manifold in a small complex neighborhood of the origin of $H^{s+1}(-\ell,\ell)\times H^s(-\ell,\ell)$, $s \geq 1$. Each set $\mathcal{T}^{2n}_{\gamma,\delta}(r)$, $r \in \mathcal{R}^{2n}_{\gamma,\delta}$ is nonempty and constitutes a well-defined analytic $2n$-torus within the phase space $H^{s+1}(-\ell,\ell)\times H^s(-\ell,\ell)$, $s \geq 1$. Every such torus is invariant under the SGE flow.*

5.5 Finite-gap KAM tori

Theorem 5.4.1 allows to define a symplectic change of variables near $\mathcal{T}^{2n}_{\gamma,\delta}$ in the phase space $H^{s+1}(-\ell,\ell)\times H^s(-\ell,\ell)$ so that the finite dimensional vectors r and D become action-angle variables on $\mathcal{T}^{2n}_{\gamma,\delta}$. In these new variables, the original Sine-Gordon Equation, as well as its small Hamiltonian perturbation, takes a form that closely resembles the Birkhoff normal form for Hamiltonian ODEs [7]. Using this observation, the following result is obtained in [64]

Theorem 5.5.1. *Consider a perturbed Sine-Gordon equation under either even- or odd-periodic boundary conditions:*

$$u_{tt} = u_{xx} - \sin u + \epsilon f'_u(u,x), \quad x \in (-\ell,\ell), \tag{5.5.1a}$$

$$u(t,x) = u(t,x+2\ell), \quad \textit{either } u(x,t) = -u(t,-x) \textit{ or } u(x,t) = u(t,-x). \tag{5.5.1b}$$

Assume that the $f(u,x)$ is a smooth function, analytic and even in u, even and 2ℓ-periodic in x and vanishing for $u = 0$ identically in x. Then, there exists a Borel subset $\mathcal{R}_\epsilon \subset \mathcal{R}^n_{\gamma,\delta}$, such that $\int_{\mathcal{R}^n_{\gamma,\delta}\setminus\mathcal{R}_\epsilon} dx \to 0$ as $\epsilon \to 0$. For any $r \in \mathcal{R}_\epsilon$, an ϵ-neighborhood of the torus $\mathcal{T}^n_{\gamma,\delta}(r)$ contains an invariant set $\mathcal{T}^{n,\varepsilon}_{\gamma,\delta}(r)$ of the perturbed equation (5.5.1)*. The invariant set $\mathcal{T}^{n,\varepsilon}_{\gamma,\delta}(r)$ is an analytic n-torus (KAM torus) in $H^{s+1}(-\ell,\ell)\times H^s(-\ell,\ell)$, $s \geq 1$. The KAM torus $\mathcal{T}^{n,\varepsilon}_{\gamma,\delta}(r)$ carries time quasi-periodic solutions to the perturbed* (5.5.1)*.*

Since the Klein-Gordon equation with the potential of the form $\mathcal{V}(u) = 1 - u^2 + \mathcal{O}(u^3)$ and small initial data can be viewed as small pertubations of the Sine-Gordon equation, it follows that almost all solutions of the latter problem are quasi-periodic in time in a small neighborhood of the finite dimensional family $\mathcal{T}^n_{\gamma,\delta}$ of small amplitude n-gap tori of the unperturbed Sine-Gordon equation. In other words, Theorem 5.5.1 completely describes long time behaviour of small amplitude KGE solutions in a specific regions of the phase space $H^s(-\ell,\ell)\times H^{s-1}(-\ell,\ell), s \geq 1$.

It is natural to expect that an analogue of Nekhoroshev's theory should hold in these settings, i.e. solutions starting near n-gap KAM tori $\mathcal{T}^{n,\varepsilon}_{\gamma,\delta}(r)$ stay close to it for very long periods of time. To the best of our knowledge, we cannot provide any direct reference to the results of this type.

5.6 Finite-dimensional KAM theory near the origin

One of the greatest technical difficulties in the study of n-gap tori consists in a very complex construction of a map that puts the original nonlinear SGE to a normal form near any such tori. The construction is much simpler, if for small periodic data $(u, v) \in H^{s+1}(-\ell, \ell) \times H^s(-\ell, \ell)$, we view the original Klein-Gordon equation as a perturbation of the linear wave equation (LWE)

$$u_{tt} = a^2 u_{xx} - b^2 u, \quad a, b > 0. \tag{5.6.1}$$

Indeed, in any of $H^s(-\ell, \ell)$, $s \in \mathbb{R}$, the collections of functions

$$\phi_n(x) = \frac{1}{\sqrt{2\ell}} e^{i\frac{\pi n}{\ell}x}, \quad n \in \mathbb{Z}, \tag{5.6.2a}$$

$$s_n(x) = \frac{1}{\sqrt{\ell}} \sin \tfrac{\pi n}{\ell} x, \ c_m(x) = \frac{1}{\sqrt{\ell}} \cos \tfrac{\pi m}{\ell} x, \quad n \geq 1, \ m \geq 0. \tag{5.6.2b}$$

provide the complete complex, respectively real, orthogonal bases. We let $\mathcal{A} = (b^2 I - \partial_{xx})^{\frac{1}{2}}$. The operator is bounded and one-to-one as a map from $H^{s+1}(-\ell, \ell) \to H^s(-\ell, \ell)$ and is diagonal in both bases, i.e.

$$\mathcal{A}\phi_n(x) = \omega_n \phi_n(x), \quad \omega_n = \left[b^2 + a^2 \tfrac{\pi n}{\ell} 2\right]^{\frac{1}{2}}, \quad n \in \mathbb{Z}, \tag{5.6.3a}$$

$$\mathcal{A}s_n(x) = \omega_n s_n(x), \ \mathcal{A}c_m(x) = \omega_n c_m(x), \quad n \geq 1, \ m \geq 0. \tag{5.6.3b}$$

For $(u, v) \in H^{s+1}(-\ell, \ell) \times H^s(-\ell, \ell)$, we let $w = \mathcal{A}^{-\frac{1}{2}} v$. In terms of variables (u, w), where $v = u_t$, the problem (5.6.1) reads

$$u_t = \mathcal{A}w, \quad w_t = -\mathcal{A}u. \tag{5.6.4}$$

The problem is Hamiltonian with the Hamiltonian

$$\mathcal{H}(u, w) = \tfrac{1}{2} \|\mathcal{A}^{\frac{1}{2}} u\|_2^2 + \tfrac{1}{2} \|\mathcal{A}^{\frac{1}{2}} w\|_2^2 \tag{5.6.5}$$

and the zeroth order symplectomorphism $J = \begin{pmatrix} 0 & 1 \\ -1 & 0 \end{pmatrix}$.

Below, we are interested in real solutions to (5.6.4). For $(u, w) \in H^s(-\ell, \ell) \times H^s(-\ell, \ell)$, it is convenient to rewrite (5.6.4) in terms of Fourier modes with respect to the real basis $\{s_n, c_n\}_{n\geq 1} \cup \{c_0\}$:

$$u(x,t) = \sum_{n\geq 1} s_n(x)\hat{u}_n(t) + \sum_{n\leq 0} c_n(x)\check{u}_n(t), \tag{5.6.6a}$$

$$w(x,t) = \sum_{n\geq 0} s_n(x)\hat{w}_n(t) + \sum_{n\leq 0} c_n(x)\check{w}_n(t). \tag{5.6.6b}$$

Upon substitution into (5.6.4), we obtain

$$\begin{cases} \frac{d}{dt}\hat{u}_n = \omega_n \hat{w}_n, \\ \frac{d}{dt}\hat{w}_n = -\omega_n \hat{u}_n, \end{cases} \quad \text{and} \quad \begin{cases} \frac{d}{dt}\check{u}_m = \omega_m \check{w}_m, \\ \frac{d}{dt}\check{w}_m = -\omega_m \check{w}_m, \end{cases} \qquad n \geq 1,\ m \geq 0. \tag{5.6.7}$$

Next, we define

$$\hat{I}_n = \hat{u}_n^2 + \hat{w}_n^2,\ \check{I}_n = \check{u}_n^2 + \check{w}_n^2, \quad n \geq 1, m \geq 0$$

and let

$$\begin{cases} \hat{u}_n = (2\hat{I}_n)^{\frac{1}{2}} \cos\hat{\theta}_n, \\ \hat{v}_n = (2\hat{I}_n)^{\frac{1}{2}} \sin\hat{\theta}_n, \end{cases} \quad \text{and} \quad \begin{cases} \check{u}_m = (2\check{I}_n)^{\frac{1}{2}} \cos\check{\theta}_m, \\ \check{v}_m = (2\hat{I}_n)^{\frac{1}{2}} \sin\hat{\theta}_m, \end{cases} \qquad \hat{\theta}_n, \check{\theta}_m \in \mathbb{T}. \tag{5.6.8}$$

In new variables, equation (5.6.4) reads

$$\dot{\hat{I}}_n = 0, \quad \dot{\hat{\theta}}_n = -\omega_n, \quad n \geq 1, \tag{5.6.9a}$$

$$\dot{\check{I}}_m = 0, \quad \dot{\check{\theta}}_m = -\omega_m, \quad m \geq 0. \tag{5.6.9b}$$

Identifying the phase space $H^s(-\ell,\ell)\times H^s(-\ell,\ell)$, with $\ell_2^s\times\mathbb{T}^\infty$, where

$$\begin{aligned}
\ell_2^s &= \Big\{ I=\big(\{\hat{I}_n\}_{n\geq 1},\{\check{I}_m\}_{m\geq 0}\big)\;\big|\;\|I\|_{\ell_2^s}<\infty\Big\}, s\in\mathbb{R},\\
\|I\|_{\ell_2^s}^2 &= \sum_{n\geq 1}\omega_n^{2s}|\hat{I}_n|^2+\sum_{m\geq 0}\omega_m^{2s}|\check{I}_m|^2,\\
\mathbb{T}^\infty &= \Big\{\theta=(\{\hat{\theta}_n\}_{n\geq 1},\{\check{\theta}_m\}_{m\geq 0})\;\big|\;\hat{\theta}_n,\check{\theta}_m\in\mathbb{T}\Big\}
\end{aligned}$$

we see that under the above transformations, problem (5.6.1) is again Hamiltonian and in the new variable, we have

$$\mathcal{H}(I,\theta)=\sum_{n\geq 1}\omega_n\hat{I}_n+\sum_{m\geq 0}\omega_n\check{I}_m. \tag{5.6.10}$$

The quantities I and θ play role of infinite-dimensional action-angle variables that take (5.6.1) to the Birkhoff normal form (5.6.9). The quantities $\frac{\omega_n}{2}\hat{I}_n$ and $\frac{\omega_m}{2}\check{I}_m$ are known as harmonic actions, while $\{\omega_m\}_{m\geq 0}$ are the characteristics frequencies of the system.

It follows from equations (5.6.9) and (5.6.10) that evolution of the linear problem (5.6.1) is essentially a linear motion on the infinite dimensional torus $\mathbb{T}^\infty$, with the frequency vector

$$\Omega=\big(\{\omega_n\}_{n\geq 1},\{\omega_m\}_{m\geq 0}\big).$$

Because each frequency ω_n, $n\geq 1$ appears in Ω twice, the system of frequencies is always resonant and no KAM theory via Kolmogorov-type iterations is possible in principle. The situation is simpler when the periodic boundary conditions are replaced with either odd- or even-periodic boundary conditions. In these cases, either sine or cosine parts of the Fourier series (5.6.6) vanishes, and we have precisely half of the original frequencies. These can be non-resonant and some perturbation analysis is possible (in fact any finite subset of $\{w_n\}_{n>0}$ is shown to be non-resonant for almost values of parameter $\frac{b^2}{a^2}\in\mathbb{R}_+$, see e.g. [15, 25, 7] and discussion there.

It is not difficult to verify that the transformation of the phase space

$$\Phi : \ell_2^s \times \mathbb{T}^\infty \to H^s(-\ell, \ell) \times H^s(-\ell, \ell)$$

that brings (5.6.1) to the Birkhoff canonical form (5.6.9) is analytic in a small complex neighborhood of

$$X = \{(I, \theta) \in \ell_2^s \times \mathbb{T}^\infty | \hat{I}_n, \check{I}_m > 0\}.$$

However, this transformation is not easy to use in the settings of the Hamiltonian perturbation theory, when dealing with the Klein-Gordon equations of the form

$$\begin{cases} u_{tt} = a^2 u_{xx} - b^2 u + \mathcal{V}'(u), \quad x \in (-\ell, \ell) \\ \mathcal{V}'(u) = \mathcal{O}(|u|^2), \end{cases} \tag{5.6.11}$$

near the origin. Most attempts of extending KAM- and Nekhoroshev-type results, reduce the transformation to a finite dimensional subspace $\mathbb{P}_N \times \mathbb{P}_N$ of $H^s(-\ell, \ell) \times H^s(-\ell, \ell)$ and study the dynamics of (5.6.11) near finite dimensional tori $\mathcal{T}^N(I) = \Phi(\{I\} \times \mathbb{T}^N)$, $I \in \mathbb{P}^N$, under the odd-periodic boundary conditions and for the initial data (u_0, w_0) that is close to $\mathcal{T}^N(I)$ when measured in a higher order Sobolev norms (higher than the order s of the original phase space $H^s(-\ell, \ell) \times H^s(-\ell, \ell)$).

In the settings described above and for sufficiently small values of initial data, it is shown that almost all solutions are close to quasi-periodic. Furthermore, depending on the distance from (u_0, v_0) to $\mathbb{P}_n \times \mathbb{P}_n$ measured in a high order Sobolev space, these solutions stay near the origin for times inverse proportional to a power of $\|u_0\|_{H^{s+1}} + \|v_0\|_{H^s}$, see [15, 16]; or for exponentially long periods of time, see [6].

As mentioned above, the approach of [15, 6, 64, 16] based on the Kolmogorov-type iterations does not work in pure periodic settings. In this situation one

has to resort to techniques similar to those employed in [26] or [25].

5.7 Infinite dimensional Nekhoroshev-type theories near the origin

In contrast to the approach considered above, where solutions evolve near finite-dimensional tori $\mathcal{T}^N(I)$, the works [7, 25] deal with near preservation of infinite-dimensional tori

$$\mathbb{T}_\infty = \Phi(\{I\} \times \mathbb{T}^\infty),$$

directly.

In both works, it is demonstrated that if the sequence of the first $N+1$ frequencies $\{\omega_0, \cdots, \omega_N\}$ is non-resonant (see [7, 25] for the concrete details), then for sufficiently large values of the order parameter $s \geq 1$, for sufficiently small values of $\epsilon > 0$ and for data satisfying

$$\|u_0\|_{H^s}^2 + \|w_0\|_{H^s}^2 \leq \epsilon^2, \tag{5.7.1}$$

the solutions to the perturbed equation (5.6.11) remain near the invariant torus

$$\Phi(\{I_0\} \times \mathbb{T}^\infty) = \mathcal{T}^\infty(I_0)$$

of the unperturbed equation (5.6.1) over a period of time proportional to ϵ^{1-N}. In other words, we have

$$\sum_{n\geq 1} |\hat{I}_n(t) - \hat{I}_n(0)|^2 \omega_n^{2s} + \sum_{n\geq 0} |\check{I}_m(t) - \check{I}_m(0)|^2 \omega_m^{2s} \leq C\epsilon^3, \tag{5.7.2}$$

for $0 \leq t \leq \epsilon^{1-N}$.

The significant difference between the latter result and those discussed in the previous section is that we do not assume concentration of the initial data in the first N Fourier modes. As a price to pay, the order $s \geq 1$ appearing in (5.7.1) and (5.7.2) is a function that grows very rapidly with N. In particular, under the assumptions of [7] and [25], we have $s \approx 2^{19}$ and $s \approx 2^9$ respectively, already for $N = 2$.

Qualitatively, equation (5.7.2) implies near conservation of infinite-dimensional tori, while quantitatively, the estimates for s and $\epsilon > 0$ are very pessimistic. As we shall see later, equation (5.7.2) holds for moderate values of s and for relatively large values of $\epsilon > 0$.

To conclude this chapter, we mention that the results in [7] and [25] are obtained using very different techniques. In the first case, the approach is close to the classical Kolmogorov iterations, i.e. the author explicitly constructs a sequence of symplectic transformations that reduce the perturbed Hamiltonian to a nearly Birkhoff canonical form. In the second approach, a family of finite-dimensional Hamiltonian trajectories associated to the truncated perturbed model (5.6.11) is embedded into a time flow of a nonlinear PDE, which is then solved up to a high-order defect.

Chapter 6

Numerical simulations

The purposes of this Chapter are twofold. First, we illustrate the convergence theories developed in Chapters 3 and 4, respectively. This is done in Section 6.1. Second, we investigate numerically the long-time behaviour of the small amplitude numerical solutions near finite-gap tori $\mathcal{T}_{\gamma,\delta}^{n,\varepsilon}(r)$ (Section 6.2) and near infinite dimensional-tori, associated to the linear wave equation (Section 6.3).

6.1 Accuracy in finite time intervals

A bulk of the thesis deals with the analysis of the spatial semi-discretization (3.0.2), however, to produce numerical solutions, (3.0.2) has to be integrated numerically in time. In connection with this, several technical issues arise which are briefly addressed below.

6.1.1 Practical Implementation

Upon semi-discretization (3.0.2), the KGE turns into the semi-linear Cauchy problem of the form

$$U_t = \mathcal{L}U + \mathcal{N}(U), \quad U(0) = U_0, \tag{6.1.1}$$

that has to be integrated numerically in time. In practice, this is done using one of the available time-stepping marching method for ODEs. Since any such method (among other operations) evaluates the vector-field of (6.1.1) several times per each time integration step, the computational cost of this procedure affects the overall efficiency of the numerical code.

In problem (6.1.1), the computational cost of the linear part $\mathcal{L}U$ is minimized in the Fourier space (for then the discrete differentiation operator $\mathcal{L}$ is diagonal), while $\mathcal{N}(U)$ is best computed in the physical space. Both operations require $\mathcal{O}(N)$ flops (floating point operations). Unfortunately, computing the sum $\mathcal{L}U + \mathcal{N}(U)$ requires use of both the direct and the inverse discrete Fourier transforms (see formulas (2.5.5a) and (2.5.5b), respectively). Since the latter operations require at least $\mathcal{O}(N \log_2 N)$ flops, the minimal computational cost of evaluating the right-hand side of (6.1.1) is $\mathcal{O}(N \log_2 N)$.

As the truncation index N increases, the Hamiltonian ODE (6.1.1) becomes extremely stiff, which precludes immediately use of any standard explicit Runge-Kutta solvers. In order to handle stiffness efficiently and to preserve the symplectic structure of the exact flow of (6.1.1), we employ a Strang-type time discretization. To do so, we split the numerical Hamiltonian of (6.1.1) as

$$\mathcal{H}(\bar{u}, \bar{v}) = \tfrac{1}{2}\Big(\langle \bar{v}, \bar{v}\rangle + a^2\langle \nabla\bar{u}, \nabla\bar{u}\rangle\Big) + \int_\Omega \mathcal{I}^2_{2N+1}[\mathcal{V}(\bar{u})] =: \mathcal{H}_1(\bar{u}, \bar{v}) + \mathcal{H}_2(\bar{u}) \tag{6.1.2a}$$

and then replace (6.1.1) with the couple of Hamiltonian equations

$$(\bar{u},\bar{v})_t = \mathcal{J}\nabla\mathcal{H}_1(\bar{u},\bar{v}), \tag{6.1.2b}$$

$$(\bar{u},\bar{v})_t = \mathcal{J}\nabla\mathcal{H}_2(\bar{u}). \tag{6.1.2c}$$

The problems (6.1.2a) and (6.1.2b) have much simpler structure than (6.1.1) and are explicitly integrable. Let Ψ_t^1 and Ψ_t^2 be their exact flows. Then a single time-step of length τ of the Strang-type scheme reads

$$(\bar{u},\bar{v})(t+\tau) = \left[\Psi_{\tau/2}^1 \circ \Psi_\tau^2 \circ \Psi_{\tau/2}^1\right](\bar{u},\bar{v})(t) =: \Phi_\tau(\bar{u},\bar{v})(t). \tag{6.1.3}$$

The discrete flow map $\Phi_\tau(\bar{u},\bar{v})$, defined in (6.1.3), is symmetric and symplectic as symmetric composition of symplectic maps Ψ_t^1 and Ψ_t^2. Furthermore, since we treat the stiff part $\mathcal{L}U$ of (6.1.1) exactly, the method (6.1.3) is A-stable and explicit.

The basic scheme (6.1.3) has classical order $p = 2$, which is too low for our purposes. Fortunately, the spectrum of $\mathcal{L}$ is purely imaginary and hence the convergence order of (6.1.3) can be lifted via the composition technique described in [54]. To be specific, in all our simulations we replace Φ_τ with

$$\Phi_\tau^s = \Phi_{\gamma_1\tau} \circ \cdots \circ \Phi_{\gamma_s\tau}, \tag{6.1.4}$$

where $s = 17$ and

$$\begin{aligned}
&\gamma_1 = \gamma_{17} = 0.13020248308889008087881763, && \gamma_6 = \gamma_{12} = 0.18453964097831570709183254,\\
&\gamma_2 = \gamma_{16} = 0.56116298177510838456196441, && \gamma_7 = \gamma_{11} = 0.25837438768632204729397911,\\
&\gamma_3 = \gamma_{15} = -0.38947496264484728640807860, && \gamma_8 = \gamma_{10} = 0.29501172360931029887096624,\\
&\gamma_4 = \gamma_{14} = 0.15884190655515560089621075, && \gamma_9 = -0.60550853383003451169892108,\\
&\gamma_5 = \gamma_{13} = -0.39590389413323757733623154.
\end{aligned}$$

The theory of [54] guarantee that the resulting A-stable, symplectic and symmetric algorithm (6.1.4) has classical order $p = 8$. Since by construction it is also explicit, a single time-integration step of (6.1.4) requires $\mathcal{O}(N \log_2 N)$ flops, which is in line with the best computational schemes available in the literature.

6.1.2 Simulations

In this section, we use the implementation procedure described above to demonstrate the computational performance of (3.0.2) in finite time intervals with regular input data. To be able to measure the computational accuracy exactly, we run series of tests using the SGE (5.1.1) posed in the real line. In these settings, the SGE is completely integrable and its exact solutions can be constructed via the inverse scattering transform (see e.g. [81] and references therein).

To be specific, we employ a subclass of exact solutions known as n-solitons (see [81])

$$V = (v_{kj})_{k,j=1}^{n}, \quad v_{kj} = \tfrac{c_j}{\lambda_k+\lambda_j} \exp\big(2i\lambda_j x - \tfrac{it}{2\lambda_j}\big), \tag{6.1.5a}$$

$$u = -4 \arg\det(I+V). \tag{6.1.5b}$$

The solutions u given in (6.1.5) describe propagation and non-linear interaction of n travelling waves in $\mathbb{R}$, whose phase shifts and velocities are given by parameters c_j and λ_j, respectively. Directly from (6.1.5) it follows that n-soliton solutions are analytic in a strip containing spatial domain $\mathbb{R}$ and are square integrable there together with their derivatives. Hence, the convergence theories of Chapters 3 and 4 apply.

A single breather scenario. To begin, we study an interaction of a coupled pair of a soliton and an anti-soliton (known as a breather). That is, we compute the initial data using (6.1.5) with $n = 2$,

$$\lambda_1 = \tfrac{2+2i}{\sqrt{8}}, \quad \lambda_2 = \tfrac{-2+2i}{\sqrt{8}}$$

and $c_i = 1$, $i = 1, 2$. In this scenario, the breather components travel at the constant speed of $v = \frac{4|\lambda_i|^2-1}{4|\lambda_i|^2+1} = \frac{3}{5}$ towards the positive direction of x-axis.

The model is numerically simulated in time interval $[0, 10]$, the resulting numerical solution and the corresponding errors are plotted in Fig. 6.1. The figures indicate that an appropriate choice of the domain truncation parameter ℓ yields accurate numerical solutions already for moderate values of the Fourier truncation index N (we used $N = 2^6$ and $\ell = 5 \log_2 N$). In fact, in this scenario the exact solution is analytic near $\mathbb{R}$ and decays exponentially to zero as $x \to \pm\infty$. Hence, the analysis of Chapter 4 applies and we expect geometric convergence. The left-bottom diagram of Fig. 6.1 indicates that this is indeed the case. The $L^2(\mathbb{R})$- and the $L^\infty(\mathbb{R})$-errors decrease geometrically as N increases from 2^3 to 2^8.

The middle-right diagram and the red line in the bottom-left diagram illustrate the conservation properties of (3.0.2), when coupled with the composite Strang-type splitting scheme (6.1.4). Since the first method preserves the Hamiltonicity of the exact KGE model and since the time flow of the second one is symplectic, the variations in the semi-discrete Hamiltonian $\bar{\mathcal{H}}(\bar{u}, \bar{v})$ are uniformly small (of magnitude 10^{-14}) independently of a concrete value of N. The bottom-right diagram of Fig. 6.1 demonstrates the overall computational efficiency of our scheme.

Two breathers interaction scenario. Case I. In our second example, we simulate a collision of a stationary and a moving breathers. The initial data is computed via (6.1.5), with $n = 4$,

$$\lambda_1 = \tfrac{1+i}{\sqrt{8}}, \quad \lambda_2 = \tfrac{-1+i}{\sqrt{8}}, \quad \lambda_3 = \tfrac{2+2i}{\sqrt{8}}, \quad \lambda_4 = \tfrac{-2+2i}{\sqrt{8}}$$

and $c_i = 1$, $i = 1, \ldots, 4$. We keep values for parameters ℓ, N and the time interval unchanged and repeat the simulations of our previous example. The numerical results, shown in Fig. 6.2, are qualitatively the same as in our

first computational example. The analyticity of the exact solution yields geometric decay of the $L^2(\mathbb{R})$- and $L^\infty(\mathbb{R})$-errors, while the semi-discrete total energy $\bar{\mathcal{H}}(\bar{u}, \bar{v})$ is preserved almost exactly.

Two breathers interaction scenario. Case II. In our third example, we let

$$\lambda_3 = \tfrac{3+2i}{\sqrt{8}}, \quad \lambda_4 = \tfrac{-3+2i}{\sqrt{8}}$$

and keep the remaining parameters to be the same as in example two. As evident from Fig. 6.3, the computational results are qualitatively identical to those displayed in Fig. 6.1 and 6.2.

Three breathers interaction scenario. To conclude this section, we use (6.1.5), with $n = 6$,

$$\lambda_1 = \tfrac{1+i}{\sqrt{8}}, \quad \lambda_2 = \tfrac{-1+i}{\sqrt{8}}, \quad \lambda_3 = \tfrac{2+2i}{\sqrt{8}}, \quad \lambda_4 = \tfrac{-2+2i}{\sqrt{8}}, \quad \lambda_5 = \tfrac{3+3i}{\sqrt{8}}, \quad \lambda_6 = \tfrac{-3+3i}{\sqrt{8}},$$

$c_i = 1$, $i = 1, \ldots, 6$. The scenario describes a collision of three moving breathers. Fig. 6.4 one more time confirms that the qualitative behaviour of $L^2(\mathbb{R})$- and $L^\infty(\mathbb{R})$-errors (blue and teal lines, respectively) depends only on the regularity of the input data. In this concrete scenario the input data is analytic near $\mathbb{R}$ and vanishes rapidly as $x \to \pm\infty$. Hence, both errors decay geometrically, in complete agreement with Theorem 4.3.1. As before, the semi-discrete Hamiltonian is nearly preserved thanks to the appropriate choice of the time-stepping marching scheme.

6.2 Long time behaviour near n-gap tori

In this section, we investigate numerically the long-time behavior scheme (3.0.2) near small amplitude finite gap tori $\mathcal{T}^{n,\varepsilon}_{\gamma,\delta}(r)$ discussed in Section 5.5. The real solutions of this type, at least for small values of n, can be found in [11]. Since these solutions are given in terms of $\theta-$function, see (5.3.1), and since the latter involves summation over $\mathbb{Z}^n$, computing them numerically for large values of n is very expensive computationally. In connection with this, see the discussion in [27].

To simplify matters, we provide simulations for 2-gap solutions only. The real solutions of this type are completely described in [34]. In particular, the solutions are given by

$$u(x,y) = \frac{2}{i}\ln\frac{\theta\Big[(0,0)^T,(\frac{1}{2},0)^T\Big](Vx+Wt;B)}{\theta\,(Vx+Wt;B)}, \tag{6.2.1}$$

where $B\in\mathbb{R}^{2\times 2}$ is a symmetric negative definite matrix and

$$\theta\Big[\zeta_1,\zeta_2\Big](z;B) = \sum_{m\in\mathbb{Z}^2} e^{\frac{1}{2}(m+\zeta_1)^T B(m+\zeta_1)+(z+2\pi i\zeta_2)^T(m+\zeta_1)}, \quad \text{where} \quad \zeta_1,\zeta_2\in\mathbb{R}^2.$$

Components of the velocity vectors $V,W\in\mathbb{R}^2$ are given explicitly by

$$V=\frac{\pi i}{2}\begin{pmatrix}0\\ \frac{\Delta}{\sqrt{q_{11}}}\end{pmatrix}, \quad W=\frac{\pi i}{2}\begin{pmatrix}2\sqrt{q_{11}}\\ \frac{q_{12}}{\sqrt{q_{11}}}\end{pmatrix}, \quad \Delta=\sqrt{q_{12}^2-4q_{11}q_{12}}.$$

Quantities q_{ij} are defined explicitly in terms of $\theta-$constants,

$$\hat\theta_{ij}[p_1,p_2] = \partial_{z_iz_j}\theta[(p_1,p_2)^T,(0,0)^T](z;B)\Big|_{z=0}, \quad 1\le i,j\le 2,$$
$$\hat\theta[p_1,p_2] = \theta[(p_1,p_2)^T,(0,0)^T](0;B)$$

by

$$q_{11} = D^{-1} \det \begin{vmatrix} \hat{\theta}[0,0] & \hat{\theta}_{12}[0,0] & \hat{\theta}_{22}[0,0] & 0 \\ 0 & \hat{\theta}_{12}[0,0] & \hat{\theta}_{22}[0,0] & \hat{\theta}[1,0] \\ \hat{\theta}[0,1] & \hat{\theta}_{12}[0,1] & \hat{\theta}_{22}[0,1] & 0 \\ 0 & \hat{\theta}_{12}[1,1] & \hat{\theta}_{22}[1,1] & \hat{\theta}[1,1] \end{vmatrix},$$

$$q_{12} = D^{-1} \det \begin{vmatrix} \hat{\theta}[0,0] & \hat{\theta}_{12}[0,0] & \hat{\theta}_{22}[0,0] & 0 \\ \hat{\theta}[1,0] & 0 & \hat{\theta}_{22}[1,0] & \hat{\theta}[1,0] \\ \hat{\theta}[0,1] & \hat{\theta}_{12}[0,1] & \hat{\theta}_{22}[0,1] & 0 \\ \hat{\theta}_{11}[1,1] & 0 & \hat{\theta}_{22}[1,1] & \hat{\theta}[1,1] \end{vmatrix},$$

$$q_{22} = D^{-1} \det \begin{vmatrix} \hat{\theta}[0,0] & \hat{\theta}_{12}[0,0] & \hat{\theta}_{22}[0,0] & 0 \\ \hat{\theta}[1,0] & \hat{\theta}_{1,2}[1,0] & 0 & \hat{\theta}[1,0] \\ \hat{\theta}_{11}[0,1] & \hat{\theta}_{12}[0,1] & \hat{\theta}[0,1] & 0 \\ \hat{\theta}_{11}[1,1] & \hat{\theta}_{12}[1,1] & 0 & \hat{\theta}[1,1] \end{vmatrix},$$

$$D = \det \begin{vmatrix} \hat{\theta}_{11}[0,0] & \hat{\theta}_{12}[0,0] & \hat{\theta}_{22}[0,0] & \hat{\theta}[0,0] \\ \hat{\theta}_{11}[1,0] & \hat{\theta}_{12}[1,0] & \hat{\theta}_{22}[1,0] & \hat{\theta}[1,0] \\ \hat{\theta}_{11}[0,1] & \hat{\theta}_{12}[0,1] & \hat{\theta}_{22}[0,1] & \hat{\theta}[0,1] \\ \hat{\theta}_{11}[1,1] & \hat{\theta}_{12}[1,1] & \hat{\theta}_{22}[1,1] & \hat{\theta}[1,1] \end{vmatrix},$$

see [34] for further details.

By Theorem 5.5.1, small perturbations of the SGE yield a family of quasi-periodic solutions [64] that fill up a KAM torus $\mathcal{T}^{n,\varepsilon}_{\gamma,\delta}(r)$ of the perturbed equation (3.0.2). It is important to note that in simulations, numerical solutions evolve in the finite-dimensional subspace $\mathbb{P}^n \times \mathbb{P}^n$ of the infinite dimensional phase space $H^{s+1}(-\ell,\ell) \times H^s(-\ell,\ell)$. Since the KAM tori are not contained in $\mathbb{P}^n \times \mathbb{P}^n$, the numerical solutions are not quasi-periodic in general. However, if the KAM tori are linearly stable, we expect the drift of numerical solutions from these tori to be very slow.

To study this drift numerically, we observe that the actions on the original unperturbed finite gap SGE tori $\mathcal{T}^n_{\gamma,\delta}(r)$ are given by gaps in the spectrum of the Lax operator $\mathcal{L}_{(u,v)}$, see the discussion in Section 5.2. Consequently, the distance between the unperturbed spectral gap and the spectral gap of operator $\mathcal{L}_{(u,v)}$ associated with the quasi-periodic KAM solutions on $\mathcal{T}^{n,\varepsilon}_{\gamma,\delta}(r)$ remains bounded for all times (again see [64] and our discussion in Section 5.5). Hence, the growth of this difference can serve as a measure of the drift of the semidiscrete numerical solutions away from the KAM tori $\mathcal{T}^{n,\varepsilon}_{\gamma,\delta}(r)$ of Section 5.5.

Example 1. In our first numerical example, we solve numerically the SGE (5.1.1) using $N = 2^6$ Fourier modes. Initial data u_0 is obtained by formula (6.2.1), with $B = -A^2$, where

$$A = 1.2 \begin{pmatrix} 2 & 0 \\ 1 & 2 \end{pmatrix}.$$

The data gives a quasi-periodic 2-gap solution of (5.1.1) in $(-\ell, \ell)$,

$$\ell = \frac{4\sqrt{q_{11}}}{\Delta}.$$

The spectral gaps occur at the eigenvalues μ^-_{-1}, μ^-_0 and μ^+_0, μ^+_1 of the Lax operator $\mathcal{L}_{(u,v)}$, see Section 5.2.

As predicted by the calculations in [75], the set $\{\mu^-_{-1}, \mu^-_0, \mu^+_0, \mu^+_1\}$ of eigenvalues is closed under reflection and complex conjugation. Accordingly, to demonstrate the long term behaviour of the semidiscrete numerical solutions given by (3.0.2), we plot $|\mu^+_0(u,v) - \mu^+_0(\bar{u},\bar{v})|$, where $\mu^+_0(u,v)$ and $\mu^+_0(\bar{u},\bar{v})$ are eigenvalues of $\mathcal{L}_{(u,v)}$ and $\mathcal{L}_{(\bar{u},\bar{v})}$, respectively. Further, since the problem is Hamiltonian, we plot also $|\mathcal{H}(u,v) - \mathcal{H}(\bar{u},\bar{v})|$.

The results of simulations in the large time interval $[0, 10^4]$ are shown in Figure 6.5. The errors remain very small for all $t \in [0, 10^4]$, see the first two diagrams of Figure 6.5. The slow linear growth in $|\mathcal{H}(u, v) - \mathcal{H}(\bar{u}, \bar{v})|$ and $|\mu_0^+(u, v) - \mu_0^+(\bar{u}, \bar{v})|$ describes a drift away from a KAM torus when solving the SGE using initial data that is not precisely sitting on the KAM torus. However, the drifts in μ_0^+ and $\mathcal{H}$ are very slow, indicating the linear stability of the associated KAM torus. Qualitatively, the numerical solutions are almost quasi-periodic in the computational domain.

To provide further illustration of the numerical Lax spectrum behaviour, we magnified the bottom-right diagram of Figure 6.5. Figure 6.6 indicates that the drift $|\mu_0^+(u, v) - \mu_0^+(\bar{u}, \bar{v})|$ behaves as a superposition of a quasi-periodic and a linear motions.

The qualitative behaviour of numerical solutions observed in Figures 6.5 and 6.6 is in fact generic. To illustrate this phenomenon, we repeated simulations several times using different values for the matrix parameter B.

Example 2. In the second example, we repeated the simulation with a slight variation in B. That is we let $B = -A^2$, where

$$A = 1.5 \begin{pmatrix} 2 & 0 \\ 1 & 2 \end{pmatrix}.$$

We use the same values for parameters ℓ and N and the same time interval $[0, 10^4]$. As before, the spectral gaps occur at the eigenvalues μ_{-1}^-, μ_0^-, μ_0^+, and μ_1^+ of the Lax operator $\mathcal{L}_{(u,v)}$. Figure 6.7 demonstrates a drift away from the KAM tori when solving the SGE numerically. As in our previous example, the drift in μ_0^+ and $\mathcal{H}$ is very slow, indicating the stability of the associated KAM torus. Figure 6.8 presents a closer look of at the evolution of $|\mu_0^+(u, v) -$

$\mu_0^+(\bar{u},\bar{v})|$. One can clearly see that qualitative behaviour $|\mu_0^+(u,v)-\mu_0^+(\bar{u},\bar{v})|$ is the same as observed in Figure 6.6.

We repeated simulations of Examples 1 and 2 using $B=-A_i^2; i=1,\cdots,4$,

$$A_1 = 1.8\begin{pmatrix} 1 & 1 \\ -1 & 2 \end{pmatrix}, \quad A_2 = 2.2\begin{pmatrix} 1 & 1 \\ -1 & 2 \end{pmatrix},$$
$$A_3 = 0.8\begin{pmatrix} 3 & 1 \\ -2 & 2 \end{pmatrix}, \quad A_4 = 1.0\begin{pmatrix} 3 & 1 \\ -2 & 2 \end{pmatrix}$$

The results of simulations are shown in Figures 6.9 – 6.16. Each simulation produces qualitatively identical results.

6.3 Long time preservation of harmonic actions

In this section, we explore long-time behaviour of small amplitude solution to the KGE with smooth potentials $\mathcal{V}(u)$ of the form

$$\mathcal{V}(u) = au^2 + bu^3 + \mathcal{O}(u^4). \tag{6.3.1}$$

As explained in Sections 5.6–5.7, in this case KGE can be viewed as a small Hamiltonian perturbation of the linear wave equation (5.6.1). In these settings, we expect the harmonic actions to be nearly preserved over very long time intervals, see the discussion in Sections 5.6–5.7. As mentioned earlier, the Birkhoff-normal form approach of [15, 6, 64, 16] works only in even-/odd-periodic settings, while general periodic boundary conditions require totally different approach, see [25]. Nevertheless, qualitatively, we expect the same long-time behaviour in each of these cases. To demonstrate this phenomenon,

we present simulations for each of these three boundary conditions. As specific potentials that satisfy (6.3.1), we take

- $\mathcal{V}(u) = \frac{b^2}{2}u^2 + c(1-\cos u)$ (the SGE scenario);
- $\mathcal{V}(u) = \frac{b^2}{2}u^2 + \frac{cu^3}{3}$ (the KGE scenario with cubic potential);
- $\mathcal{V}(u) = \frac{b^2}{2}u^2 + c(1-\cos u) + d(1-\frac{\cos 2u}{2})$ (the double SGE scenario);
- $\mathcal{V}(u) = \frac{b^2}{2}u^2 + c(\cosh u - 1)$ (the Hyperbolic SGE (HSGE)).

The SGE scenario. To begin, we consider the SGE subject to one of the following initial conditions

$$u_0(x) = \sin\left(\sin\left(\frac{\pi}{\ell}x\right) + \cos\left(\frac{\pi}{\ell}x\right)\right), \quad v_0(x) = \cos\left(\frac{\pi}{\ell}x\right), \tag{6.3.2a}$$

$$u_0(x) = \epsilon\left(1 - \left(\frac{x^2}{\ell^2}\right)^2\right), \quad v_0(x) = 0, \tag{6.3.2b}$$

$$u_0(x) = \epsilon x\left(1 - \left(\frac{x^2}{\ell^2}\right)^2\right), \quad v_0(x) = 0, \tag{6.3.2c}$$

that respectively correspond to periodic/even-periodic/odd-periodic scenarios. Further, we let $\epsilon = 0.1$, $\ell = \pi$, $N = 2^6$ and $t \in [0, 10^4]$. The variation in the first six harmonic actions associated to numerical solution $(\bar{u}, \bar{v})$ are depicted in Figures 6.17–6.19. We can clearly see that higher is the frequency, smaller is the relative error in the corresponding action.

This behaviour is in complete agreement with the perturbation theory of [15, 25, 7] discussed in Section 5.6. The qualitative behavior of numerical solutions observed in Figures 6.17–6.19 is, in fact, generic. To illustrate

this phenomenon, we repeated simulations several times using the remaining potentials mentioned above.

The KGE scenario with cubic potential. We apply the same initial conditions (6.3.2) to the KGE (1.1.1) with potential $\mathcal{V}(u) = \frac{b^2}{2}u^2 + \frac{c}{3}u^3$ where $b, c \in \mathbb{R}$. We used the same values for parameters ℓ and N and the same time interval $[0, 10^4]$ as in the first example. The long-time behavior of the harmonic actions is shown in Figures 6.20–6.22. The qualitative behavior observed is similar to that of Figures 6.17–6.19.

We repeated simulations of the first two examples using the remaining two potentials. The double SGE settings (Figures 6.23–6.25) and the HSGE potential (Figures 6.26–6.28) yield results similar to those observed in Figures 6.17–6.22.

The harmonic actions are nearly preserved over very long time intervals. The deviations of the numerically computed actions from their initial positions are getting smaller as the corresponding frequencies increase. The behaviour of the harmonic actions is qualitatively the same for even-, odd- and periodic boundary conditions. It is worth mentioning that in all our simulations, we used relatively large value of ϵ that controls the size of our data and relatively small value of N, that controls the size of the perturbation $(\mathcal{I} - \mathcal{I}_n)\mathcal{V}(u)$. Nevertheless, in all computational scenarios, long time dynamics of numerical solutions is rather regular and fits well within the framework of the perturbation theory discussed in Sections 5.6–5.7. Hence, we have strong numerical evidences that quantitative estimates for the parameters s and N are far from being realistic. In other words, the KAM and Nechoroshev theories require significant refinements.

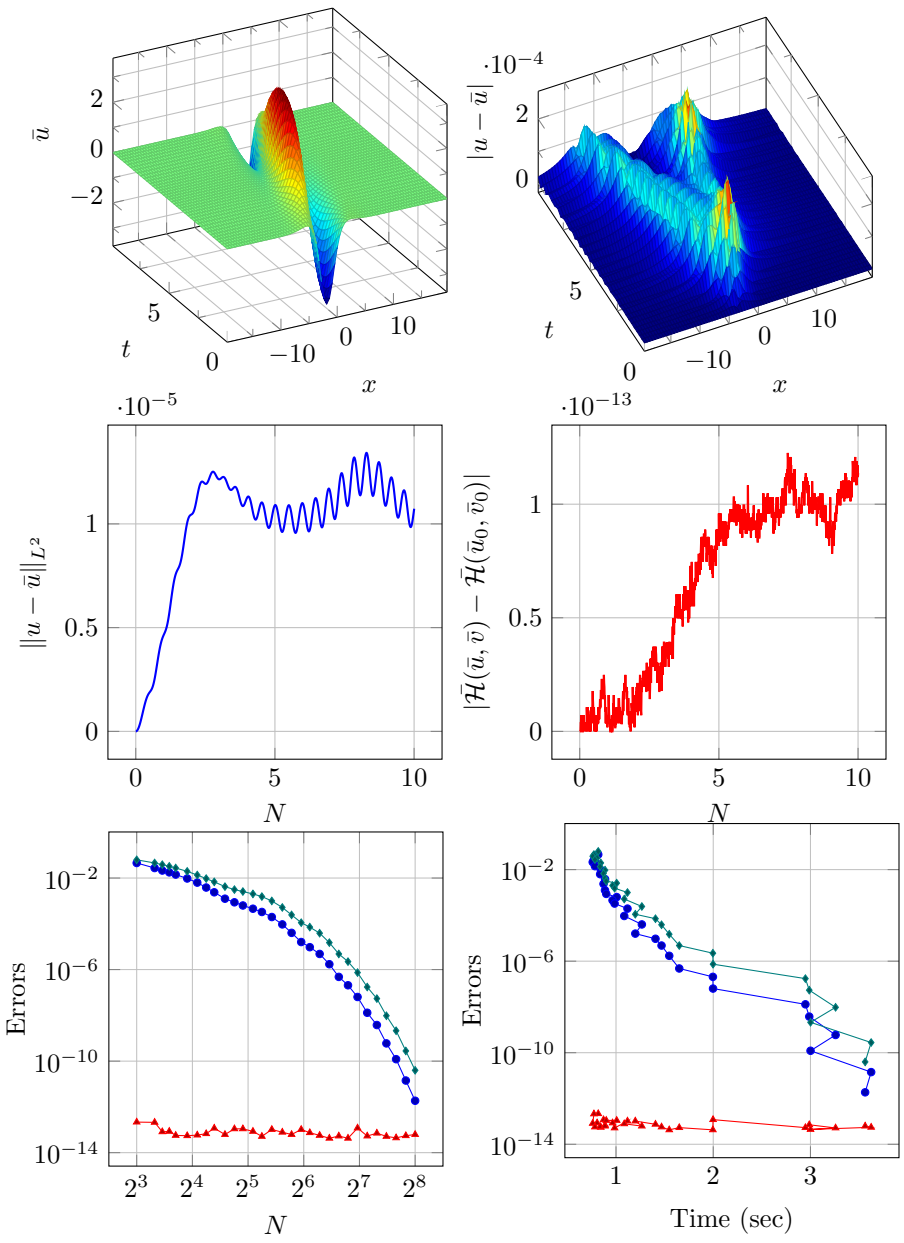

Figure 6.1: A single breather scenario. The top row, $N = 2^6$: the numerical solution $\bar{u}$ (left), the pointwise error $|u - \bar{u}|$ (right). The middle row, $N = 2^6$: the L^2-error $\|u - \bar{u}\|_{L^2}$ evolution (left), error in the total energy $|\bar{\mathcal{H}}(\bar{u}, \bar{v}) - \bar{\mathcal{H}}(\bar{u}_0, \bar{v}_0)|$ (right). The bottom row: the accuracy as a function of N (left); the accuracy as a function of execution time (right).

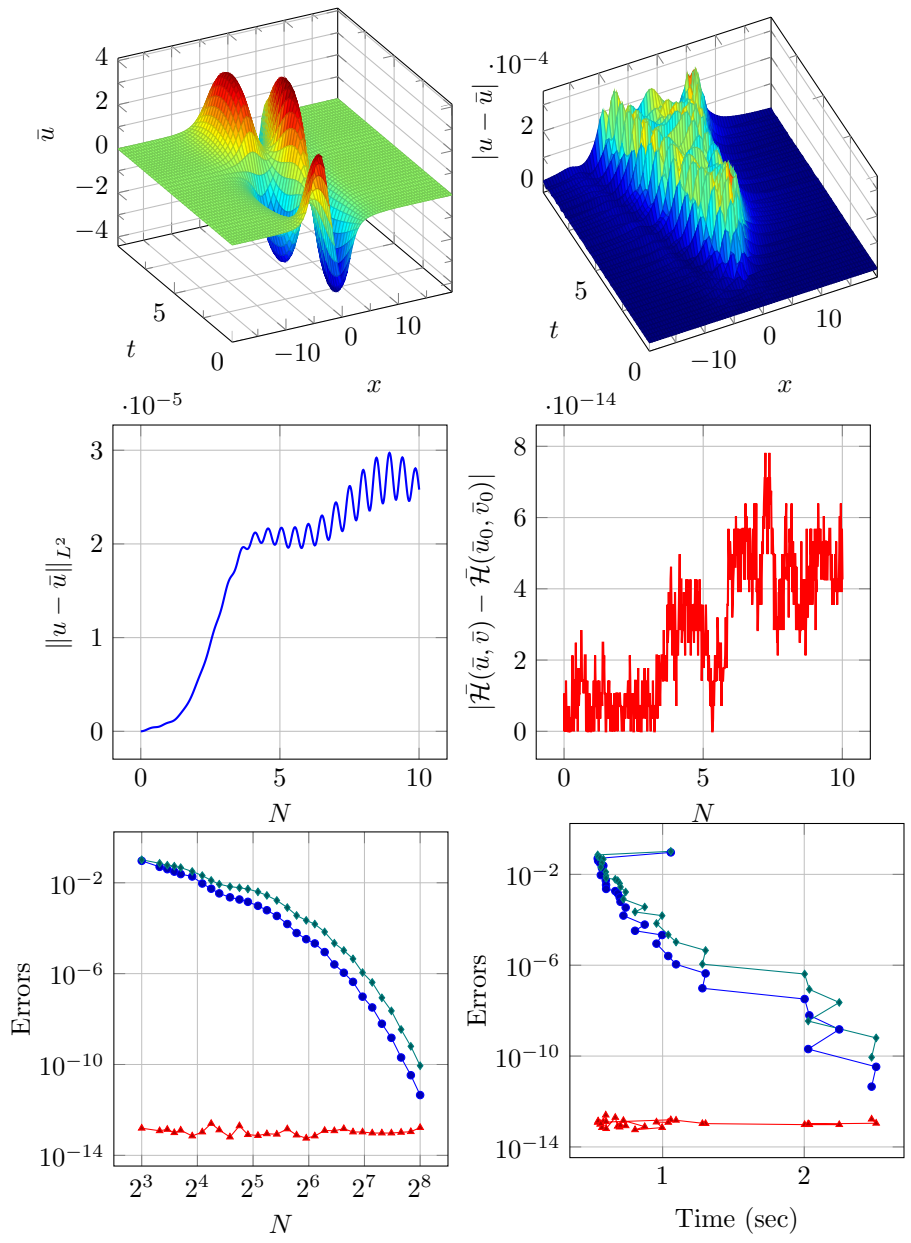

Figure 6.2: Two breathers interaction scenario. Case I. The top row, $N = 2^6$: the numerical solution $\bar{u}$ (left), the pointwise error $|u-\bar{u}|$ (right). The middle row, $N = 2^6$: the L^2-error $\|u-\bar{u}\|_{L^2}$ evolution (left), error in the total energy $|\mathcal{H}(\bar{u},\bar{v})-\mathcal{H}(\bar{u}_0,\bar{v}_0)|$ (right). The bottom row: the accuracy as a function of N (left); the accuracy as a function of execution time (right).

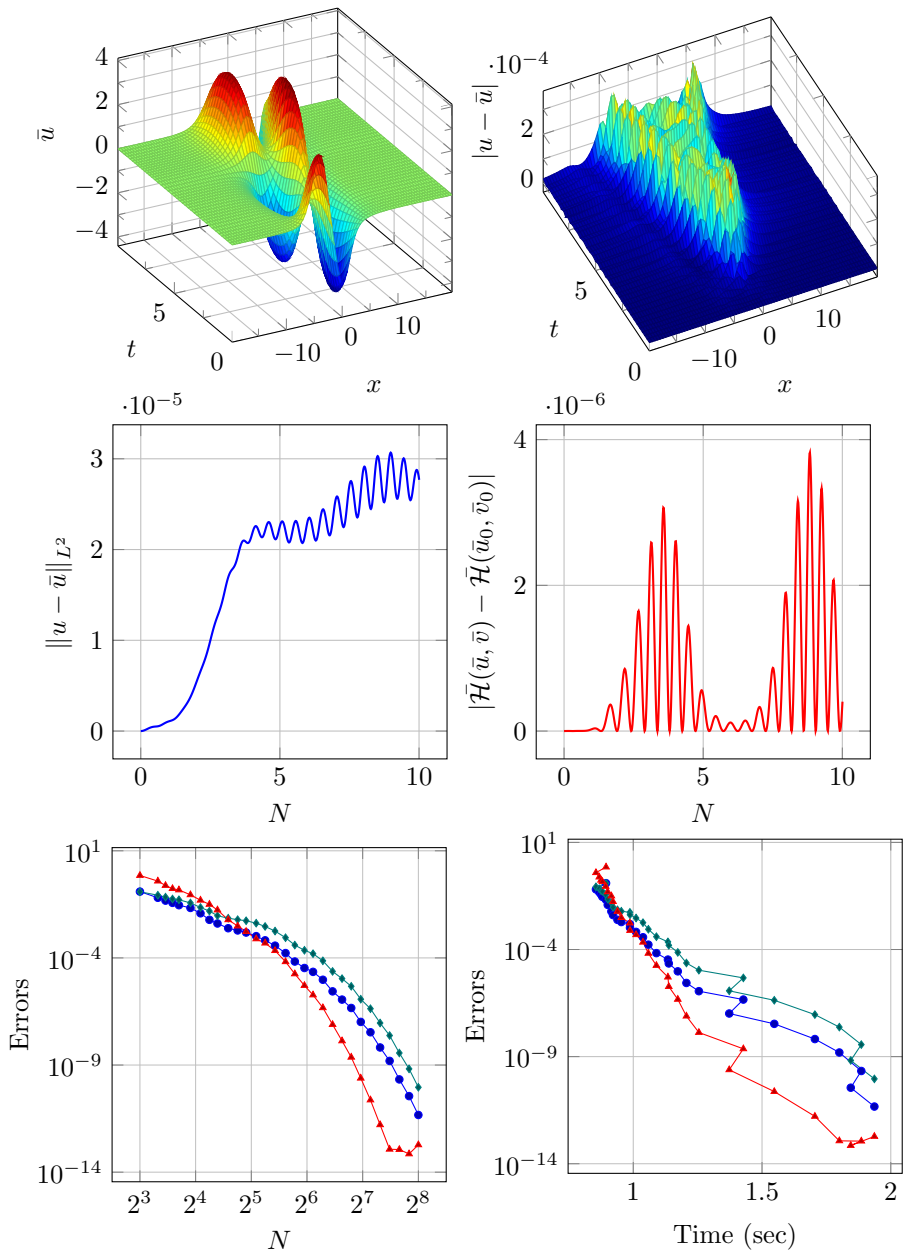

Figure 6.3: Two breathers interaction scenario. Case II. The top row, $N = 2^6$: the numerical solution $\bar{u}$ (left), the pointwise error $|u - \bar{u}|$ (right). The middle row, $N = 2^6$: the L^2-error $\|u - \bar{u}\|_{L^2}$ evolution (left), error in the total energy $|\bar{\mathcal{H}}(\bar{u}, \bar{v}) - \bar{\mathcal{H}}(\bar{u}_0, \bar{v}_0)|$ (right). The bottom row: the accuracy as a function of N (left); the accuracy as a function of execution time (right).

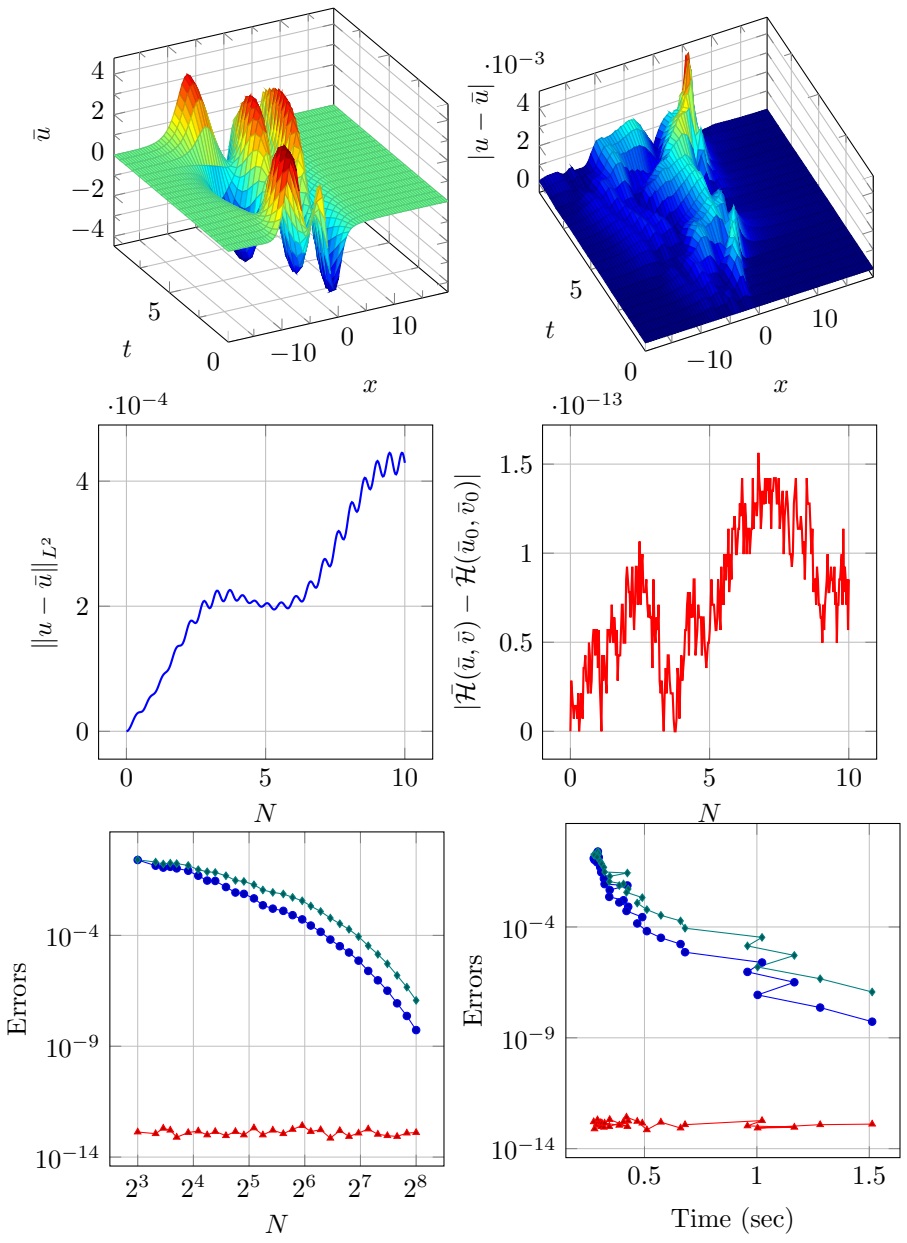

Figure 6.4: Three breathers interaction scenario. The top row, $N = 2^6$: the numerical solution $\bar{u}$ (left), the pointwise error $|u - \bar{u}|$ (right). The middle row, $N = 2^6$: the L^2-error $\|u-\bar{u}\|_{L^2}$ evolution (left), error in the total energy $|\mathcal{H}(\bar{u},\bar{v}) - \mathcal{H}(\bar{u}_0,\bar{v}_0)|$ (right). The bottom row: the accuracy as a function of N (left); the accuracy as a function of execution time (right).

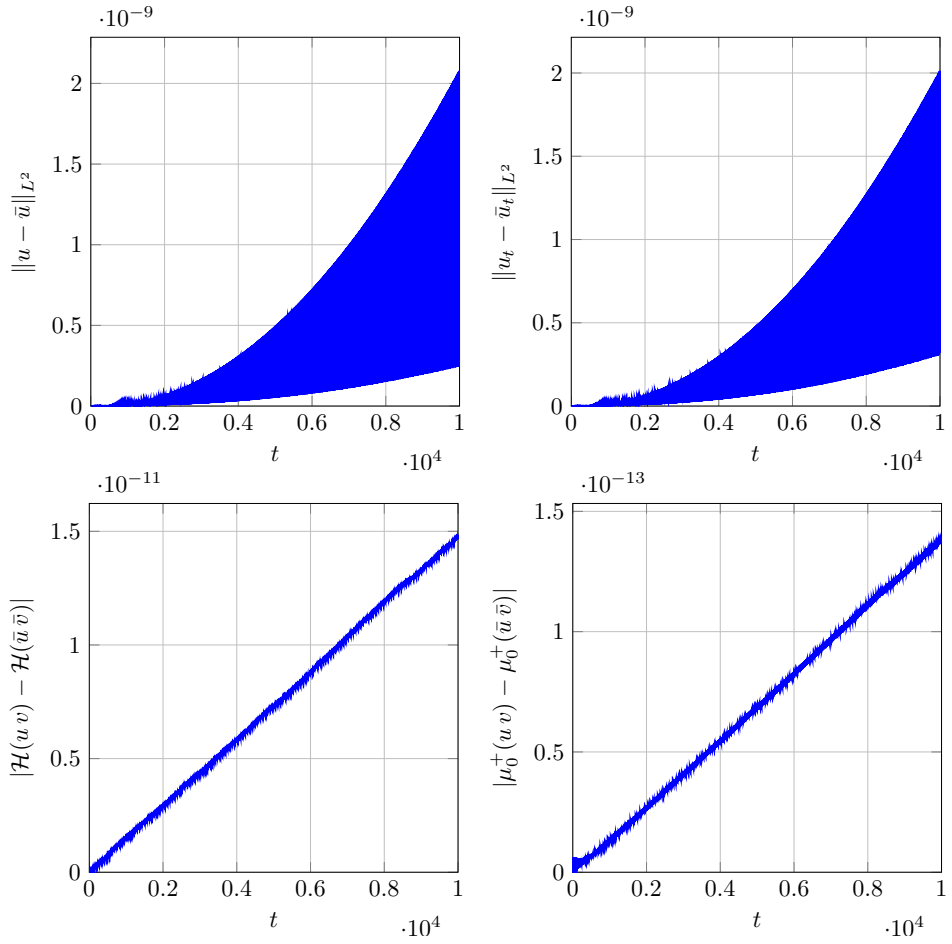

Figure 6.5: The long-time behavior of our semidiscretization method for initial conditions associated with small finite gap solutions to the SGE (left to right and top to bottom): $\|u - \bar{u}\|_{L^2}$, $\|u_t - \bar{u}_t\|_{L^2}$, $|\mathcal{H}(u, v) - \mathcal{H}(\bar{u}, \bar{v})|$, $|\mu_0^+(u, v) - \mu_0^+(\bar{u}, \bar{v})|$, with $N = 2^6$.

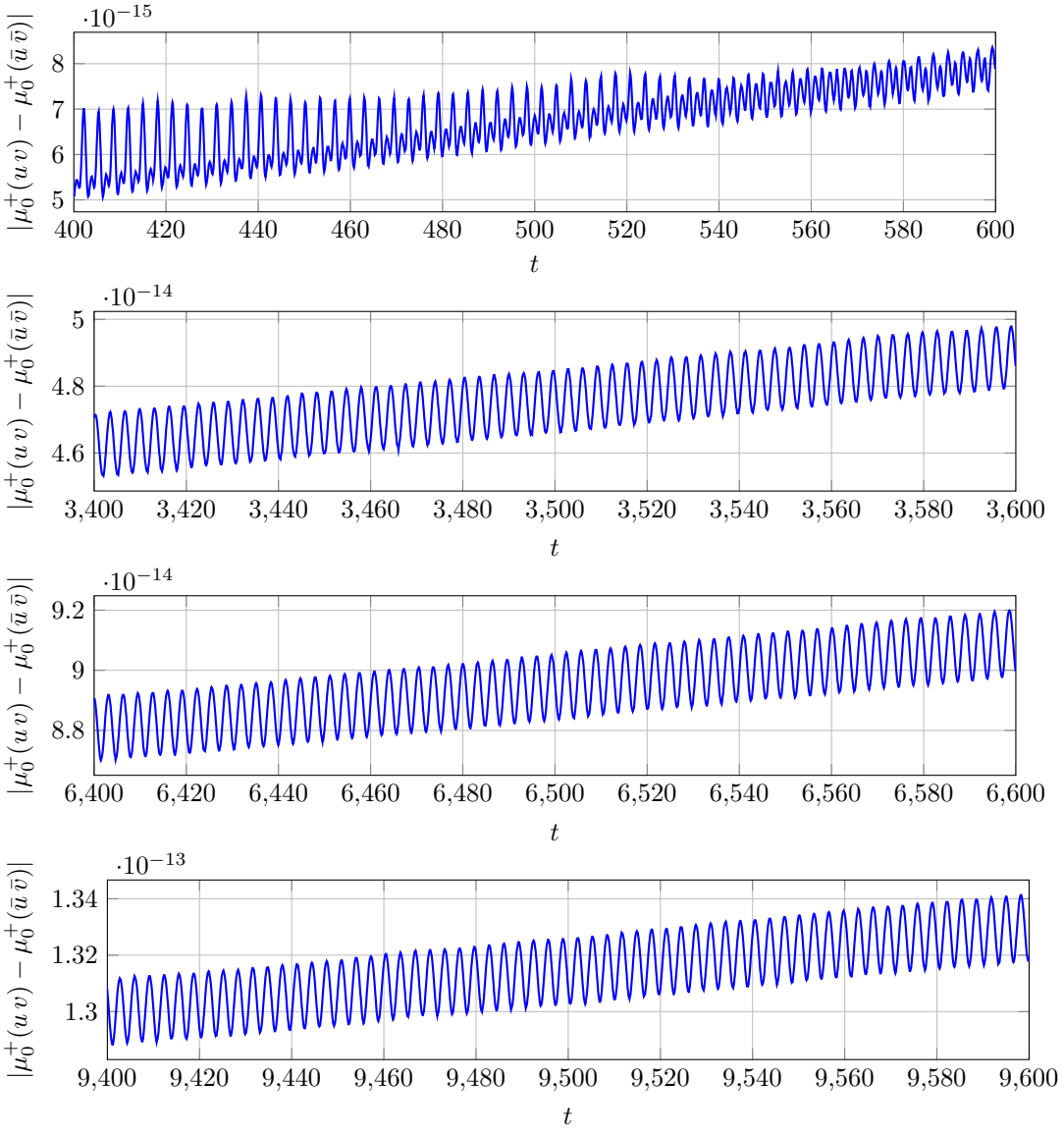

Figure 6.6: Long time dynamics of $|\mu_0^+(u,v) - \mu_0^+(\bar{u},\bar{v})|$ as a function of time.

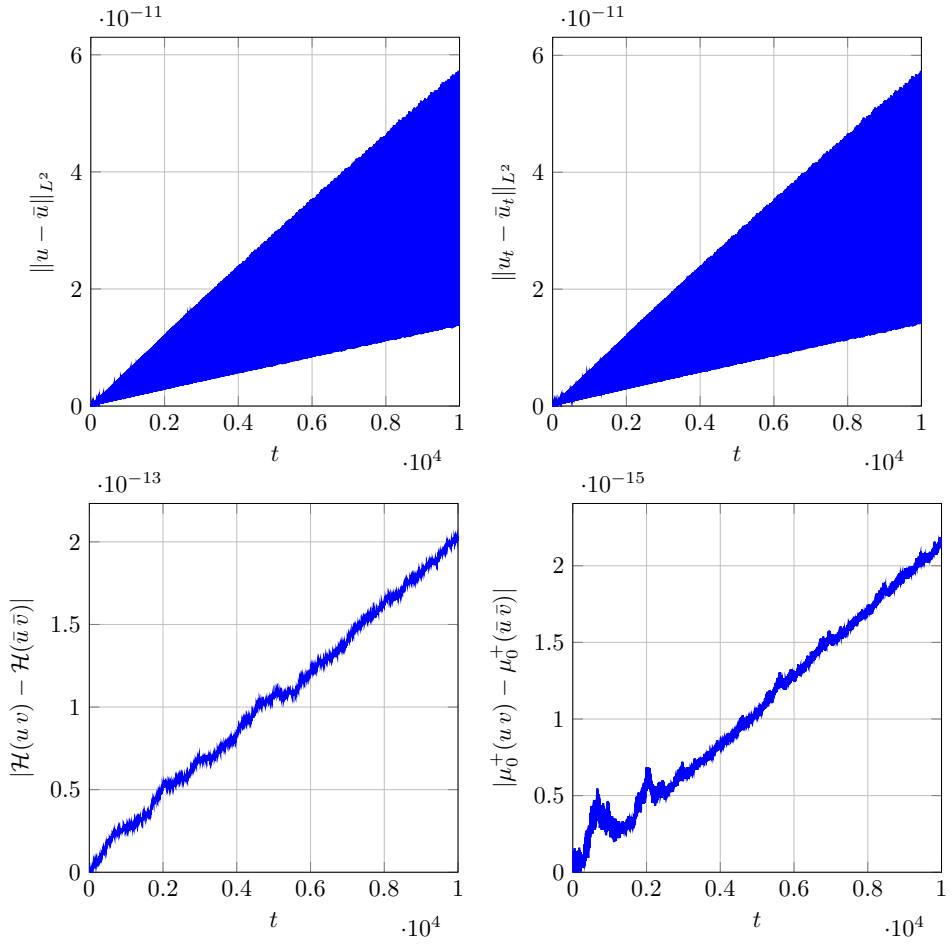

Figure 6.7: The long-time behavior of our semidiscretization method for initial conditions associated with small finite gap solutions to the SGE (left to right and top to bottom): $\|u - \bar{u}\|_{L^2}$, $\|u_t - \bar{u}_t\|_{L^2}$, $|\mathcal{H}(u, v) - \mathcal{H}(\bar{u}, \bar{v})|$, $|\mu_0^+(u, v) - \mu_0^+(\bar{u}, \bar{v})|$, with $N = 2^6$.

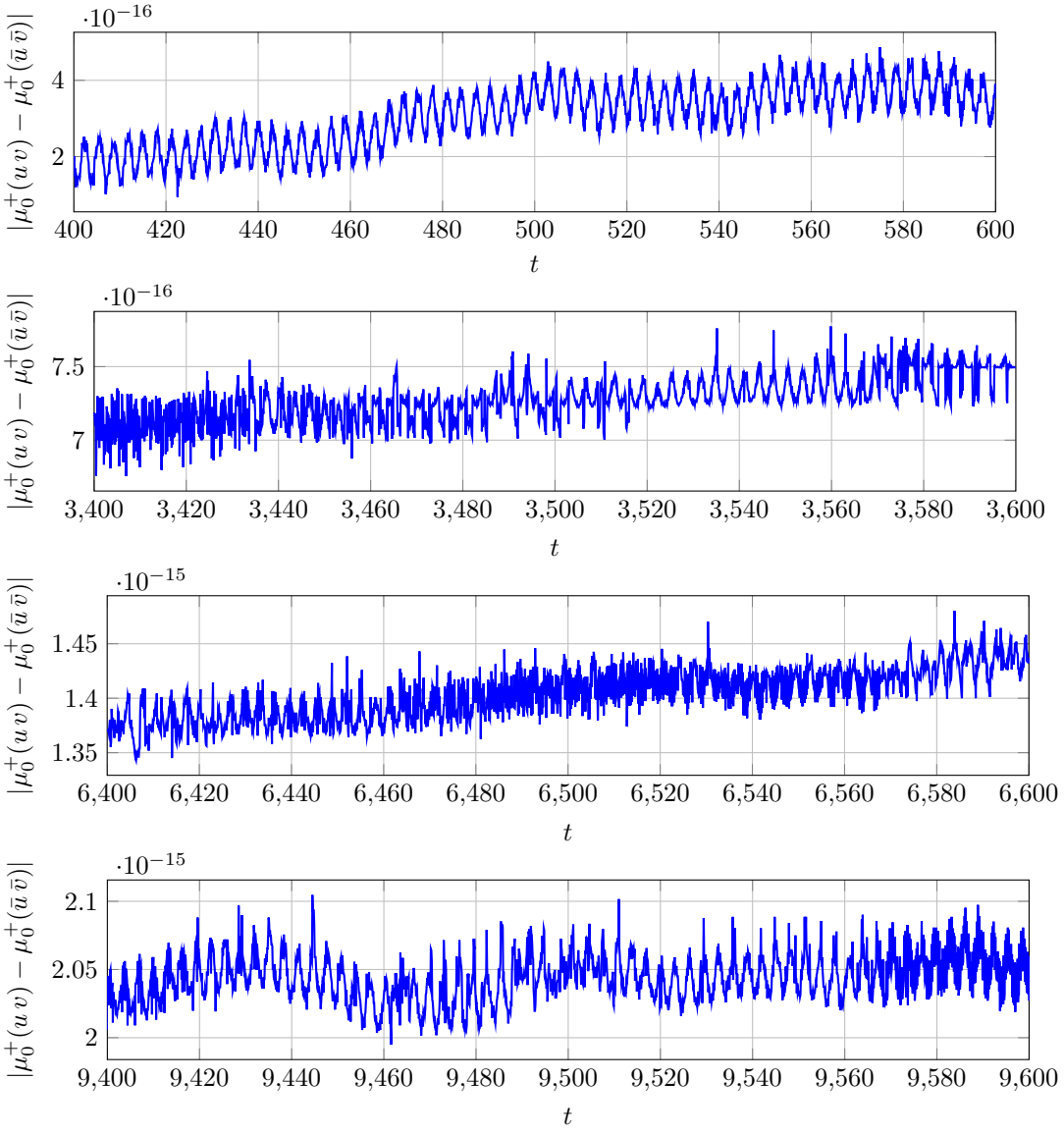

Figure 6.8: Long time dynamics of $|\mu_0^+(u,v) - \mu_0^+(\bar{u},\bar{v})|$ as a function of time.

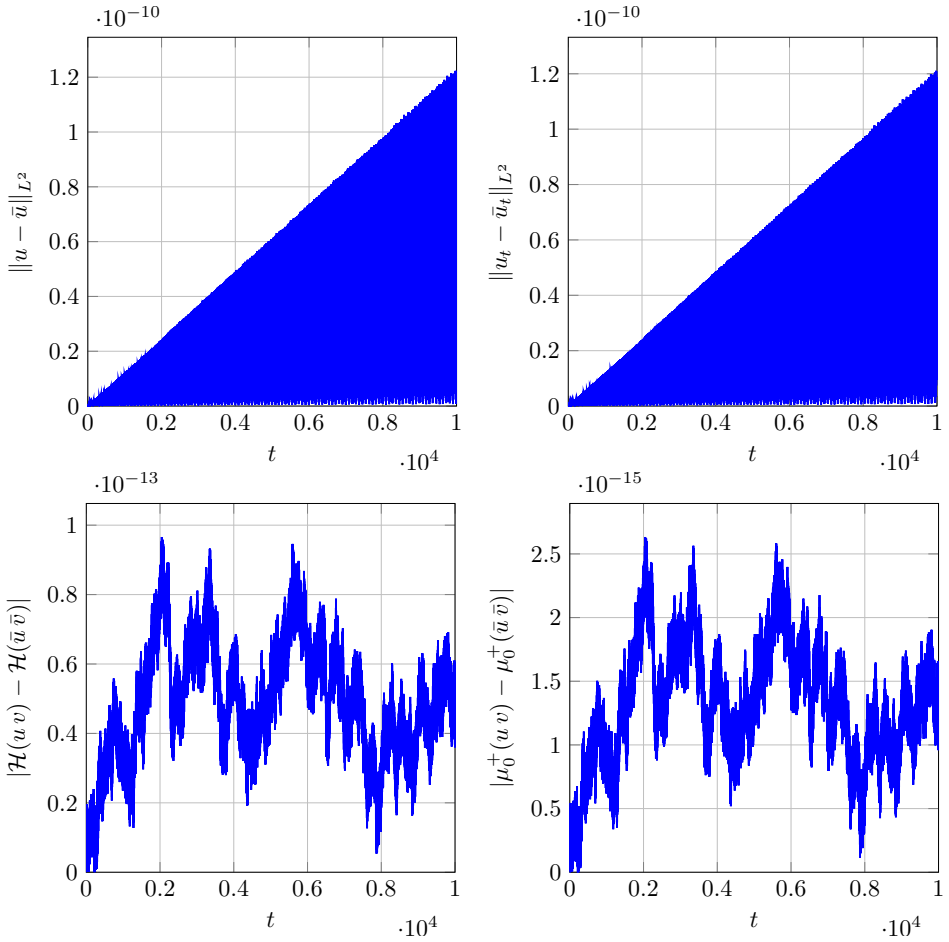

Figure 6.9: The long-time behavior of our semidiscretization method for initial conditions associated with small finite gap solutions to the SGE (left to right and top to bottom): $\|u - \bar{u}\|_{L^2}$, $\|u_t - \bar{u}_t\|_{L^2}$, $|\mathcal{H}(u, v) - \mathcal{H}(\bar{u}, \bar{v})|$, $|\mu_0^+(u, v) - \mu_0^+(\bar{u}, \bar{v})|$, with $N = 2^6$.

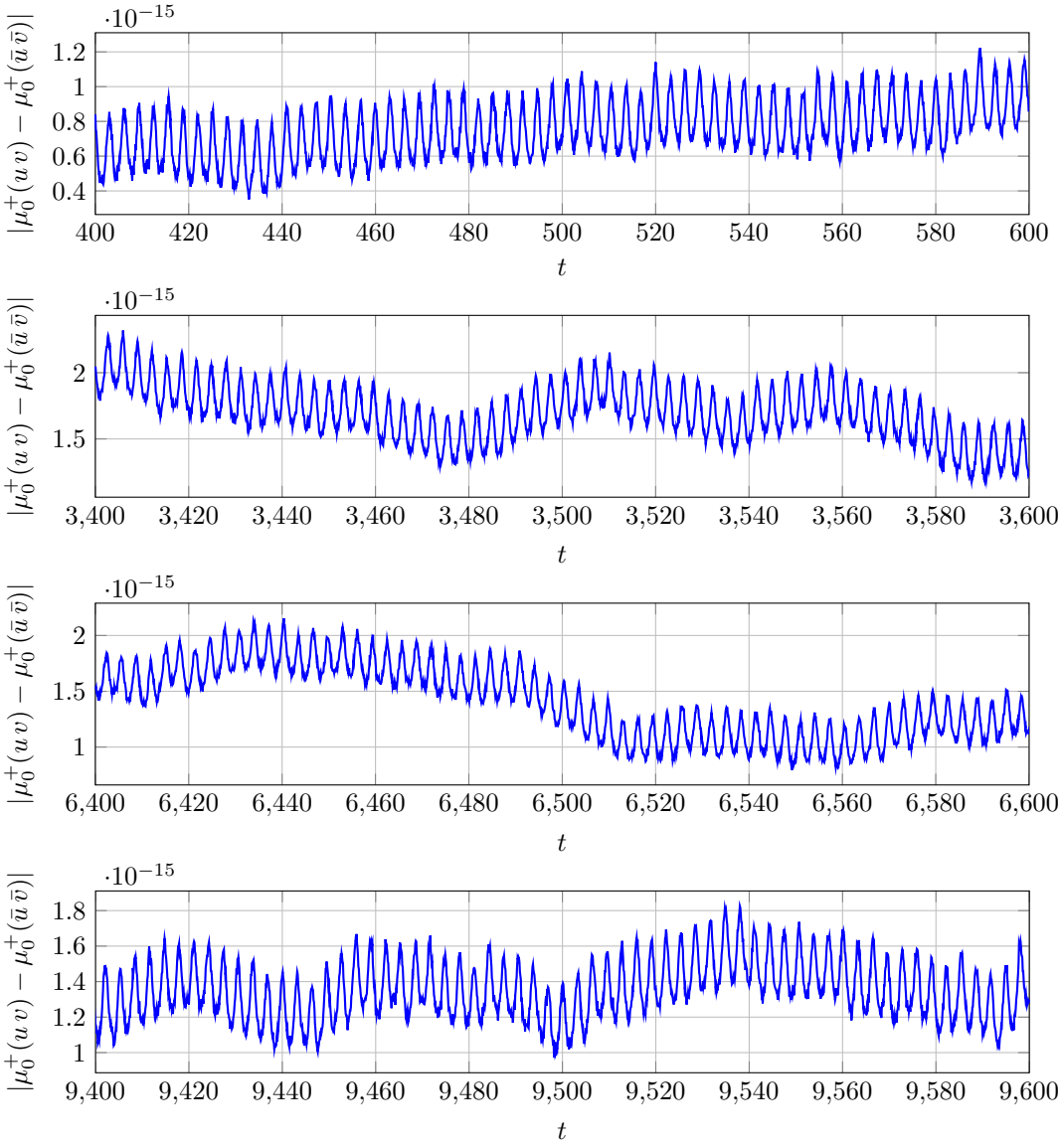

Figure 6.10: Long time dynamics of $|\mu_0^+(u,v) - \mu_0^+(\bar{u},\bar{v})|$ as a function of time.

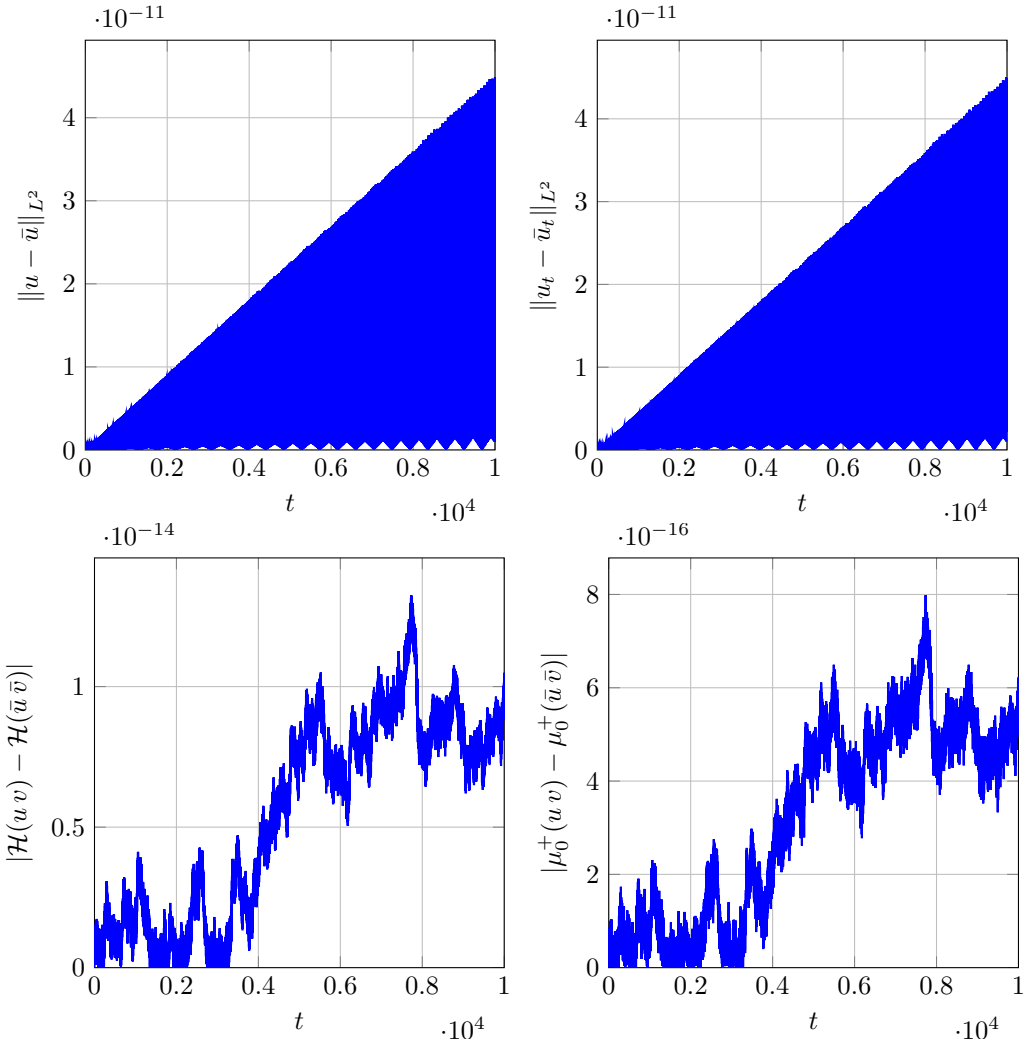

Figure 6.11: The long-time behavior of our semidiscretization method for initial conditions associated with small finite gap solutions to the SGE (left to right and top to bottom): $\|u - \bar{u}\|_{L^2}$, $\|u_t - \bar{u}_t\|_{L^2}$, $|\mathcal{H}(u, v) - \mathcal{H}(\bar{u}, \bar{v})|$, $|\mu_0^+(u, v) - \mu_0^+(\bar{u}, \bar{v})|$, with $N = 2^6$.

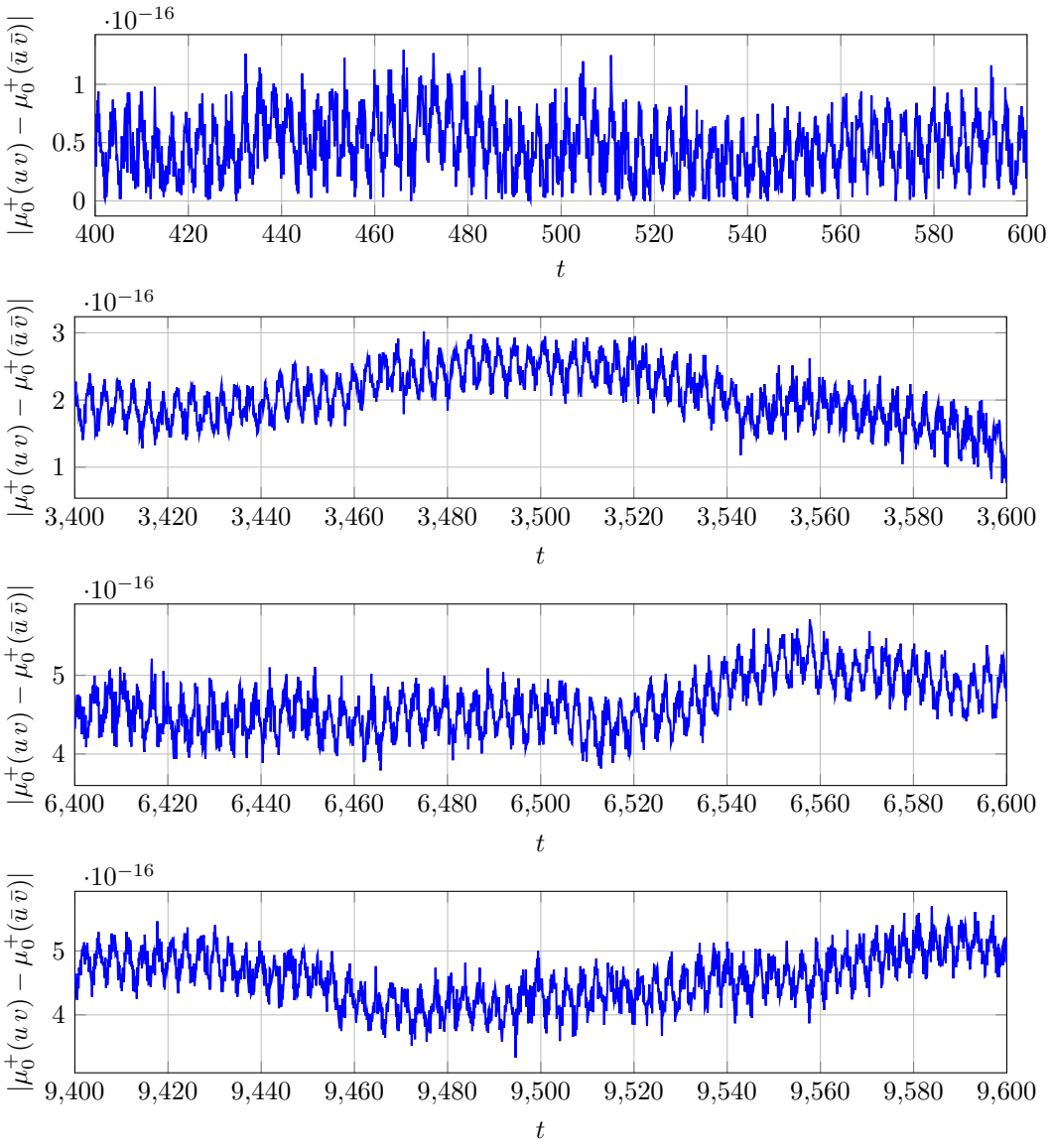

Figure 6.12: Long time dynamics $|\mu_0^+(u,v) - \mu_0^+(\bar{u},\bar{v})|$ as a function of time.

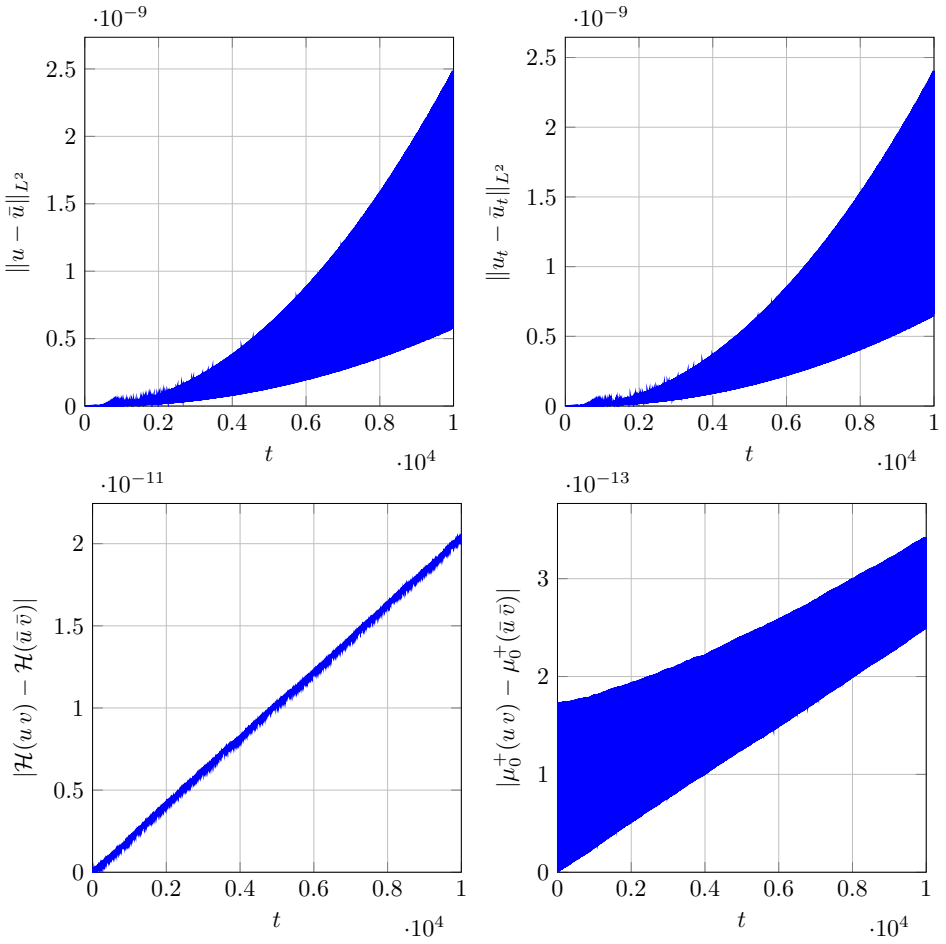

Figure 6.13: The long-time behavior of our semidiscretization method for initial conditions associated with small finite gap solutions to the SGE (left to right and top to bottom): $\|u - \bar{u}\|_{L^2}$, $\|u_t - \bar{u}_t\|_{L^2}$, $|\mathcal{H}(u, v) - \mathcal{H}(\bar{u}, \bar{v})|$, $|\mu_0^+(u, v) - \mu_0^+(\bar{u}, \bar{v})|$, with $N = 2^6$.

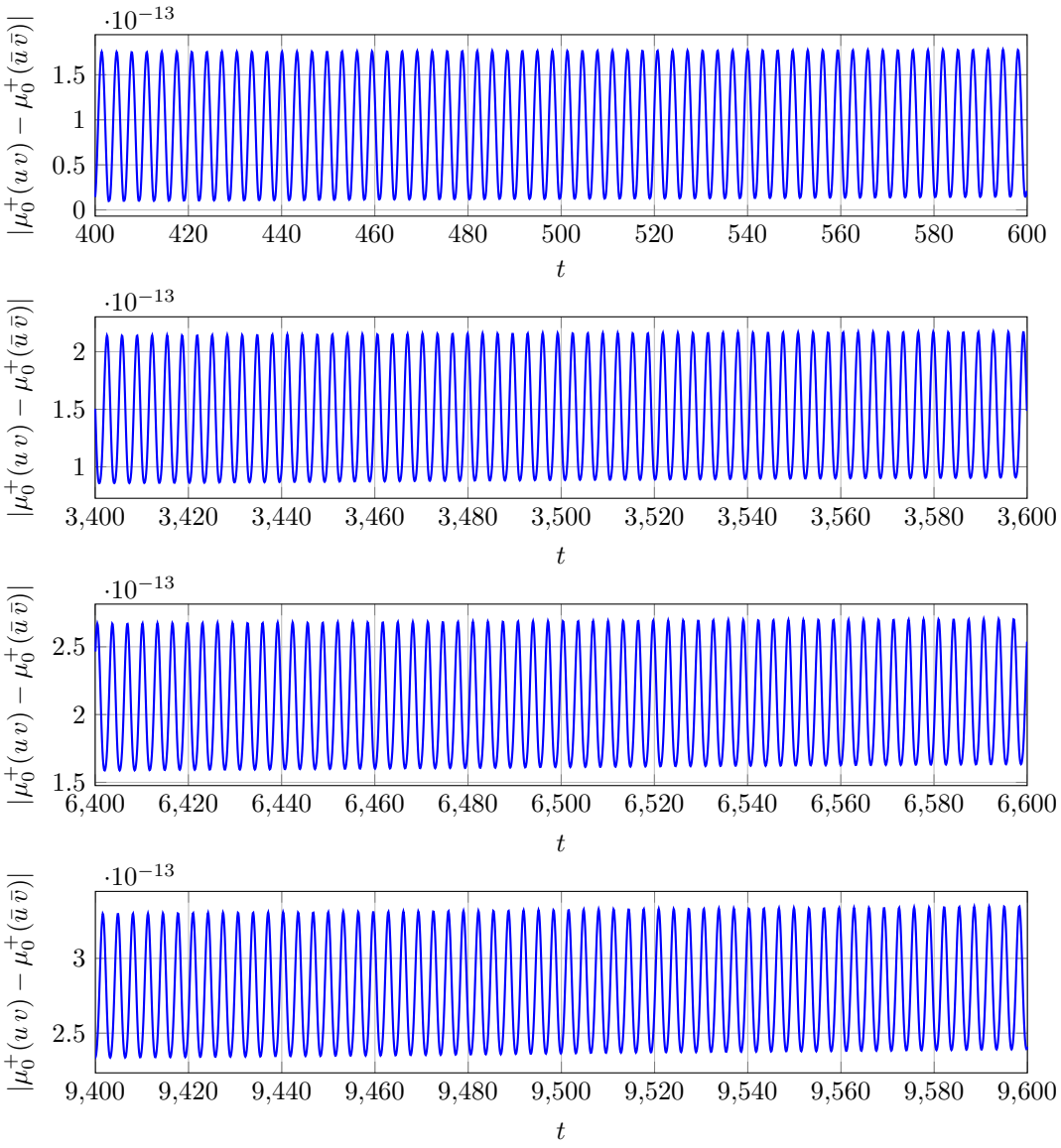

Figure 6.14: Long time dynamics of $|\mu_0^+(u,v) - \mu_0^+(\bar{u},\bar{v})|$ as a function of time

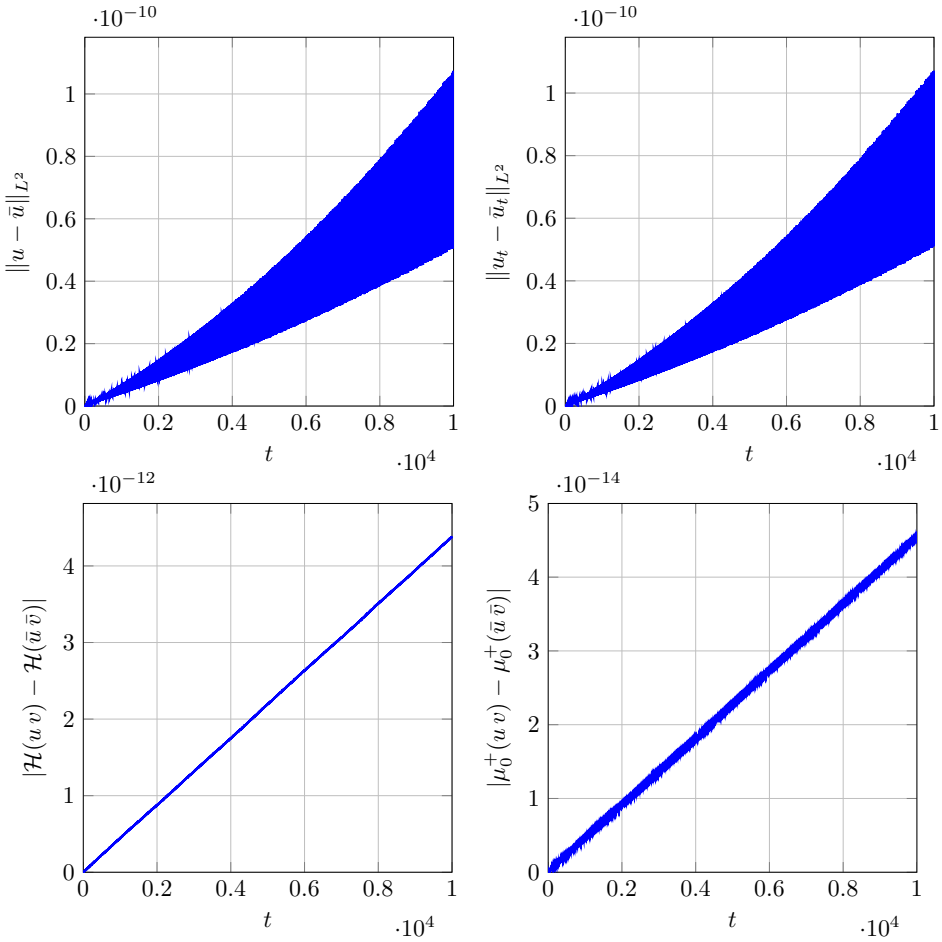

Figure 6.15: The long-time behavior of our semidiscretization method for initial conditions associated with small finite gap solutions to the SGE (left to right and top to bottom): $\|u - \bar{u}\|_{L^2}$, $\|u_t - \bar{u}_t\|_{L^2}$, $|\mathcal{H}(u, v) - \mathcal{H}(\bar{u}, \bar{v})|$, $|\mu_0^+(u, v) - \mu_0^+(\bar{u}, \bar{v})|$, with $N = 2^6$.

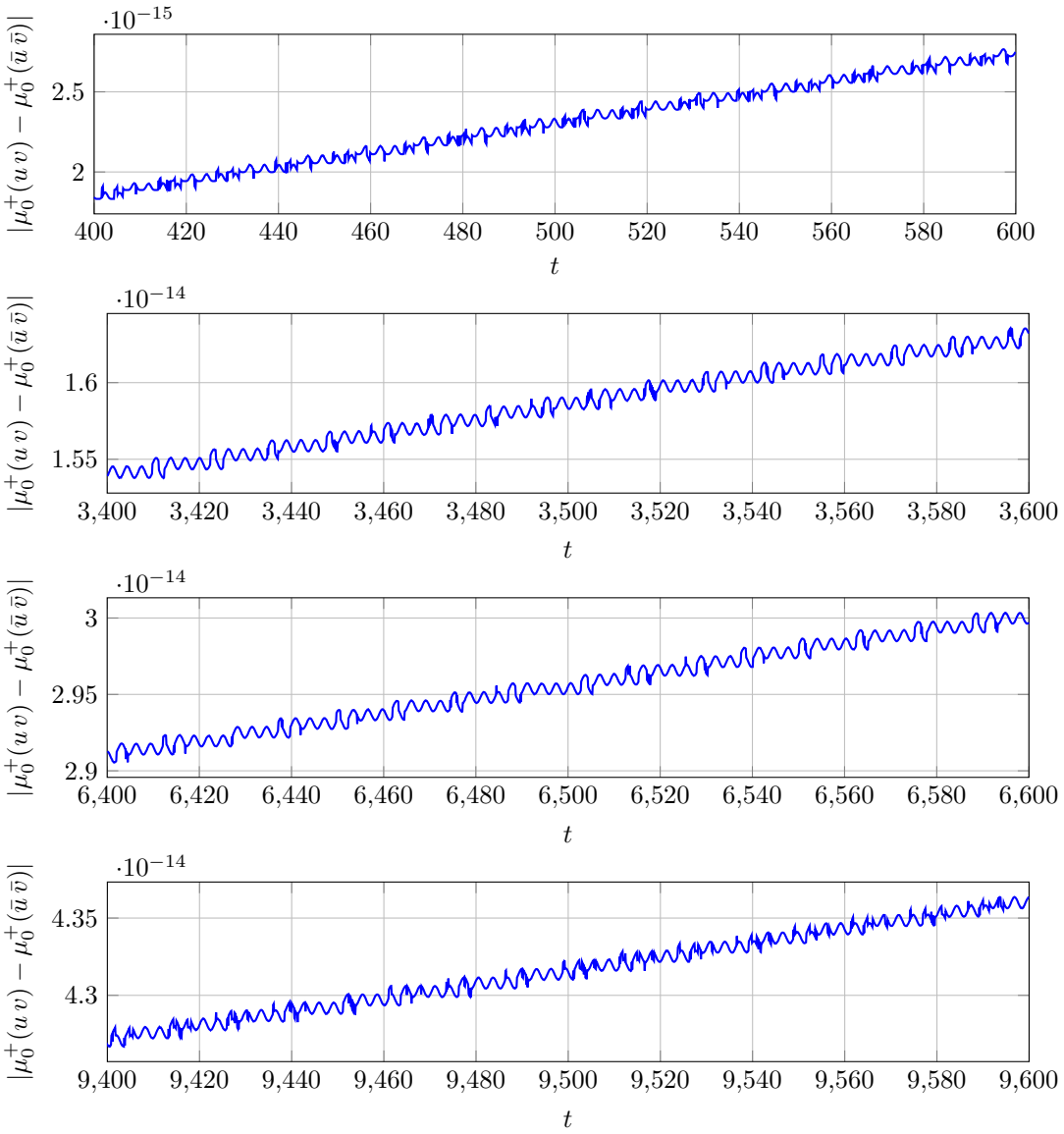

Figure 6.16: Long time dynamics of $|\mu_0^+(u,v) - \mu_0^+(\bar{u},\bar{v})|$ as a function of time.

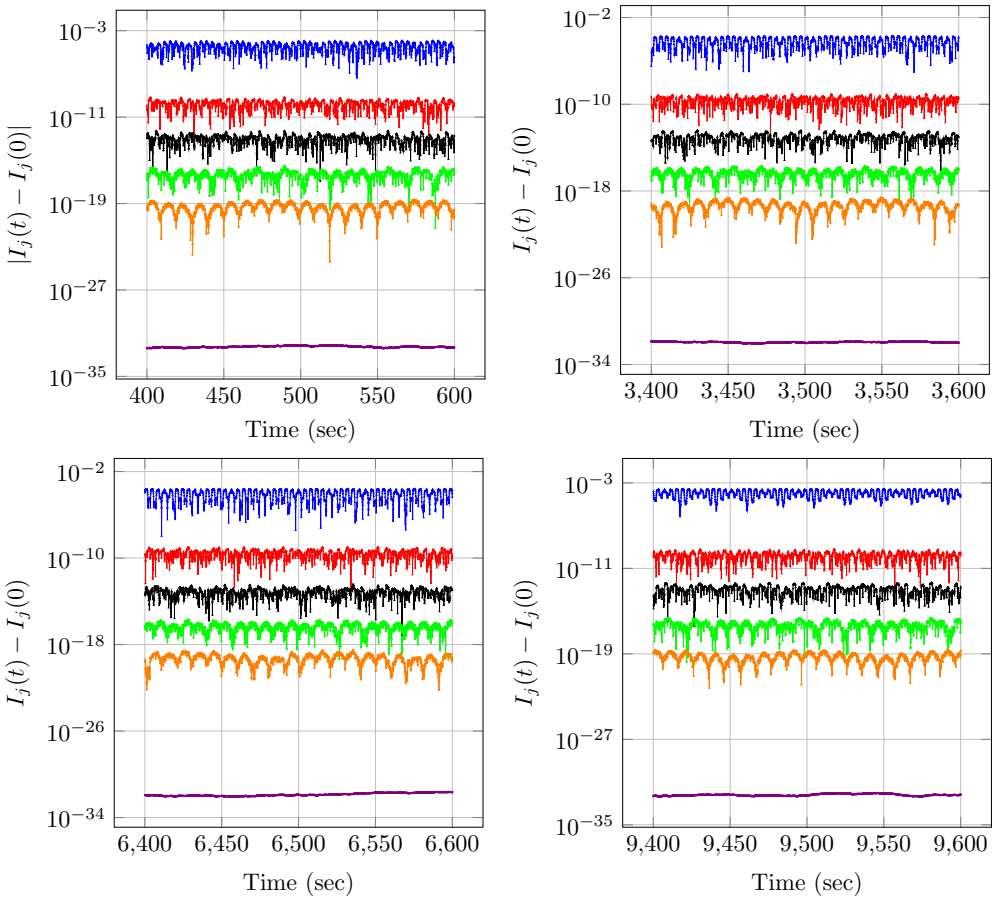

Figure 6.17: Near-conservation of the harmonic actions plotted as a function of time (SGE, periodic boundary conditions).

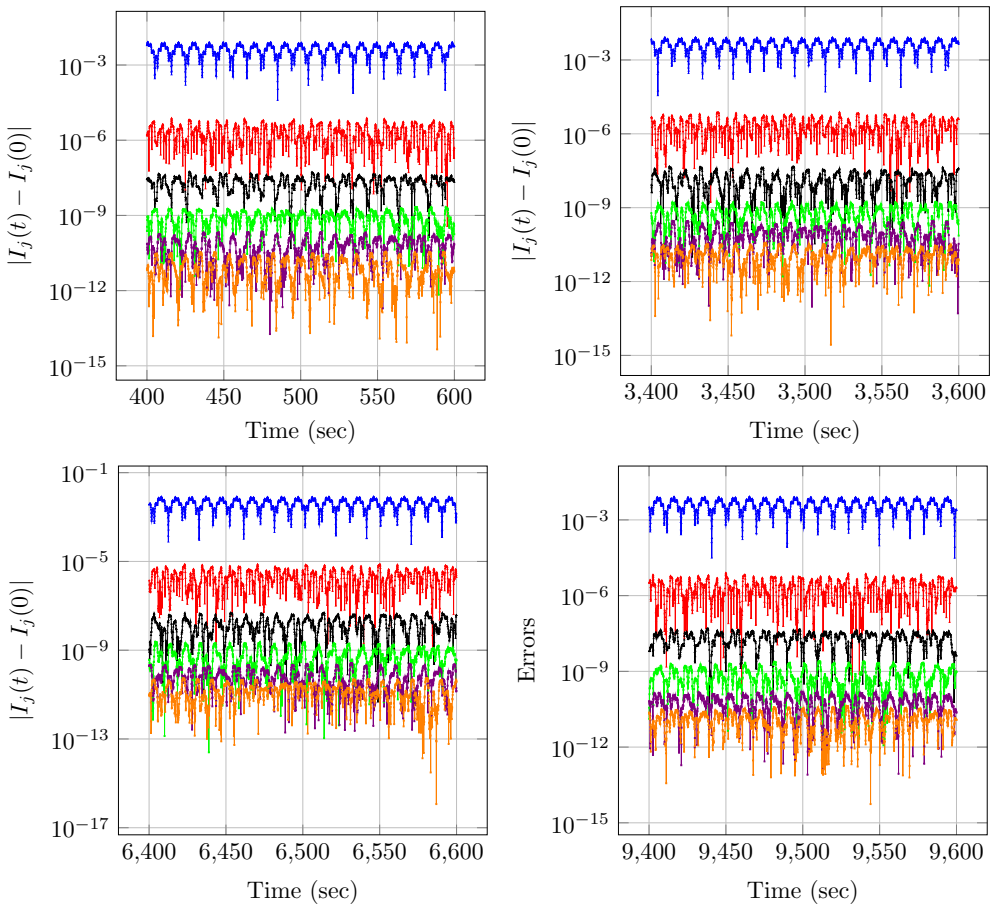

Figure 6.18: Near-conservation of the harmonic actions plotted as a function of time (SGE, even-periodic boundary conditions).

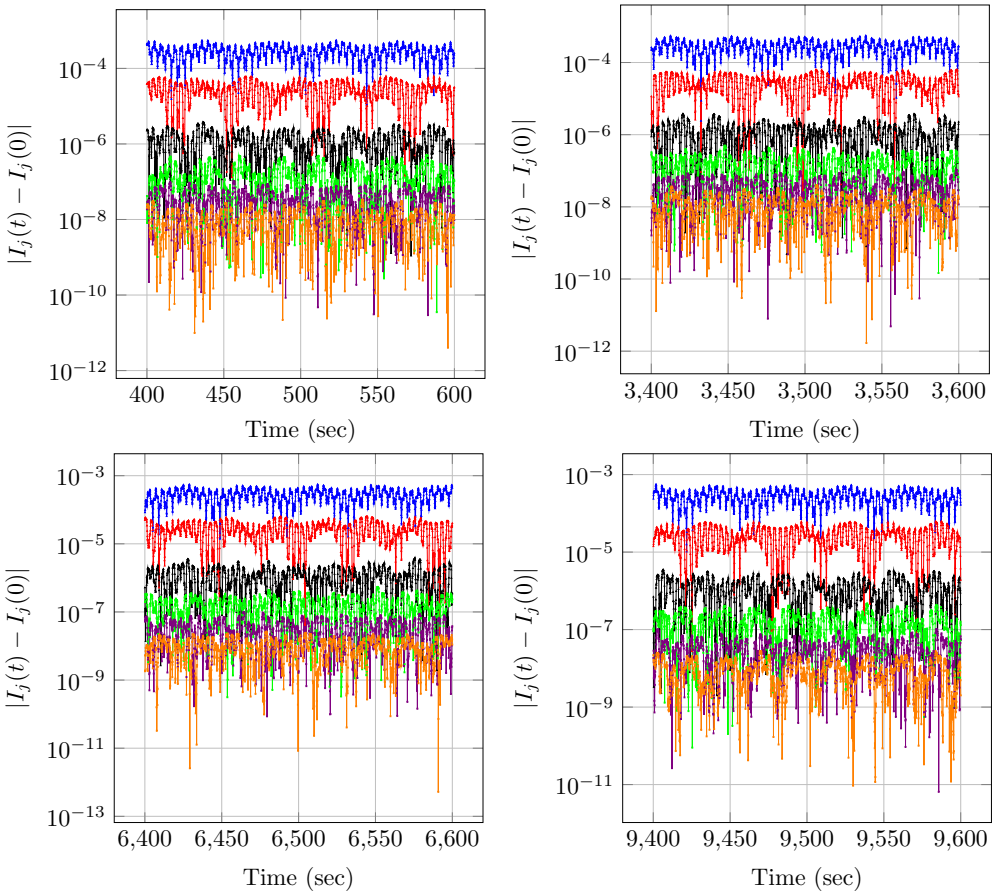

Figure 6.19: Near-conservation of the harmonic actions plotted as a function of time (SGE, odd-periodic boundary conditions).

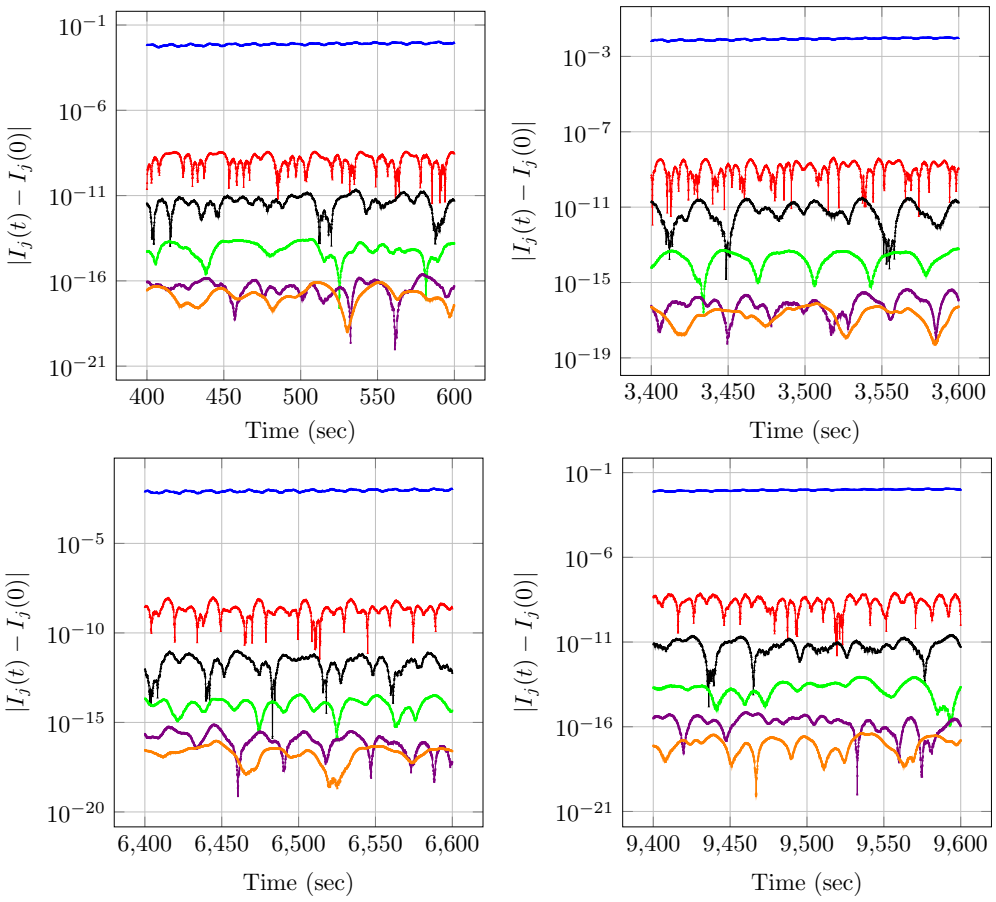

Figure 6.20: Near-conservation of the harmonic actions plotted as a function of time (KGE with cubic potential, periodic boundary conditions).

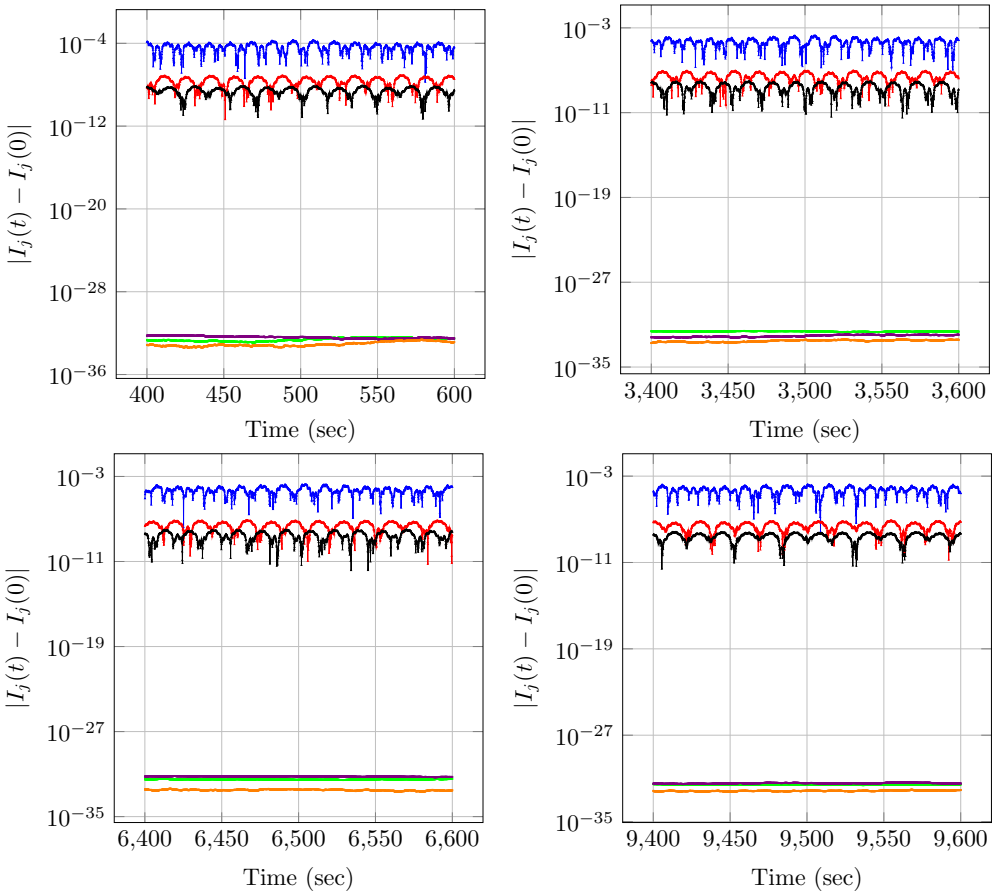

Figure 6.21: Near-conservation of the harmonic actions plotted as a function of time (KGE with cubic potential, even-periodic boundary conditions).

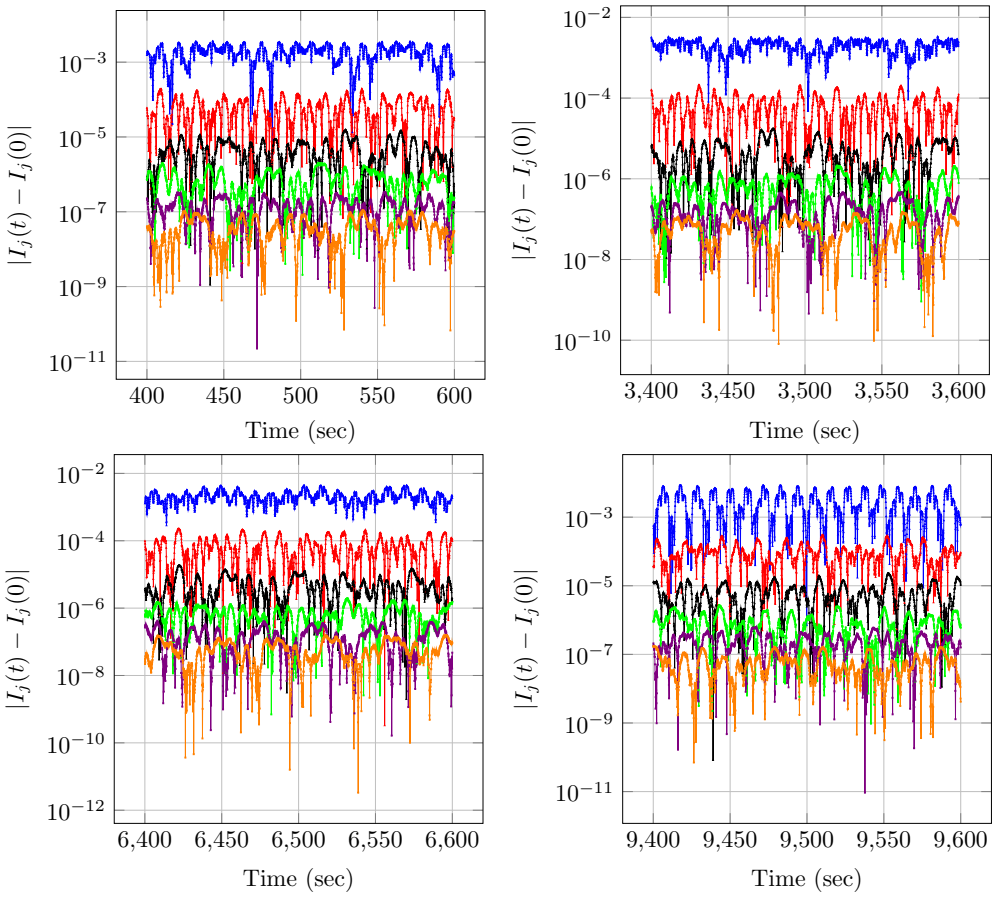

Figure 6.22: Near-conservation of the harmonic actions plotted as a function of time (KGE with cubic potential, odd-periodic boundary conditions).

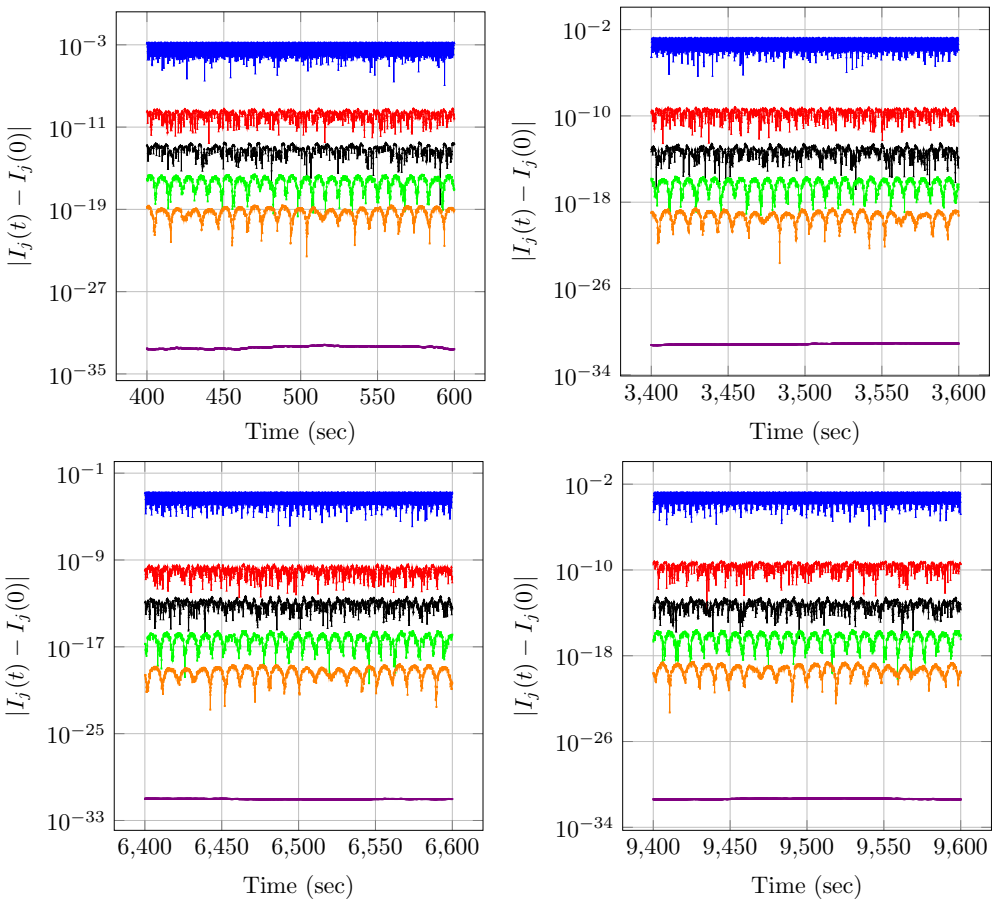

Figure 6.23: Near-conservation of the harmonic actions plotted as a function of time (double SGE, periodic boundary conditions).

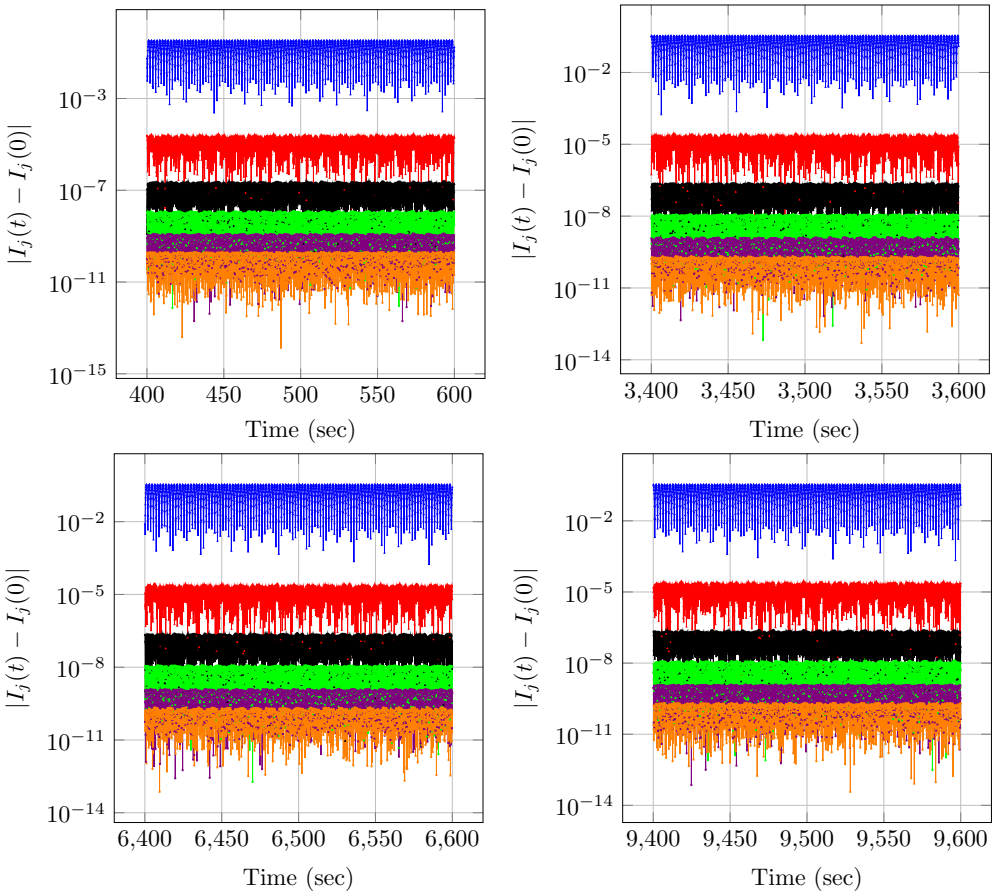

Figure 6.24: Near-conservation of the harmonic actions plotted as a function of time (double SGE, even-periodic boundary conditions).

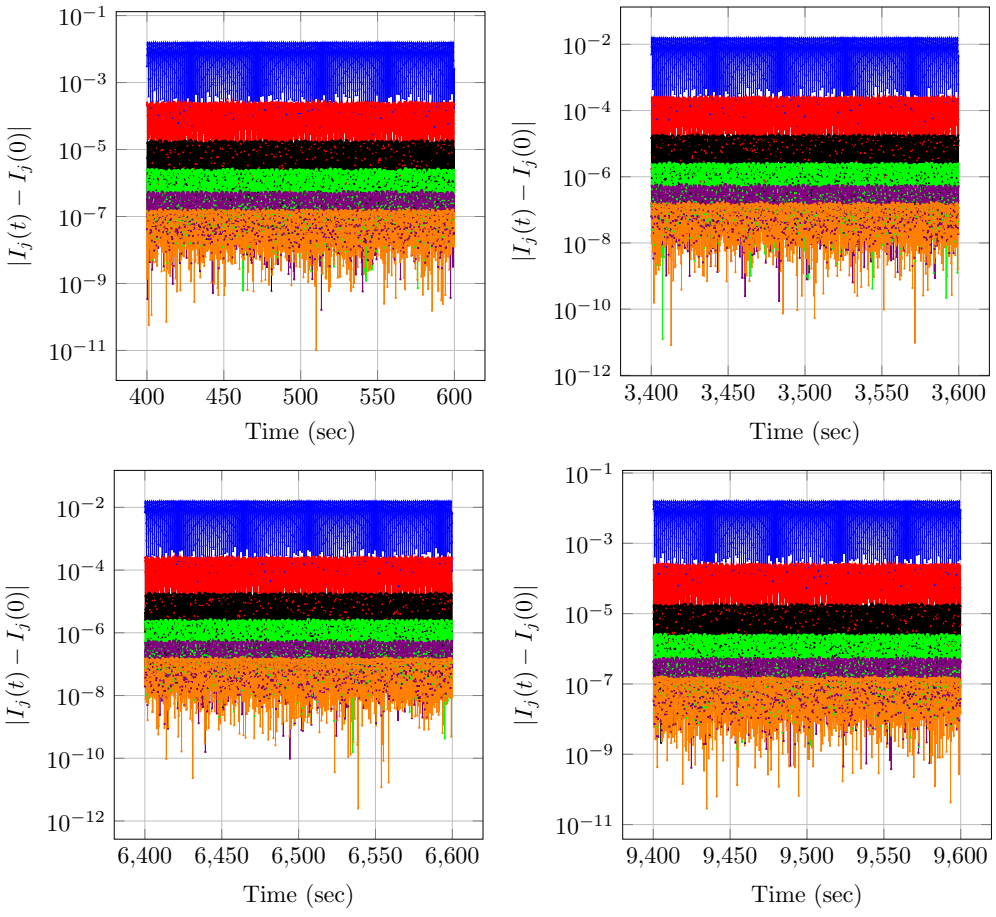

Figure 6.25: Near-conservation of the harmonic actions plotted as a function of time (double SGE, odd-periodic boundary conditions).

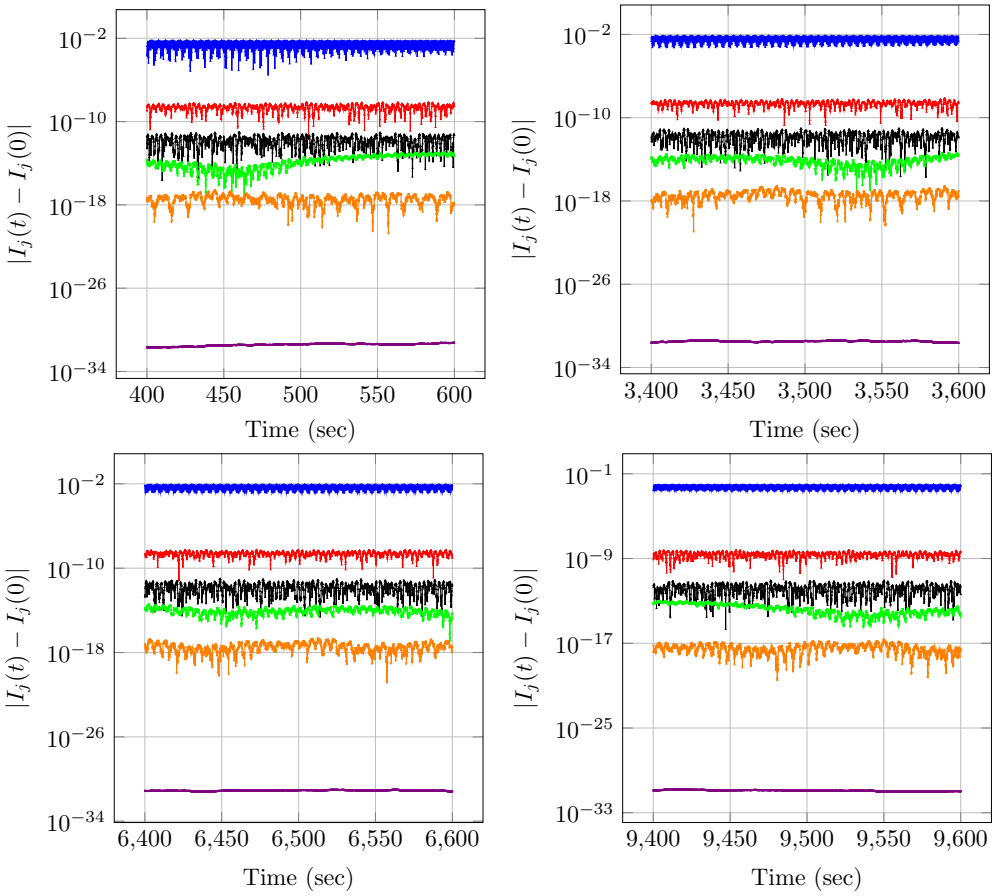

Figure 6.26: Near-conservation of the harmonic actions plotted as a function of time (HSGE, periodic boundary conditions).

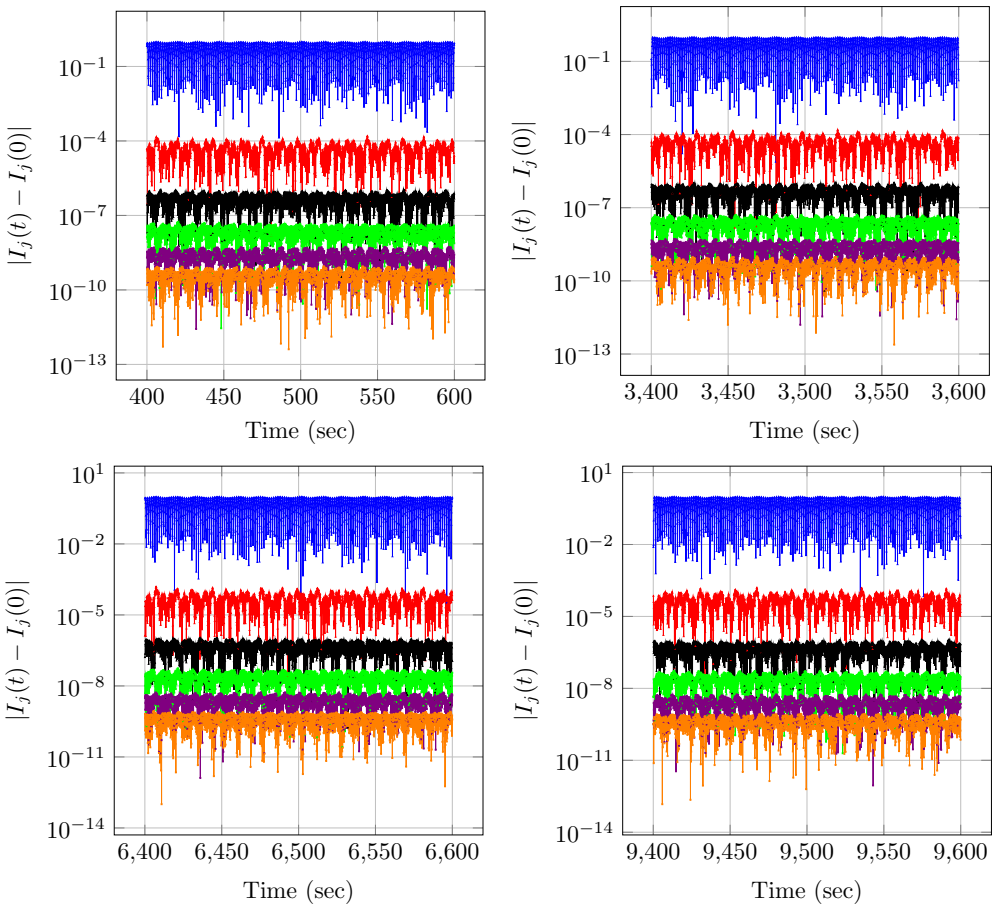

Figure 6.27: Near-conservation of the harmonic actions plotted as a function of time (HSGE, even-periodic boundary conditions).

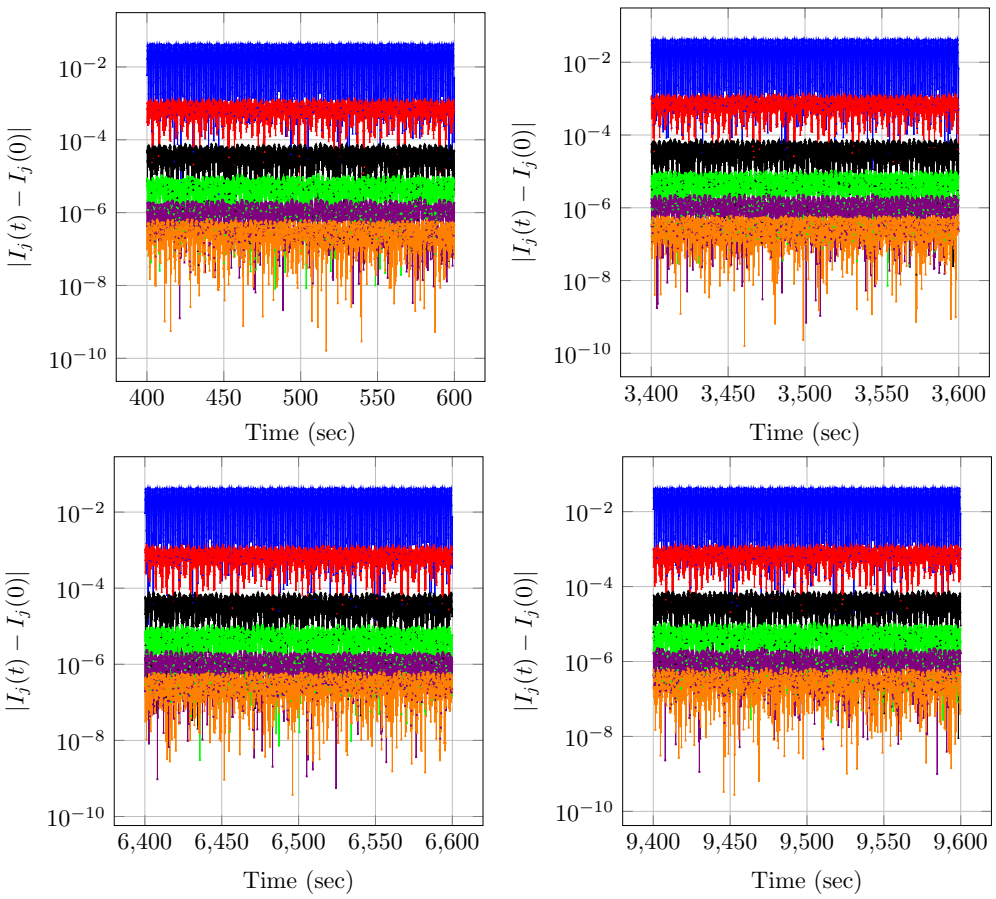

Figure 6.28: Near-conservation of the harmonic actions plotted as a function of time (HSGE, odd-periodic boundary conditions).

Chapter 7

Conclusion

In conclusion, in this thesis we undertook a comprehensive investigation of the Klein-Gordon Equation (KGE) using a combined theoretical and numerical approach.

In the literature, most of known numerical schemes deal with the KGE posed on bounded spatial domains. When the domain is unbounded it is standard to truncate it and then apply conventional schemes designed for bounded domains. To the best of our knowledge there exists no rigorous treatment of the numerical error induced by the domain truncation. In the thesis, we demonstrated that this error is properly controlled, provided the truncated domain is sufficiently large to capture the essential features of the input data.

The spectral methods in general are known to converge extremely fast. In context of various types of spectral schemes applied to KGE the (sub-)geometric convergence rate was reported by large number of researches. However, to the best of our knowledge, rigorous mathematical proofs have not appeared in the numerical literature. In Chapter 4, we employed the ideas of [82] to demonstrate (sub-)geometric convergence for analytic data.

In a number of realistic scenarios, the pseudo-spectral Fourier-type schemes can be viewed as a small Hamiltonian perturbation of the SGE and/or the linear wave equation (LWE). In these cases, it is natural to expect that the qualitative behaviour of the semidiscrete flow resembles closely the flow generated by the SGE/LWE. Despite multiple attempts to construct an infinite dimensional analogue of KAM theory, the available results are far from being satisfactory. The available results rely on assumptions which are extremely pessimistic. In Chapter 6 of the thesis, we provided comprehensive numerical simulations, indicating that the long-time dynamics of semidiscrete solutions is close to the dynamics of the unperturbed SGE/LWE models for a much wider set of parameters than predicted by available theories.

Suggestion for possible future work. Future work could involve two directions. One path would be to extend the analysis to encompass a wider range of potentials. This could involve exploring the applicability of the Fourier-type pseudo-spectral to more general classes of potentials. The second direction would be investigating the long-time behavior of solutions under different perturbation scenarios. In particular, future work could apply an adaptation of the KAM theory to investigate 'stickiness' of the semidiscrete KAM tori observed numerically in Sections 6.2–6.3.

Bibliography

[1] M.J. Ablowitz, D.J. Kaup, A.C. Newell, and H. Segur. Method for solving the Sine-Gordon equation. *Physical Review Letters*, 30(25):1262, 1973.

[2] M.J. Ablowitz and H. Segur. *Solitons and the Inverse Scattering Transform*. Society for Industrial and Applied Mathematics, 1981.

[3] R.A. Adams and J.J.F Fournier. *Sobolev Spaces*. Elsevier, 2nd edition, 2003.

[4] S. Aseeri, O. Batrasev, M. Icardi, B. Leu, A. Liu, N. Li, M.K. Muite, E. Müller, B. Palen, M. Quell, H. Servat, P. Sheth, R. Speck, M. VanMoer, and J. Vienne. Solving the Klein-Gordon equation using Fourier spectral methods: A benchmark test for computer performance. *Proceedings of the Symposium on High Performance Computing*, pages 182–191, 2015.

[5] P. Baldi, M. Berti, and R. Montalto. KAM for autonomous quasi-linear perturbations of KdV. *Annales de l'Institut Henri Poincaré C, Analyse non linéaire*, 33(6):1589–1638, November 2016.

[6] D. Bambusi. Long time stability of some small amplitude solutions in nonlinear Schrödinger equations. *Communications in mathematical physics*, 189(1):205–226, 1997.

[7] D. Bambusi. Birkhoff normal form for some nonlinear PDEs. *Communications in Mathematical Physics*, 234(2):253–285, 2003.

[8] D. Bambusi. *An introduction to Birkhoff normal form*. Universita di Milano, 2014.

[9] W. Bao and X. Zhao. A uniformly accurate multiscale time integrator spectral method for the Klein-Gordon-Zakarov system in the high-plasma-frequency limit regime. *Journal of Computational Physics*, 327:270–293, 2015.

[10] A. Barone, F. Esposito, C.J. Magee, and A.C. Scott. Theory and applications of the Sine-Gordon equation. *La Rivista del Nuovo Cimento (1971-1977)*, 1(2):227–267, 1971.

[11] E.D. Belokolos, A.I. Bobenko, V.Z. Enolskii, A.R. Its, and V.B. Matveev. *Algebro-geometric approach to nonlinear integrable equations*, volume 1994. Springer, Berlin, 1994.

[12] G. Ben-Yu, P.J. Pascual, M. J. Rodriguez, and L. Vazquez. Numerical solution of the Sine-Gordon equation. *Applied Mathematics and Computation*, 18(1):1–14, 1986.

[13] S. Berberian. *Introduction to Hilbert space*. New York: Oxford University Press, 1961.

[14] G. Berikelashvili, S. Kharibegashvili O. Jokhadze, and B. Midodashvili. Finite difference solution of a nonlinear Klein-Gordon equation with an external source. *Mathematics of Computation*, 80(274):847–862, 2010.

[15] J. Bourgain. Construction of approximative and almost periodic solutions of perturbed linear Schrödinger and wave equations. *Geometric & Functional Analysis GAFA*, 6(2):201–230, 1996.

[16] J. Bourgain. On diffusion in high-dimensional Hamiltonian systems and PDE. *Journal d'Analyse Mathématique*, 80(1):1–35, 2000.

[17] J.P. Boyd. *Chebyshev and Fourier Spectral Methods*. Dover Publications, Inc., New York, 2000.

[18] P. Brenner and W. Wahl. Global classical solutions of nonlinear wave equations. *International Journal of Computer Mathematics*, 176(1):87–121, 1981.

[19] H. Brezis. *Functional Analysis, Sobolev Spaces and Partial Differential Equations*. Springer, New-York, Dordrecht, Heidelberg, London, 2011.

[20] F.E. Browder. On non-linear wave equations. *Math. Z.*, 80:249–264, 1962.

[21] P.L. Butzer and R.J. Nessel. *Fourier Analysis and Approximation*. Academic Press, 1971.

[22] C. Canuto, A. Quarteroni, M.Y. Hussani, and T.A. Zang. *Spectral Methods: Fundamental in Single Domains*. Springer-Verlag. Berlin, Heidelberg, 2006.

[23] K. Chadan, D. Colton, L. Päivärinta, and W. Rundell. *An Introduction to Inverse Scattering and Inverse Spectral Problems*. Society for Industrial and Applied Mathematics, 1997.

[24] H. Chen, S. Lu, and W. Chen. A fully discrete spectral method for the nonlinear time fractional Klein-Gordon equation. *Taiwanese Journal of Mathematics*, 21(1):231–251, 2017.

[25] D. Cohen, E. Hairer, and C. Lubich. Long-time analysis of nonlinearly perturbed wave equations via modulated Fourier expansions. *Archive for Rational Mechanics and Analysis*, 187(2):341–368, 2008.

[26] W. Craig. Newton's method and periodic solutions of nonlinear wave equations. *Communications on Pure and Applied Mathematics*, 46(11):1409–1498, 1993.

[27] B. Deconinck, M. Heil, A. Bobenko, M. Van Hoeij, and M. Schmies. Computing Riemann theta functions. *Mathematics of Computation*, 73(247):1417–1442, 2004.

[28] M. Dehghan and A. Shokri. Numerical solution of Klein-Gordon equations using radial basis functions. *Journal of Computational and Applied Mathematics*, 230:400–410, 2009.

[29] M. Dehghan and A. Taleei. Numerical solution of the Yukawa-coupled Klein-Gordon-Schrödinger equations via a Chebyshev pseudospectral multidomain method. *Applied Mathematical Modelling*, 36(6):2340–2349, 2012.

[30] A. Delshams and P. Gutiérrez. Effective stability and KAM theory. *Journal of Differential Equations*, 128(2):415–490, 1996.

[31] R.K. Dodd, I.C. Eibeck, J.D. Gibbon, and H.C. Morris. *Solitons and Nonlinear Wave Equations*. Academic London, 1982.

[32] X. Dong, Z. Xu, and X. Zhao. On time-splitting pseudospectral discretization for nonlinear Klein-Gordon equation in nonrelativistic limit regime. *Communications in Computational Physics*, 16(2):440–466, 2014.

[33] B.A. Dubrovin. Theory of operators and real algebraic geometry. *Global Analysis—Studies and Applications III*, pages 42–59, 2006.

[34] B.A. Dubrovin and S.M. Natanzon. Real two-zone solutions of the Sine-Gordon equation. *Functional Analysis and Its Applications*, 16(1):21–33, 1982.

[35] D.B. Duncan. Sympletic finite difference approximations of the nonlinear Klein-Gordon equation. *SIAM Journal on Numerical Analysis*, 34(5):1742–1760, 1997.

[36] F.H. Easif, S.A. Manaa, and D. Mekaeel. The finite difference method for ϕ^4 - nonlinear Klein-Gordon equation. *IOSR Journal of Engineering (IOSRJEN)*, 3(11):01–05, 2013.

[37] E.G. Ekomasov and R.K. Salimov. Pseudo-spectral Fourier method as applied to finding localized spherical soliton solutions of $(3 + 1)$-dimensional Klein-Gordon equations. *Journal of Computational Mathematics and Mathematical Physics*, 56(9):1604–1610, 2016.

[38] A.H. Encinasa, J. Martín-Vaqueroa, A. Queiruga-Diosa, and V. Gayoso-Martínezb. Efficient high-order finite difference methods for nonlinear Klein-Gordon equations. *Nonlinear Analysis: Modelling and Control*, 20(2):274–290, 2015.

[39] K. Erwin. *Introductory functional analysis with applications*. New York: Wiley, 1978.

[40] L.C. Evans. *Weak Convergence Methods for Nonlinear Partial Differential Equations*. CBMS Regional Conference Series in Mathematics, AMS, Providence, RI., 74th edition, 1990.

[41] R. Feola and F. Giuliani. Long time dynamics of quasi-linear Hamiltonian Klein-Gordon equations on the circle. *Journal of Dynamics and Differential Equations*, 2023.

[42] A.B. Ferrari and E.S. Titi. Gevrey regularity for nonlinear analytic parabolic equations. *Communications in Partial Differential Equations*, 23(1-2):424–448, 1998.

[43] C. Foias and R. Temam. Gevrey class regularity for the solutions of the Navier-Stokes equations. *Journal of Functional Analysis*, 87(2):359–369, 1989.

[44] I. Fukuda and M. Tsutsumi. On coupled Klein-Gordon-Schrödinger equations, II. *Journal of mathematical Analysis and Applications*, 66(2):358–378, 1978.

[45] J. Garnet and E. Trubowitz. Gaps and bands on one-dimensional Schrödinger operator II. *Commentarii Mathematici Helvetici*, 62:18–37, 1987.

[46] J. Geng and J. You. A KAM theorem for Hamiltonian partial differential equations in higher dimensional spaces. *Communications in Mathematical Physics*, 262(2):343–372, 2006.

[47] J. Ginibre and G. Velo. The global Cauchy problem for the nonlinear Klein-Gordon equation. *Math. Z.*, 189:487–505, 1985.

[48] J. Ginibre and G. Velo. The global Cauchy problem for the nonlinear Klein-Gordon equation-II. *Ann. Inst. Henri Poincare*, 6:15–35, 1989.

[49] F. Giuliani. *KAM for quasi-linear PDE's*. PhD thesis, 2017.

[50] L. Grafakos. *Modern Fourier Analysis*. Springer, 2009.

[51] L. Grafakos. *Classical Fourier Analysis*. Springer, 3rd edition, 2014.

[52] B. Grebert. Birkhoff normal form and Hamiltonian PDEs. *Partial differential equations and applications*, 2007.

[53] B. Guo and Z.Q. Wang. A collocation method for generalized nonlinear Klein-Gordon equation. *Advances in Computational Mathematics*, 40(2):377–398, 2014.

[54] E. Hairer, C. Lubich, and G. Wanner. *Geometric Numerical Integration*. Springer, 2006.

[55] H. Han and Z. Zhang. An analysis of the finite-difference method for one-dimensional Klein-Gordon equation on unbounded domain. *Applied Numerical Mathematics*, 59(7):1568–1583, 2009.

[56] J. Hesthaven, S. Gottlieb, and D. Gottlieb. *Spectral Method for Time-Dependent Problems*. Cambridge University Press, Cambridge, UK, 2007.

[57] S. Ibrahim, M. Majdoub, and M. Masmoudi. Global solutions for a semilinear, two dimensional Klein-Gordon equation with exponential-type nonlinearity. *Commun. Pure Appl. Math.*, 59:1639–1658, 2006.

[58] I. Javid and A. Rustam. Numerical solution of Klein/Sine-Gordon equations by spectral method coupled with Chebyshev wavelets. *Applied Mathematics*, 7(17):2097–2109, 2016.

[59] W. John. The Sine-Gordon equations: Complete and partial integrability. *Journal of Mathematical Physics*, 25(7):2226–2235, 1984.

[60] K. Jörgens. Das anfangswertproblem im grossen für eine Klasse nichtlinearer wellengleichungen. *Math. Z.*, 77:295–308, 1961.

[61] J. Jost. *Compact Riemann Surfaces*. Springer-Verlag, 2006.

[62] S. Klainerman, Q. Wang, and S. Yang. Global solution for massive Maxwell-Klein-Gordon equations. *arXiv*, 2018.

[63] D.A. Kopriva. *Implementing Spectral Methods for Partial Differential Equations: Algorithms for Scientists and Engineers*. Springer, 2009.

[64] S.B. Kuksin. *Analysis of Hamiltonian PDEs*, volume 19. Clarendon Press, 2000.

[65] M. Lakestani and M. Dehghan. Collocation and finite difference-collocation methods for the solution of nonlinear Klein-Gordon equation. *Computer Physics Communications*, 181(8):1392–1401, 2010.

[66] N. Latioui, A. Guesmia, and A. Ouaoua. Well-posedness and stability for a system of Klein-Gordon equations. *International Journal of Analysis and Applications*, 20:10–10, 2022.

[67] P.D. Lax. *Functional analysis*. New York: Wiley, 2002.

[68] X. Li, B.Y. Guo, and L. Vazquez. A Legendre spectral method for solving the nonlinear Klein-Gordon equation. *Mathematics Applied and Computation*, 15:19–36, 1996.

[69] J.L. Lions. *Equations Differentielles Operationnelles et problemes aux limites*. Grundlehren der Math. Wiss., Bd. 111. Springer, 1961.

[70] C. Liu, A. Iserles, and X. Wu. Symmetric and arbitrarily high-order Birkhoff-Hermite time integrators and their long-time behaviour for solving nonlinear Klein-Gordon equations. *Journal of Computational Physics*, 356:1–30, 2018.

[71] Gafari Abiodun Lukumon. Numerical solution of the klein-gordon equation in an unbounded domain., 2018.

[72] Y. Luo, Y. Yang, M.S. Ahmed, T. Yu, M. Zhang, L. Wang, and H. Xu. Global existence and blow up of the solution for nonlinear Klein-Gordon equation with general power type nonlinearities at three initial energy levels. *Applied Numerical Mathematics*, https://doi.org/10.1016/j.apnum.2018.05.018, 2018.

[73] Y. Ma. Global solutions of quasilinear wave Klein-Gordon system in two-space dimension: Technical tools. *Journal of Hyperbolic Differential Equations*, 14(4):591–625, 2017.

[74] G. Mastroianni and G.V. Milovanović. *Interpolation Processes. Basic theory and applications*. Springer-Verlag, Berlin, 2008.

[75] H.P. McKean. The Sine-Gordon and Sinh-Gordon equations on the circle. *Communications on Pure and Applied Mathematics*, 34(2):197–257, 1981.

[76] R. Miranda. *Algebraic Curves and Riemann Surfaces*, volume 5. American Mathematical Society, 1995.

[77] A. Mohebbia, Z. Asgarib, and A. Shahrezaee. Fast and high accuracy numerical methods for the solution of nonlinear Klein-Gordon equations. *Verlag der Zeitschrift für Naturforschung Tubingen - Mainz*, 66a:735–744, 2011.

[78] J. Moser. Various aspects of integrable Hamiltonian systems. In *Proc. CIME Conference, Bressansone, Italy, 1978. Progr. Math. 8.* Birkhäuser, 1980.

[79] M. Nakamura and T. Ozawa. The Cauchy problem for nonlinear Klein-Gordon equations in the Sobolev spaces. *Publ. RMS, Kyoto Univ.*, 37:255–293, 2001.

[80] A.C. Newell. The inverse scattering transform. In *Solitons*, pages 177–242. Springer Berlin Heidelberg, Berlin, Heidelberg, 1980.

[81] S. Novikov, S.V. Manakov, L.P. Pitaevskii, and V.E. Zakharov. *Theory of Solitons, The inverse Scatterring Method.* Springer Science and Business Media, 1984.

[82] S. Panizzi. On the domain of analyticity of solutions to semilinear Klein–Gordon equations. *Nonlinear Analysis*, 75:2841–2850, 2012.

[83] J.E. Pasciak. Spectral and pseudo spectral methods for advection equations. *Math. Comp.*, 35:1081–1092, 1980.

[84] N. Polat and H. Taskesen. On the existence of global solutions for a nonlinear Klein-Gordon equation. *Faculty of Sciences and Mathematics, University of Nis, Serbia*, 28(5):1073–1079, 2014.

[85] S. Roman. The formula of Faa di Bruno. *Amer. Math. Monthly*, 87:805–809, 1980.

[86] H.L. Royden and P.M. Fitzpatrick. *Real analysis*. Pearson Education Asia Limited and China Machine Press., 4th edition, 2010.

[87] J. Rubinstein. Sine-Gordon equation. *Journal of Mathematical Physics*, 11(1):258–266, 1970.

[88] J. Shen, T. Tang, and L. Wang. *Spectral Method: Algorithms, Analysis and Applications*. Springer-verlag. Berlin, Heidelberg, 2011.

[89] S. Shindin, N. Parumasur, and G. Lukumon. Numerical analysis of Fourier pseudospectral methods for the Klein–Gordon equation with smooth potentials. *Afrika Matematika*, 33(3):85, 2022.

[90] Z. Songmu. *Nonlinear evolution equations*. Boca Raton, Fla: Chapman and Hall/CRC Press, 2004.

[91] E.M. Stein and R. Shakarchi. *Fourier Analysis, An Introduction*. Princeton University Press, 2003.

[92] E.M. Stein and G. Weiss. *Introduction to Fourier Analysis on Euclidean Spaces*. Princeton University Press, 1971.

[93] Q.F. Wang and D. Cheng. Numerical solution of damped nonlinear Klein-Gordon equations using variational method and finite element approach. *Journal of Applied Mathematics and Computation*, 162:381–401, 2005.

[94] C. E. Wayne. An introduction to KAMs theory. Preprint, 8, 2008.

[95] C.E. Wayne. An introduction to KAM theory. In *Dynamical systems and probabilistic methods in partial differential equations (Berkeley, CA, 1994)*, volume 31, pages 3–29, 1994.

[96] R.A. Weder. Scattering theory for the Klein-Gordon equation. *J. Functional Analysis*, 27:100–117, 1978.

[97] B. Weizhu and D. Xuanchun. Analysis and comparison of numerical methods for the Klein-Gordon equation in the nonrelativistic limit regime. *Numerische Mathematik*, 120(2):189–229, 2012.

[98] Y. Widmer. On the integrability of the Sine-Gordon equation. *arXiv*, 2015.

[99] S. Xia and J. Zhang. Global well-posedness and scattering for a nonlinear Klein-Gordon equation in low dimensions. *American Institute of Phyics*, 92:351–378, 2013.

[100] R. Xu and Y. Ding. Global solutions and finite time blow up for damped Klein-Gordon equation. *Acta Mathematica Scientia*, 33(3):634–652, 2013.

[101] F. Yin, T. Tian, J. Song, and M. Zhu. Spectral methods using Legendre wavelets for nonlinear Klein/Sine-Gordon equations. *Journal of Computational and Applied Mathematics*, 275:321–334, 2015.